



1 **Data supporting the North Atlantic Climate System: Integrated Studies (ACSIS) programme,**  
2 **including atmospheric composition, oceanographic and sea ice observations (2016-2022) and output**  
3 **from ocean, atmosphere, land and sea-ice models (1950-2050)**

4 Alex T. Archibald<sup>1, 2</sup>, Bablu Sinha<sup>3</sup>, Maria R. Russo<sup>1, 2</sup>, Emily Matthews<sup>5</sup>, Freya A. Squires<sup>6</sup>, N. Luke  
5 Abraham<sup>1, 2</sup>, Stephane J.-B Bauguitte<sup>4</sup>, Thomas. J. Bannan<sup>5</sup>, Thomas G. Bell<sup>7</sup>, David Berry<sup>8</sup>, Lucy J.  
6 Carpenter<sup>9</sup>, Hugh Coe<sup>5, 10</sup>, Andrew Coward<sup>3</sup>, Peter Edwards<sup>9,11</sup>, Daniel Feltham<sup>12</sup>, Dwayne Heard<sup>13</sup>, Jim  
7 Hopkins<sup>9,11</sup>, James Keeble<sup>1, 2</sup>, Elizabeth C. Kent<sup>3</sup>, Brian A. King<sup>3</sup>, Isobel R. Lawrence<sup>14,15</sup>, James Lee<sup>9,15</sup>,  
8 Claire R. Macintosh<sup>16</sup>, Alex Megann<sup>3</sup>, Bengamin I. Moat<sup>3</sup>, Katie Read<sup>9,11</sup>, Chris Reed<sup>4</sup>, Malcolm J.  
9 Roberts<sup>17</sup>, Reinhard Schiemann<sup>18</sup>, David Schroeder<sup>12</sup>, Timothy J. Smyth<sup>7</sup>, Loren Temple<sup>9</sup>, Navaneeth  
10 Thamban<sup>5</sup>, Lisa Whalley<sup>13,19</sup>, Simon Williams<sup>3</sup>, Huihui Wu<sup>5</sup>, Ming-Xi Yang<sup>7</sup>

11  
12 <sup>1</sup>National Centre for Atmospheric Science, University of Cambridge, Cambridge, United Kingdom  
13 <sup>2</sup>Yusuf Hamied Department of Chemistry, University of Cambridge, Cambridge CB2 1EW, United Kingdom  
14 <sup>3</sup>National oceanography Centre, United Kingdom.  
15 <sup>4</sup>Facility for Airborne Atmospheric Measurements Airborne Laboratory, Cranfield University, Cranfield MK43 0AL, United  
16 Kingdom  
17 <sup>5</sup>Department of Earth and Environmental Science, Centre for Atmospheric Science, University of Manchester, Manchester  
18 M13 9PL, United Kingdom  
19 <sup>6</sup>British Antarctic Survey, Cambridge CB3 0ET, United Kingdom  
20 <sup>7</sup>Plymouth Marine Laboratory, Plymouth PL1 3DH, United Kingdom  
21 <sup>8</sup>WMO, Geneva, Switzerland  
22 <sup>9</sup>Wolfson Atmospheric Chemistry Laboratories, Department of Chemistry, University of York, York YO10 5DD, United  
23 Kingdom  
24 <sup>10</sup>National Centre for Atmospheric Science, University of Manchester, Manchester M13 9PL, United Kingdom  
25 <sup>11</sup>National Centre for Atmospheric Science, University of York, York, United Kingdom  
26 <sup>12</sup>CPOM, University of Reading, Reading, UK  
27 <sup>13</sup>School of Chemistry, University of Leeds, Leeds LS2 9JT , United Kingdom  
28 <sup>14</sup>ESA ESRIN, Via Galileo Galilei, 1, 00044 Frascati RM, Italy.  
29 <sup>15</sup>CPOM, University of Leeds, Leeds, United Kingdom  
30 <sup>16</sup>ESA Climate Office, United Kingdom  
31 <sup>17</sup>Met Office Hadley Centre, Exeter, UK.  
32 <sup>18</sup>National Centre for Atmospheric Science, Department of Meteorology, University of Reading, Reading, UK  
33 <sup>19</sup>National Centre for Atmospheric Science, University of Leeds, Leeds, United Kingdom

34  
35  
36  
37



38  
39

40 *Correspondence to:* Alex Archibald ([ata27@cam.ac.uk](mailto:ata27@cam.ac.uk)) and Bablu Sinha ([bablu@noc.ac.uk](mailto:bablu@noc.ac.uk))

41 **Abstract.** The North Atlantic Climate System: Integrated Study (ACSIS) was a large multidisciplinary research programme  
42 funded by the United Kingdom's Natural Environment Research Council (NERC). ACSIS ran from 2016-22 and brought  
43 together around 80 scientists from seven leading UK-based environmental research institutes to deliver major advances in  
44 understanding North Atlantic climate variability and extremes. Here we present an overview of the data generated by the  
45 ACSIS programme. The datasets cover the full North Atlantic System comprising: the North Atlantic Ocean, the atmosphere  
46 above it including its composition, Arctic Sea Ice and the Greenland Ice Sheet.

47

48 Atmospheric composition datasets include measurements from 7 aircraft campaigns (between 3 and 10 flights each, 0-10km  
49 altitude range) in the north eastern Atlantic (~40°W-5°E, ~15°N-55°N) made at intervals of from 6 months to 2 years between  
50 February 2017 and may 2022. The flights measured chemical species (including greenhouse gases, ozone precursors and  
51 VOCs) and aerosols (organic, SO<sub>4</sub>, NH<sub>4</sub>, NO<sub>3</sub>, and nss-Cl) (<https://dx.doi.org/10.5285/6285564c34a246fc9ba5ce053d85e5e7>  
52 (FAAM et al. (2024))). Ground based stations at the Cape Verde Atmospheric Observatory (CVAO), Penlee Point Atmospheric  
53 Observatory (PPAO) and Plymouth Marine Laboratory (PML) recorded ozone, ozone precursors, halocarbons, as well as  
54 greenhouse gases (CO<sub>2</sub>, methane), SO<sub>2</sub> and photolysis rates. (CVAO,  
55 <http://catalogue.ceda.ac.uk/uuid/81693aad69409100b1b9a247b9ae75d5>, National Centre for Atmospheric Science et al.  
56 (2014)), O<sub>3</sub> and CH<sub>4</sub> (PPAO, <https://catalogue.ceda.ac.uk/uuid/8f1ff8ea77534e08b03983685990a9b0> (Plymouth Marine  
57 Laboratory and Yang (2024)) and aerosols (PML, <https://dx.doi.org/10.5285/e74491c96ef24df29a9342a3d57b5939>, Smyth  
58 (2024)).

59

60 Complementary model simulations of atmospheric composition were performed with the UK Earth System Model, UKESM1,  
61 for the period 1982 to 2020 using CMIP6 historical forcing up to 2014 and SSP3-7.0 scenario from 2015-2020. Model  
62 temperature and winds were relaxed towards ERA reanalysis. Monthly mean model data for ozone, NO, NO<sub>2</sub>, CO, methane,  
63 stratospheric ozone tracers and 30 regionally emitted tracers are available to download  
64 (<https://data.ceda.ac.uk/badc/acsis/UKESM1-hindcasts>, Abraham (2024)).

65

66 ACSIS also generated new ocean heat content diagnostics <https://doi.org/10/g6wm>, <https://doi.org/10/g8g2>, Moat et al.  
67 (2021a-b) and gridded temperature and salinity based on objectively mapped Argo measurements  
68 <https://doi.org/10.5285/fe8e524d-7f04-41f3-e053-6c86abc04d51> (King (2023)).

69 An ensemble of atmosphere-forced global ocean-sea ice simulations using the NEMO-CICE model was performed with  
70 horizontal resolutions of ¼° and 1/12° covering the period 1958-2020 using several different atmosphere reanalysis based



71 surface forcing datasets, supplemented by additional global simulations and standalone sea ice model simulations with  
72 advanced sea ice physics using the CICE model (<http://catalogue.ceda.ac.uk/uuid/770a885a8bc34d51ad71e87ef346d6a8>,  
73 Megann et al. (2021e)). Output is stored as monthly averages and includes 3D potential temperature, salinity, zonal, meridional  
74 and vertical velocity; 2D sea surface height, mixed layer depth, surface heat and freshwater fluxes, ice concentration and  
75 thickness and a wide variety of other variables.

76

77 In addition to the data presented here we provide a brief overview of several other datasets that were generated during ACSIS  
78 which have been described previously in the literature.

### 79 **1. The North Atlantic Climate System**

80 The North Atlantic Climate System Integrated Study (ACSIS) was a 6 year research programme (2016-2022) commissioned  
81 by The UK Natural Environment Research Council (NERC) as part of the first wave of a new series of Long Term Science  
82 Multi-centre (LTSM) projects. ACSIS connected research in the physical and chemical components of the atmosphere-  
83 hydrosphere-cryosphere nexus within the North Atlantic region and provided an opportunity for NERC scientists from  
84 different disciplines to come together and deliver new insights into a region undergoing rapid change in: the ocean and  
85 atmosphere temperatures and circulation, in sea ice thickness and extent, and in key atmospheric constituents such as ozone,  
86 methane and aerosols (Sutton et al., 2018). The ACSIS team included members of the National Centre for Atmospheric Science  
87 (NCAS), Plymouth Marine Laboratory (PML), the National Oceanography Centre (NOC), the British Antarctic Survey (BAS),  
88 the National Centre for Earth Observation (NCEO), the Centre for Polar Observation and Modelling (CPOM), and the Met  
89 Office.

90

91 ACSIS was designed to answer key questions about the North Atlantic Climate System:

92 1) How have changes in natural and anthropogenic emissions and atmospheric circulation combined to shape multi-year trends  
93 in North Atlantic atmospheric composition and radiative forcing? 2) How have natural variability and radiative forcing  
94 combined to shape multi-year trends in the North Atlantic physical climate system? 3) To what extent are changes in the North  
95 Atlantic climate system predictable on multi-year timescales?

96

97 In order to answer these questions, ACSIS was arranged into a series of interlinked work packages involving a broad  
98 representation of scientists from the different NERC centres involved in ACSIS. These work packages delivered new scientific  
99 understanding, delivered through several key synthesis papers (Sutton et al., 2018, Robson et al., 2018, 2020, Hirschi et al.,  
00 2020) as well as a wealth of data. Key objectives of the ACSIS project were to:

01 A) Provide the UK science community with sustained observations, data syntheses, leading-edge numerical simulations and  
02 analysis tools to facilitate world-class research on changes in the North Atlantic climate system and their impacts. B) To



03 provide a quantitative and multivariate description of how the North Atlantic climate system is changing. C) To determine the  
04 primary drivers and processes that are shaping changes in the North Atlantic climate system now and will shape changes in  
05 the near future. D) To determine the extent to which future changes in the North Atlantic climate system are predictable.

06 In this paper we focus on objective (A) of the ACSIS project, which included the creation of new datasets to underpin the  
07 ACSIS project and support wider work on the North Atlantic climate system by the UK and international science communities.

08

09 In this paper we outline the underpinning datasets generated as part of the ACSIS project, how they can be obtained (guided  
10 by the FAIR principles (Wilkinson et al., 2016)), and the motivation for their creation.

### 11 1.1 Overview of data holdings

12 A summary of the datasets that are generated by ACSIS and freely available to the community is given in Table 1. Note that  
13 the new data presented in this paper are archived across two platforms: the British Oceanographic Data Centre,  
14 <https://www.bodc.ac.uk> (ocean observations) and the Centre for Environmental Data Analysis, <https://www.ceda.ac.uk> (all  
15 other data). A schematic map giving an overview of the footprints of all the observational datasets can be found in Fig 4 of  
16 Sutton et al. (2018). The three general areas covered are: atmospheric composition covering aircraft and ground station data  
17 along with nudged historical atmospheric chemistry/circulation model simulations; ocean observations covering gridded in  
18 situ temperature and salinity (0-2000m) and 0-1000m heat content; forced historical ocean-ice simulations at eddy permitting  
19 and eddy resolving resolutions and standalone Arctic sea ice simulations. In subsequent sections 2, 3 and 4, we describe the  
20 individual archived datasets in detail. Several other datasets, previously described in the literature, have been generated by the  
21 ACSIS programme including simulations to generate volcanic forcing data for climate models, coupled climate model  
22 simulations with a high resolution atmosphere and/or ocean, gridded sea-surface temperature based on in situ ocean  
23 observations, and observation based estimates of the Atlantic Meridional Overturning Circulation and Arctic wide sea ice  
24 thickness. For completeness, and because the new datasets described here will likely be used in conjunction with the already  
25 published datasets, we provide a brief overview of the latter in Section 5.

26

27 **Table 1.** Overview of the data described in this paper with links to the sub-sections where the data are described in detail.

Title	Data, weblink, and citation	Accessibility	Subsection
Aircraft missions	Gas and aerosol data collected on board the Facility for Airborne Atmospheric Measurements <a href="https://dx.doi.org/10.5285/6285564c34a246fc9ba5ce053d85e5e7">https://dx.doi.org/10.5285/6285564c34a246fc9ba5ce053d85e5e7</a> FAAM et al. (2024)	Open access for merged 10s data; registration/login to CEDA	2.1



		required for full temporal resolution.	
Ground based observational atmospheric composition time series	<p>Atmospheric composition, including ozone, methane, carbon monoxide, VOCs and aerosol parameters from the Cape Verde Atmospheric Observatory (CVAO) <a href="http://catalogue.ceda.ac.uk/uuid/81693aad69409100b1b9a247b9ae75d5">http://catalogue.ceda.ac.uk/uuid/81693aad69409100b1b9a247b9ae75d5</a> National Centre for Atmospheric Science et al. (2014)</p> <p>Penlee Point Atmospheric Observatory (PPAO) <a href="https://catalogue.ceda.ac.uk/uuid/8f1ff8ea77534e08b03983685990a9b0">https://catalogue.ceda.ac.uk/uuid/8f1ff8ea77534e08b03983685990a9b0</a> Plymouth Marine Laboratory and Yang (2024). Plymouth Marine Laboratory <a href="https://catalogue.ceda.ac.uk/uuid/e74491c96ef24df29a9342a3d57b5939">https://catalogue.ceda.ac.uk/uuid/e74491c96ef24df29a9342a3d57b5939</a> Smyth (2024)</p>	CVAO data require registration/login to CEDA. PPAO and PML data are open access.	2.2, 2.3
Nudged atmosphere model simulations with atmospheric composition	<p>Simulated atmospheric composition from 1981-2020 with atmospheric circulation nudged to ERA5 reanalysis <a href="https://data.ceda.ac.uk/badc/acsis/UKESM1-hindcasts">https://data.ceda.ac.uk/badc/acsis/UKESM1-hindcasts</a> Abraham (2024)</p>	Open access for selected atmospheric composition variables. Requires registration/login on JASMIN and Met Office MASS account for access to comprehensive dataset.	2.4
Ocean circulation and heat content	<p>Objectively interpolated (gridded) ocean temperature and salinity (0-2000m) <a href="https://doi.org/10.5285/fe8e524d-7f04-41f3-e053-6c86abc04d51">https://doi.org/10.5285/fe8e524d-7f04-41f3-e053-6c86abc04d51</a> King (2023)</p> <p>Upper Ocean (0-1000m) heat content time series</p>	Open access.	3.1,



	<p><a href="https://doi.org/10/g6wm">https://doi.org/10/g6wm</a> Moat et al. (2021a)  <a href="https://doi.org/10/g8g2">https://doi.org/10/g8g2</a> Moat et al. (2021b)</p>		
<p>Ocean-sea ice and standalone sea ice simulations</p>	<p>NEMO-CICE global ocean simulations with default sea ice physics 1°, 1/4° and 1/12° up to 2020</p> <p><a href="https://dx.doi.org/10.5285/119a5d4795c94d2e94f610647640edc0">https://dx.doi.org/10.5285/119a5d4795c94d2e94f610647640edc0</a> Megann et al. (2021b)  <a href="https://dx.doi.org/10.5285/a0708d25b4fc44c5ab1b06e12fef2f2e">https://dx.doi.org/10.5285/a0708d25b4fc44c5ab1b06e12fef2f2e</a>, Megann et al (2021c)  <a href="https://dx.doi.org/10.5285/4c545155dfd145a1b02a5d0e577ae37d">https://dx.doi.org/10.5285/4c545155dfd145a1b02a5d0e577ae37d</a>, Megann et al. (2021d)  <a href="https://dx.doi.org/10.5285/e02c8424657846468c1ff3a5acd0b1ab">https://dx.doi.org/10.5285/e02c8424657846468c1ff3a5acd0b1ab</a> Megann et al. (2022a)  <a href="https://dx.doi.org/10.5285/399b0f762a004657a411a9ea7203493a">https://dx.doi.org/10.5285/399b0f762a004657a411a9ea7203493a</a> (Megann et al. (2022b)</p> <p>NEMO-CICE global ocean simulations with improved sea ice physics 1/4° up to 2020 and standalone Arctic sea ice simulations:</p> <p><a href="http://catalogue.ceda.ac.uk/uuid/770a885a8bc34d51ad71e87ef346d6a8">http://catalogue.ceda.ac.uk/uuid/770a885a8bc34d51ad71e87ef346d6a8</a> Megann et al. (2021e)</p>	open access	3.2.2, 4.1

28 **2. Composition data sets**

29 The composition of the atmosphere is changing at an unprecedented pace. Changes in the levels of stratospheric ozone, surface  
 30 ozone and other secondary pollutants are driven by human activities (e.g., Griffiths et al., 2021; Keeble et al., 2020; Turnock  
 31 et al., 2020). The North Atlantic region has undergone significant growth and decline in air pollution over the last three decades  
 32 and modelling studies have all shown the significant human health benefits of these more recent reductions (Turnock et al.  
 33 2016; Archibald et al., 2017; Daskalakis et al., 2016). But whilst we have a broad understanding of the distribution of key air  
 34 pollutants and short lived climate forcers, our understanding of the variability of these species and their trends is hampered  
 35 across the North Atlantic owing to a paucity of observations. The North Atlantic is frequently impacted by the transport of



36 transboundary pollution from anthropogenic sources and fires (Boylan et al., 2015; Helmig et al., 2015; Kumar et al., 2013),  
37 as well as from local natural marine and shipping emissions (e.g., Yang et al., 2016a). High altitude research stations in the  
38 Eastern North Atlantic in the Azores (Mt. Pico) and Canary Islands (Izána), coastal observatories on the west coast of Ireland  
39 (Mace Head) and in the Cape Verde Islands have provided long term data sets with which to better understand the sources and  
40 processes controlling reactive trace gases and aerosols across the North Atlantic.

41

42 In ACSIS a series of work packages were conducted to a) further our understanding of the distribution and variability of key  
43 trace gases and aerosols using aircraft campaigns and long-term measurements, b) understand the processes controlling these  
44 and c) improve model simulations, which can be used to forecast the future evolution of these species. In the following sections  
45 we outline the data that were generated to support these objectives.

## 46 2.1 Aircraft campaigns in the North Atlantic

47 A series of (daytime) research flights were carried out across the North Atlantic Ocean from February 2017 – May 2022.  
48 Measurements were collected using the UK's Atmospheric Research Aircraft (ARA). The ARA is a BAe-146-301 which has  
49 been in service since 2004 and is managed by the Facility for Airborne Atmospheric Measurements (FAAM), an airborne  
50 laboratory funded by the UK government. The FAAM aircraft is capable of carrying a 4-tonne instrument load and can operate  
51 at altitudes between 50 and 30000 ft (15–9140 m), allowing the study of processes in the troposphere and boundary layer.  
52 ARA missions as part of ACSIS provide the longest record of composition change in the lower free troposphere over the North  
53 Atlantic (Sutton et al., 2018) and further complemented historic research flights conducted with the ARA in the region (e.g.,  
54 Parrington et al., 2012; Reeves et al., 2002) and more recent flights by other platforms (e.g., ATom (Wofsy et al., 2018),  
55 NAAMES (e.g., Behrenfeld et al., 2019; Sinclair et al., 2020) and ACE-ENA (Zawadowicz et al., 2021)). A wide range of  
56 instrumentation are fitted on the ARA, including measurements of key meteorological parameters such as temperature,  
57 humidity, wind speed and direction as well as a range of in situ trace gas measurements including carbon monoxide (CO),  
58 ozone (O<sub>3</sub>), oxides of nitrogen (NO<sub>x</sub>=NO+NO<sub>2</sub>), and the greenhouse gases carbon dioxide (CO<sub>2</sub>) and methane (CH<sub>4</sub>). Table 2  
59 below summarises the measurement techniques and uncertainties onboard the ARA that were used during ACSIS flights.

60

61 **Table 2.** A summary of atmospheric chemistry instrumentation used during the ACSIS flights onboard the FAAM BAe-146-  
62 301 Atmospheric Research Aircraft.

Measur ement	Instrumentation	Time resolution	Precision 3σ	Uncertainty	Timescale	Data available in merge file
O <sub>3</sub>	Thermo 49i ozone photometer	4 sec	6 ppb	3 ppb / 3%	2017-2021	X
O <sub>3</sub>	2BTechnologies Model 205 ozone photometer	2 sec	4 nmol mol <sup>-1</sup>	5 ppb / 3% for O <sub>3</sub> > 100 nmol mol <sup>-1</sup>	2022-present	X



CO	AeroLaser AL5002 (VUV RF)	1 sec	6 ppb	2 ppb	2005-2019	X
CO <sub>2</sub>	Los Gatos Research FGGA (OA-ICOS)	1 sec	1.5 ppm	0.5 ppm	2011-present	X
CH <sub>4</sub>	Los Gatos Research FGGA (OA-ICOS)	1 sec	6 ppb	3 ppb	2011-present	X
NO	Chemiluminescence Air Quality Design Inc	10 sec	10 ppt	24%	2009-2019	X
NO <sub>2</sub>	Chemiluminescence Air Quality Design Inc	10 sec	13 ppt	41%	2009-2019	X
NO	Chemiluminescence Air Quality Design Inc (upgraded)	0.1 sec	30 ppt	24%	2019-present	X
NO <sub>2</sub>	Chemiluminescence Air Quality Design Inc (upgraded)	0.1 sec	60 ppt	41%	2019-present	X
SO <sub>2</sub>	University of York laser-induced fluorescence sulfur dioxide detector (LIF-SO <sub>2</sub> )	1 sec	225 ppt	15 %	2022-present	X
Solar Actinic flux	Ocean Optics QE Pro, up and downward facing UV-vis (280-700 nm) spectrometers	1 sec	TBC	5 %	2019-present	X
HCHO	LIF pulsed 353.370 nm spectrometer, Thermo Scientific Model TFL 3000 Novawave	1 sec	n/a	n/a	2019-present	
VOCs	Whole Air Samples and offline analysis by GC-FID or GC-MS	n/a			2005-present	
Other gases	University of Manchester High Resolution-Time of Flight-Chemical Ionisation Mass Spectrometer (ToF-CIMS)	0.25 sec		10-20%	2019-present	
HONO	ToF-CIMS	0.25 sec	n/a	20%		
HCN	ToF-CIMS	0.25 sec		30%		X
BrO	ToF-CIMS	0.25 sec	n/a	40%		
BrCl	ToF-CIMS	0.25 sec	n/a	40%		
CINO <sub>2</sub>	ToF-CIMS	0.25 sec		30%		X
Cl <sub>2</sub>	ToF-CIMS	0.25 sec	n/a	20%		
ClO	ToF-CIMS	0.25 sec	n/a	40%		
HPMTF §	ToF-CIMS	0.25 sec	n/a	n/a		
Urea	ToF-CIMS	0.25 sec	30 ppt	25%		X





Aerosol	University of Manchester Aerosol Mass Spectrometer (AMS)				2019-present (excl. 2020)
Organic	AMS	8-15 sec	0.03 $\mu\text{g}/\text{m}^3$	38%	X
SO <sub>4</sub>	AMS	8-15 sec	0.03 $\mu\text{g}/\text{m}^3$	36%	X
NH <sub>4</sub>	AMS	8-15 sec	0.03 $\mu\text{g}/\text{m}^3$	34%	X
NO <sub>3</sub>	AMS	8-15 sec	0.03 $\mu\text{g}/\text{m}^3$	34%	X
nss-Cl	AMS	8-15 sec	0.03 $\mu\text{g}/\text{m}^3$	n/a	X

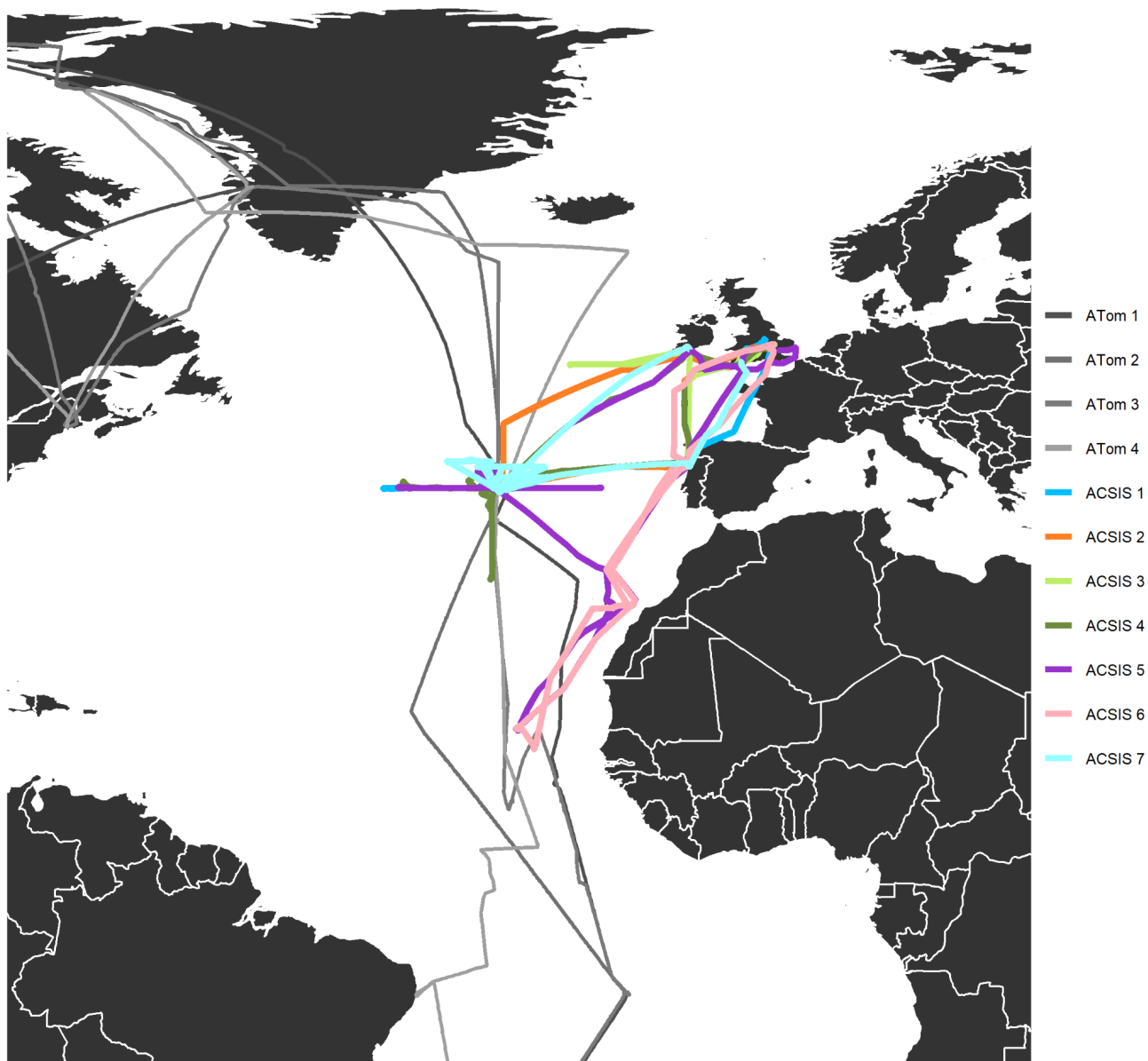
63 <sup>§</sup>Hydroperoxy methyl thioformate.

64

65 Figure 1 shows the location of the ACSIS flight tracks, coloured by campaign number. There were a total of 45 flights as part  
66 of the ACSIS campaign, comprising close to 200 hours of measurement data. Measurements were made from approximately  
67 50 m over the sea surface to 7600 m. ACSIS 1, 2, 4, 5 and 7 were predominantly based out of the Azores, whilst flights for  
68 ACSIS 3 were based out of Cork, Ireland and ACSIS 6 flights based out of Cape Verde.



69



70

71

72 **Figure 1.** A map of flight tracks for the seven ACSIS ARA campaigns. Part of the NASA ATom flight campaign flight tracks  
73 are shown in grey for comparison.

74



75 Also shown in Fig. 1 are part of the flight tracks for the NASA Atmospheric Tomography Mission (ATom) mission. The  
76 ATom campaigns aimed to improve the representation of reactive gases and short-lived climate forcers in global atmospheric  
77 chemistry and climate models by measuring atmospheric composition along a global circuit flight track (Prather et al., 2017).  
78 Four ATom campaigns occurred between August 2016 and May 2018. The ATom data set is complementary to that collected  
79 during the ACSIS flight campaigns; ATom flights provided a broad overview on a global scale, whereas ACSIS flights  
80 intensively measured the North Atlantic region. ACSIS-1 overlapped with ATom2 and ACSIS-2 overlapped with ATom3.

81

### 82 **2.1.1 Bulk Analysis of Data**

83 Data collected during flights from all 7 ACSIS campaigns have been analysed together to give insights into the spatial and  
84 vertical characteristics of atmospheric composition over the North Atlantic Ocean. Table 3 summarises the flights and times  
85 that were used in this bulk analysis.

86

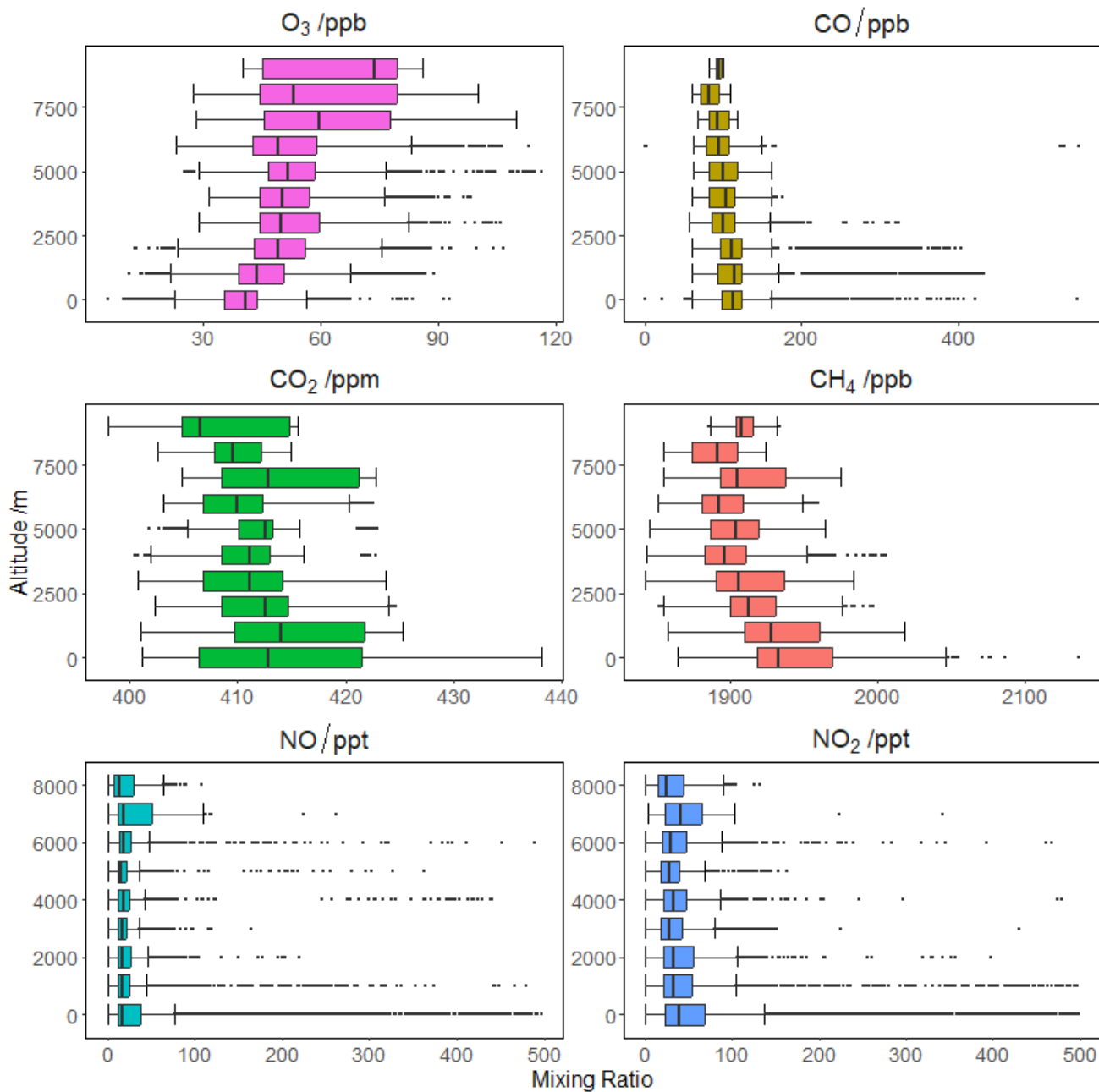
87 **Table 3.** Summary of flights used in bulk analysis of atmospheric composition data.

Campaign	Flight Numbers	Date Range	Comments
AC SIS 1	B996, B997, B998, B999, C001, C002	13/02/2017 – 16/02/2017	
AC SIS 2	C066, C067, C068, C070, C071	19/10/2017 – 23/10/2017	
AC SIS 3	C103, C105, C106	14/05/2018 – 17/05/2018	No greenhouse gas data available due to the FGGA fault.
AC SIS 4	C139, C140, C141, C142, C143, C144, C145	19/02/2019 – 22/02/2019	No VOC data on CEDA
AC SIS 5	C199, C200, C201, C202, C203, C204, C205, C210, C211, C212	13/08/2019 – 22/08/2019	
AC SIS 6	C215, C216, C217, C226, C227, C228, C229	04/02/2020 – 14/02/2020	
AC SIS 7	C288, C289, C290, C291, C292, C293, C294	03/05/2022 – 09/05/2022	

88

### 89 **2.1.3 Vertical Distribution of Pollutants**

90 Data from all seven campaigns have been combined and grouped into 1000 m altitude bins. Figure 2 shows the vertical  
91 distribution of O<sub>3</sub>, CO, CO<sub>2</sub>, CH<sub>4</sub>, NO and NO<sub>2</sub>.



92  
93  
94  
95  
96

**Figure 2.** Box plots showing the vertical distribution of O<sub>3</sub>, CO, CO<sub>2</sub>, CH<sub>4</sub>, NO and NO<sub>2</sub> for all seven ACSIS campaigns. Note that due to sporadic high mixing ratios of CO, NO and NO<sub>2</sub> at low altitudes these data have been filtered to only show data below 600 ppbv for CO and 500 pptv for NO and NO<sub>2</sub>.



### 97 **2.1.2 Data archive**

98 To accompany this paper a 10 second averaged merge file has been created for each flight listed in Table 3  
99 (<https://dx.doi.org/10.5285/6285564c34a246fc9ba5ce053d85e5e7>, Facility for Airborne Atmospheric Measurements et al.,  
2024). The merge files are open access and designed to be a tool for an initial exploration of the data and to highlight the  
101 breadth of the atmospheric composition data collected during the ACSIS programme. However, for further analysis the original  
102 frequency data should be used and details of where these files can be found is included in the header information of the merge  
103 files The merged files are in ascii format and consist of a short explanatory paragraph followed by a list of variables and finally  
104 the data arranged as columns, with one variable per column with rows corresponding to the values at each 10s time interval. .

### 105 **2.2 Cape Verde Atmospheric Observatory (CVAO)**

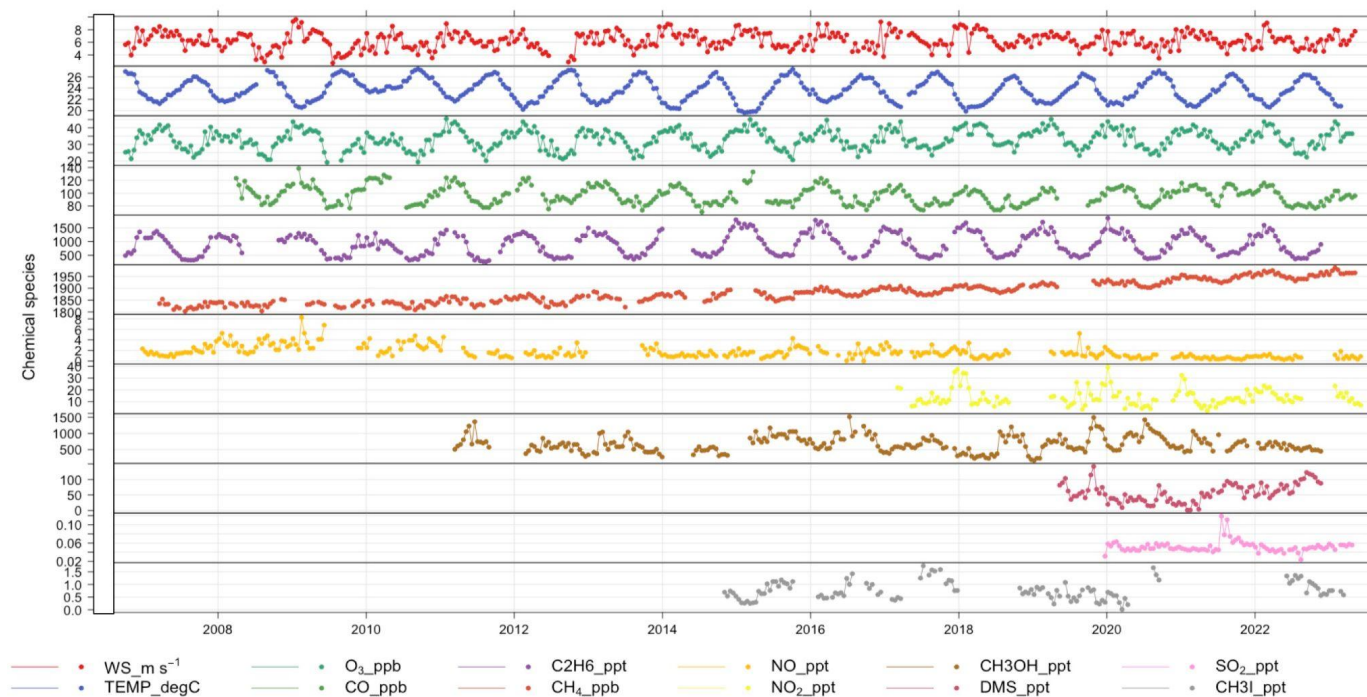
106 The Global GAW Cape Verde Atmospheric Observatory is situated in Calhau on the island of Sao Vicente in the Republic of  
107 Cabo Verde (16.848°N, 24.871°W, 10m asl, <https://amof.ac.uk/observatory/cape-verde-atmospheric-observatory-cvao/>).  
108 Measurements were started in October 2006 to further our understanding of atmospheric chemistry within the tropical marine  
109 boundary layer and North Atlantic region. The site receives air from a wide variety of sources with 10-day back trajectories  
110 reaching to North America, Europe and sub-Saharan Africa (see Carpenter et al. (2010) for details). Long term high frequency  
111 measurements allow investigation into the trends of climate gases such as CO<sub>2</sub> and CH<sub>4</sub> whilst measurements of pollutants  
112 from the continents such as hydrocarbons and nitrogen oxides provide better constraints of global emission changes and their  
113 effect on the long-term background of the North Atlantic (e.g., Helmig et al., 2016). The Observatory regularly hosts field  
114 campaigns which focus on process studies such as sea-surface interactions and the role of aerosols in atmospheric chemistry  
115 (Read et al., 2008, McFiggans et al., 2009, Lawler et al., 2011, Van Pinxteren et al., 2020). Recent work has provided evidence  
116 for the rapid photolysis of nitrate aerosol as an important source of HONO and NO<sub>2</sub> to the marine troposphere (Andersen et  
117 al., 2021). Andersen et al. (2023) confirmed the ubiquity of this so-called “renoxification” source of HONO and NO<sub>x</sub> in the  
118 remote Atlantic troposphere using HONO observations at the CVAO and from aircraft in the surrounding remote Atlantic  
119 troposphere and showed evidence for renoxification occurring on marine and mixed marine/dust and biomass burning aerosols  
120 with an efficiency that increased with relative humidity and decreased with the concentration of nitrate. Table 4 provides a  
121 summary of the chemical species recorded at the CVAO.

122  
123 **Table 4.** Summary of atmospheric data recorded at CVAO.

Measurement	Instrumentation	Time resolution	Precision (1hr)	Timescale
O <sub>3</sub>	Thermo 49i ozone monitor	10 sec	0.5 ppb	2006-present
CO	Aerolaser AL5001/ Picarro G4201	4 sec	1 ppb	2008-present



NO	Chemiluminescence instrument	Air	5 min	1.4 ppt	2006-present
	Quality Design Inc. (AQD), USA				
NO <sub>2</sub>	Chemiluminescence instrument	Air	5 min	4.4 ppt	2017-present
	Quality Design Inc. (AQD), USA				
VOCs	GC-FID		1 hour		2006-present
OVOCs	GC-FID		1 hour		2014-present
Short-lived halocarbons	GC-MS-TOF		1 hour		2014-present
CFCs/HCFCs	GC-MS-TOF		1 hour		2022-present
DMS	GC-FID		1 hour		2012-present
Photolysis rates	Spectral radiometer		1 min		2016-present
CO <sub>2</sub>	Picarro G4201		4 sec	10 ppb	2012-present
CH <sub>4</sub>	Picarro G4201		4 sec	0.3 ppb	2012-present
SO <sub>2</sub>	Thermo 43i HL		5 sec		2019-present
Total Gaseous Mercury	Tekran		1 min		2014-2019





25

26 **Figure 3.** Time series of Cape Verde data showing a range of the species and meteorological parameters measured..

27

### 28 **2.2.1 Ozone**

29 Ozone concentrations at the CVAO show seasonal variability with highest concentrations in spring and lowest in summer,  
30 consistent with its role as a secondary pollutant. During the period 2007-2022, ozone steadily increased at a rate of 0.16 +/-  
31 0.08 ppbV/year. In summer, the site occasionally receives air from the southern hemisphere during the early stages of the  
32 Atlantic cyclonic activity, which leads to very low concentrations of ozone (<10 ppb) observed along with episodes of intense  
33 precipitation. Ozone data from the CVAO contributed to the Tropospheric Ozone Assessment Report (TOAR) (Schultz et al.,  
34 2017).

35

### 36 **2.2.2 Carbon monoxide**

37 Carbon monoxide is a primary pollutant emitted from anthropogenic sources and from biomass burning. Between 2008-2016  
38 levels were decreasing at a rate of 0.6 +/- 0.8 ppbV/ year. Since 2016 CO has been decreasing at a slower rate of 0.14 +/- 0.9  
39 ppbV/year.

40

### 41 **2.2.3 Methane**

42 Global methane concentrations have increased substantially over the last 10 years and this has been attributed to a combination  
43 of increased primary emissions of hydrocarbons and increased emissions from wetlands due to increasing temperatures  
44 (Jackson et al, 2020, Thompson et al., 2018). At the CVAO methane has been increasing steadily (8 +/- 0.4 ppbV/year) however  
45 in the last couple of years (2020-2023) the rate has increased by almost 60% to 14 +/- 1.8 ppbV/year. Observations of ethane  
46 and other hydrocarbons can give an indication as to whether changes in methane are due to changes in emissions or in oxidant  
47 levels and whether increased emissions are natural or anthropogenic (Helmig et al, 2016). Ethane shows an increasing trend  
48 of 17.5 +/- 5 pptV until 2020 and then strongly decreases after that 27.1 +/- 17 pptV.

49

### 50 **2.2.4 NO<sub>x</sub>**

51 NO<sub>x</sub> mixing ratios at the CVAO peak around solar noon at 20–30 pptv, in contrast to model simulations that predict a midday  
52 minimum due to conversion of NO<sub>2</sub> to HNO<sub>3</sub> through reaction of OH (Reed et al. 2017). Inclusion of the rapid photolysis of  
53 nitrate aerosol to produce HONO and NO<sub>2</sub> is required to successfully simulate the observed diurnal cycles of these gases at  
54 the CVAO (Reed et al. 2017; Andersen et al. 2023). In extremely clean air containing low levels of CO and VOCs, Andersen  
55 et al. (ACP, 2022) showed good agreement between NO<sub>2</sub> levels observed at the CVAO and those derived from the  
56 photostationary state (PSS), utilising measured NO, O<sub>3</sub>, and jNO<sub>2</sub> and photo-chemical box model predictions of peroxy  
57 radicals. However, in clean air containing small amounts of aged pollution, as typically encountered in winter, higher levels



:58 of NO<sub>2</sub> were observed than inferred from the PSS, implying underestimation of peroxy radicals or unattributed NO<sub>2</sub>  
:59 measurement artefacts.

:60

### :61 **2.2.5 Data archive**

:62 Cape Verde data collected under the auspices of ACSIS is available from CEDA:  
:63 <http://catalogue.ceda.ac.uk/uuid/81693aad69409100b1b9a247b9ae75d5> (National Centre for Atmospheric Science et al.  
:64 (2014)). Note that there are a number of subdirectories, some of which are not relevant to the data described in this paper. The  
:65 relevant subdirectories are labelled with the variable or variable group and the time period (e.g. Cape Verde Atmospheric  
:66 Observatory: Ozone measurements (2006 onwards)). The data format is ASCII, consisting of a header explaining the variables  
:67 listed followed by the data in columnar format (one column per variable), with the data values in rows appearing in  
:68 chronological order. We note that specific Cape Verde data is also archived at the World Data Centre for Greenhouse Gases,  
:69 <https://gaw.kishou.go.jp> (CO<sub>2</sub>, CH<sub>4</sub> and CO) and at EBAS, <https://ebas.nilu.no> (VOCs, NO<sub>x</sub>, SO<sub>2</sub> and halocarbons).

### :70 **2.3 Penlee Point Atmospheric Observatory**

:71 Penlee Point Atmospheric Observatory (PPAO; 50° 19.08' N, 4° 11.35' W;  
:72 <https://www.westernchannelobservatory.org.uk/penlee/>) was established by the Plymouth Marine Laboratory (PML) in 2014  
:73 on the southwest coast of the United Kingdom. At the western mouth of the Plymouth Sound and near the tip of the Rame  
:74 Peninsula, PPAO is a few tens of metres away from the water edge and about 11 m above mean sea level. The site is exposed  
:75 to marine air over a very wide sector. Typical south-westerly winds tend to bring relatively clean background air coming off  
:76 the North Atlantic. Winds from the southeast are often contaminated by exhaust plumes from passing ships, while winds from  
:77 the north are influenced by terrestrial emissions.

:78 In close proximity to the Western Channel Observatory marine sampling stations, high frequency observations at PPAO enable  
:79 both long-term and process-based studies of atmosphere-ocean interactions. Current/recent work has assessed trace gas  
:80 burdens and air-sea fluxes including greenhouse gases (Yang et al. 2016b, 2016c, 2019a), volatile organic carbon (Phillips et  
:81 al., 2021), sulfur- (Yang et al., 2016c), halogen- (Sommariva et al., 2018), and nitrogen-containing gases (ongoing). Further  
:82 works include aerosol composition and fluxes, with particular foci on ship emissions (ongoing as a part of the ACRUISE  
:83 project), sea spray production (Yang et al., 2019b), macro/micro nutrient deposition (White et al., 2021), and reaction between  
:84 atmospheric ozone and the sea surface microlayer (Loades et al., 2020)

:85 Continuous observations most relevant to ACSIS include ground-based ozone and methane from PPAO as well as column  
:86 aerosols from the rooftop of PML (10 km north/northeast of PPAO). These measurements are detailed in Table 5.

:87 **Table 5.** Overview of the measurements made at PPAO.





Measurement	Instrumentation	Time resolution	Accuracy	Timescale
O <sub>3</sub>	(a) 2B 205 ozone monitor; (b) Thermo 49i ozone monitor	10 sec	≤1 ppb	(a) May 2014 – Sept 2018 (b) Sept 2018 – present
CH <sub>4</sub>	(a) Picarro G2311-f; (b) Los Gatos Research Fast Greenhouse Gas Analyzer	0.1 sec until Aug 2016; 1 sec since Aug 2016	≤ 3 ppb	(a) May 2014 – Sept 2015 (b) Sept 2015 – present
Aerosols	POM sunphotometer	10 min (when clear sky and during the day)	≤0.01 at 550 nm	2001 – present

.88

.89

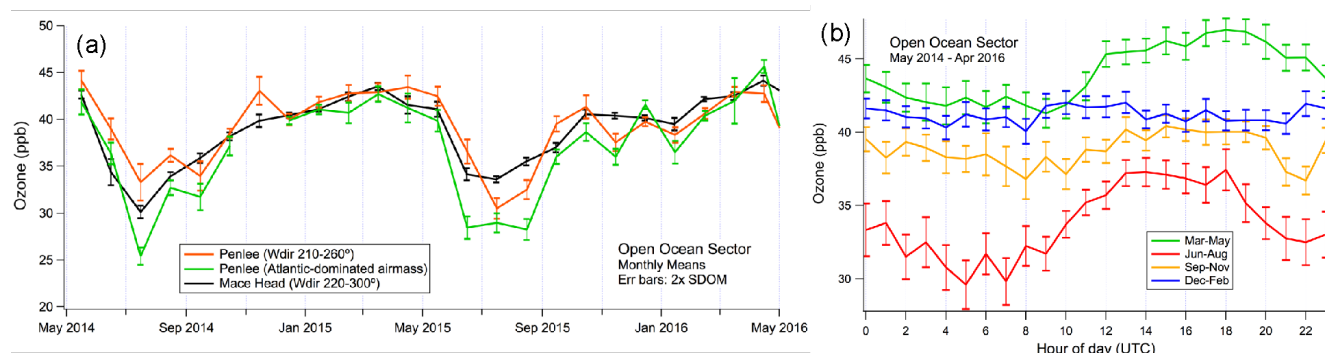
### .90 **2.3.1 Ozone**

.91 We first examine the ground-based O<sub>3</sub> observation, focusing especially on variability within the open ocean (e.g. Atlantic)  
 .92 wind sector. Here we limit our analysis to the first two years of observations (May 2014 to Apr 2016), when air mass dispersion  
 .93 modelling (NAME) was available to assess the air mass history (see Yang and Fleming, 2019). Due to its short lifetime, we  
 .94 expect O<sub>3</sub> to be more sensitive than CH<sub>4</sub> to local sources/sinks and heterogeneities associated with a coastal environment. This  
 .95 presents a good opportunity to compare two different methods of identifying the open ocean wind sector: 1) by air mass history,  
 .96 and 2) by local wind direction.

.97 Monthly mean O<sub>3</sub> observations from the North Atlantic were similar between Penlee Point and Mace Head, both showing  
 .98 spring maxima and summer minima (Figure 4). Defining the PPAO open ocean sector either by local wind direction (210 to  
 .99 260°) or by air mass history (>80% in the Atlantic Ocean region over the last 5 days) results in fairly consistent monthly mean  
 .00 O<sub>3</sub> over most months. The difference between the two methods appears to be slightly larger in summer; possibly due to the  
 .01 diurnal sea breeze effect. In subsequent analyses, we define the open ocean (Atlantic) wind sector by local wind direction only  
 .02 as the NAME modelling for PPAO is unavailable after Mar 2017.

.03

.04

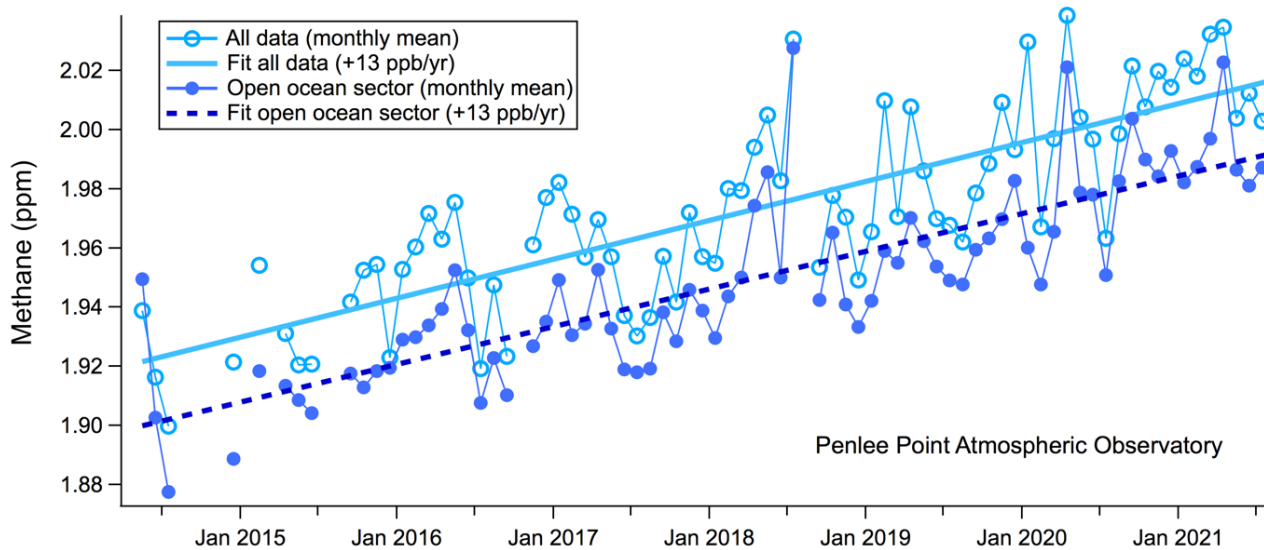


05  
06 **Figure 4.** (a) Monthly mean ozone mixing ratio from Mace Head and from PPAO (two different definitions of open ocean  
07 sector are shown). (b) Diurnal variability in ozone mixing ratio for different seasons. Error bars indicate standard error.  
08

09 Ozone from the open ocean wind sector shows quite a strong seasonal variability. This is likely due to a combination of  
10 variability in sources, sinks, and atmospheric transport (see e.g., Monks et al. (2014) for a discussion on these processes).  
11 The diurnal profiles of  $O_3$  are very different in different seasons (**Fig. 4 (b)**), with the largest day-night difference in summer  
12 and almost no difference in winter, owing to the increasing strength of photochemical production and the longer lifetime of  
13  $O_3$  respectively. The nighttime decrease in  $O_3$  is greatest in summer and smaller during the other seasons, probably in large  
14 part due to deposition to the ocean surface.

### 16 2.3.2 Methane

17  
18 The long-term increase in the dry-air mixing ratio of  $CH_4$  (Figure 5) is significant, 13 ppb/yr, and in line with observations  
19 made globally (e.g., Nisbet et al. 2019). The mean mixing ratio from the Atlantic wind sector (here roughly defined as wind  
20 direction between 210 and 260 degrees) is lower than the mean of all data, but shows the same trend. The overall mean  $CH_4$   
21 is about 0.02-0.03 ppm higher than the open-ocean mean.  
22  
23



24

25 **Figure 5:** Long-term measurements of methane made at PPAO highlighting the strong increase in methane.

26

27 Methane shows a mean seasonal amplitude of 0.03 ppm (relative difference of 1.5%). The summer minimum is most likely  
28 due to increased sink of methane by the OH radical. These data suggest no significant deviation from the long-term trend over  
29 the last few years (2019-2022), when it has been postulated that the COVID lockdowns changed the atmospheric oxidising  
30 capacity and so the OH sink (e.g., Stevenson et al., 2022).

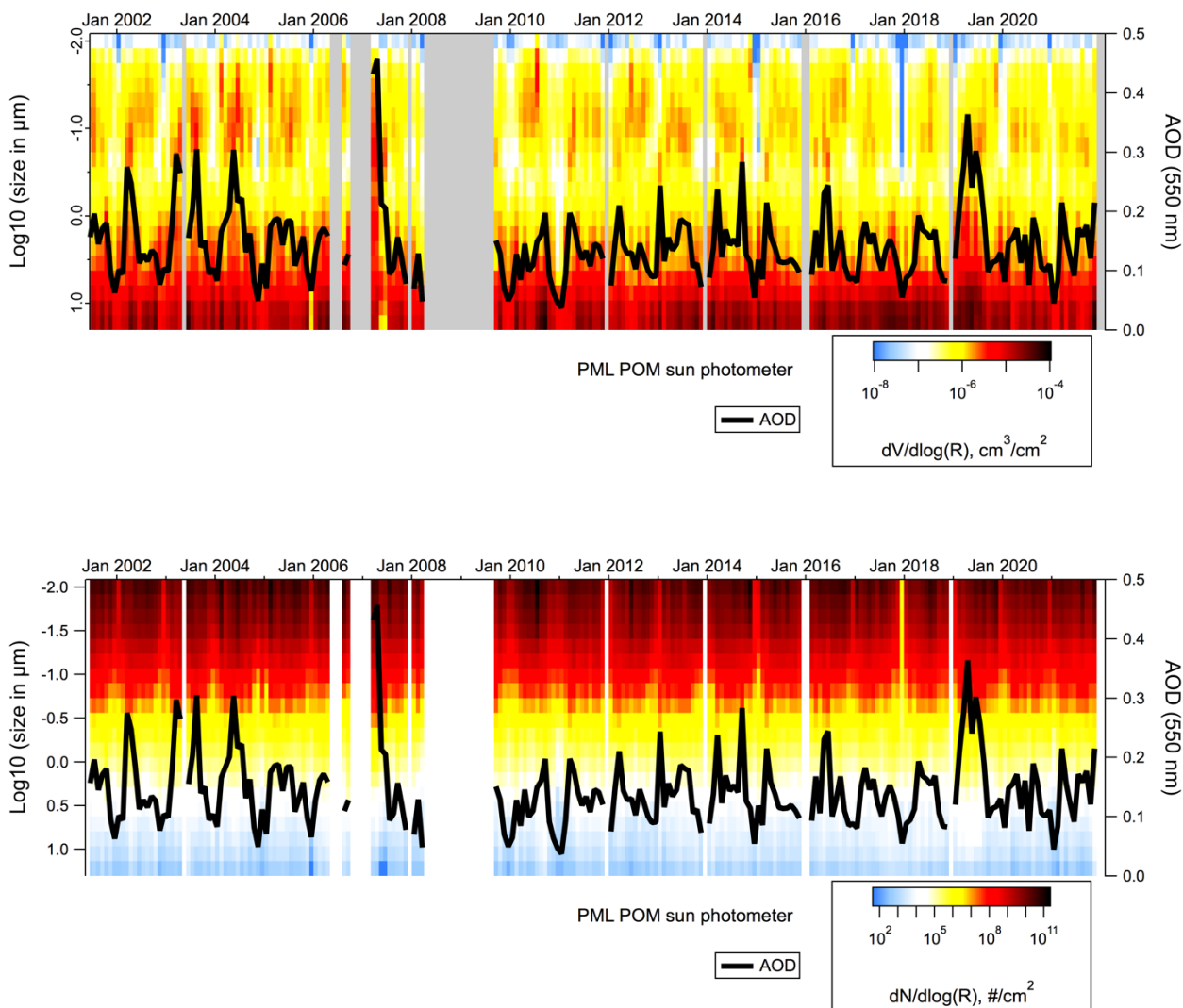
31

### 32 **2.3.3 Aerosols from sunphotometers**

33 Long-term aerosol measurements (starting from 2001) have been made from the rooftop of PML (50.3661° N, 4.1482° W,  
34 about 10 km NNE of Penlee Point). The retrieved, cloud-filtered data are averaged to monthly intervals as shown in Figure 6.  
35 Overall there is no obvious long term trend in Aerosol Optical Depth (AOD) at this site, in contrast to many other locations in  
36 Western Europe that tend to show a gradual reduction. This may be because of the predominance of sea spray aerosols at this  
37 location (Yang et al. 2020).

38

39 The inferred size distributions are also shown (Fig. 6b). The volume distribution ( $dV/d\log(R)$ ) is dominated by super-micron  
40 aerosols, while the number distribution ( $dN/d\log(R)$ ) is dominated by sub-micron aerosols. There appears to be a gradual  
41 reduction in springtime aerosol maximum at around 100 nm radius from 2010 to 2021, which could be related to reduced  
42 terrestrial or ship anthropogenic emissions (e.g. due to air quality related regulations).



43  
44

45

46 **Figure 6.** Long-term aerosol observations from the PML rooftop (monthly mean).

47

### 48 2.3.4 Data archive

49 Penlee Point Atmospheric Observatory data is archived at the CEDA:  
50 <https://catalogue.ceda.ac.uk/uuid/8f1ff8ea77534e08b03983685990a9b0> (Plymouth Marine Laboratory and Yang (2024)).  
51 Data from the PML sun photometer can be found at <https://dx.doi.org/10.5285/e74491e96ef24df29a9342a3d57b5939> (Smyth  
52 (2024)) The data format is ASCII, consisting of a header explaining the variables listed followed by the data in columnar  
53 format (one column per variable), with the data values in rows appearing in chronological order.



## 54 2.4 Atmospheric composition modelling with UKESM1

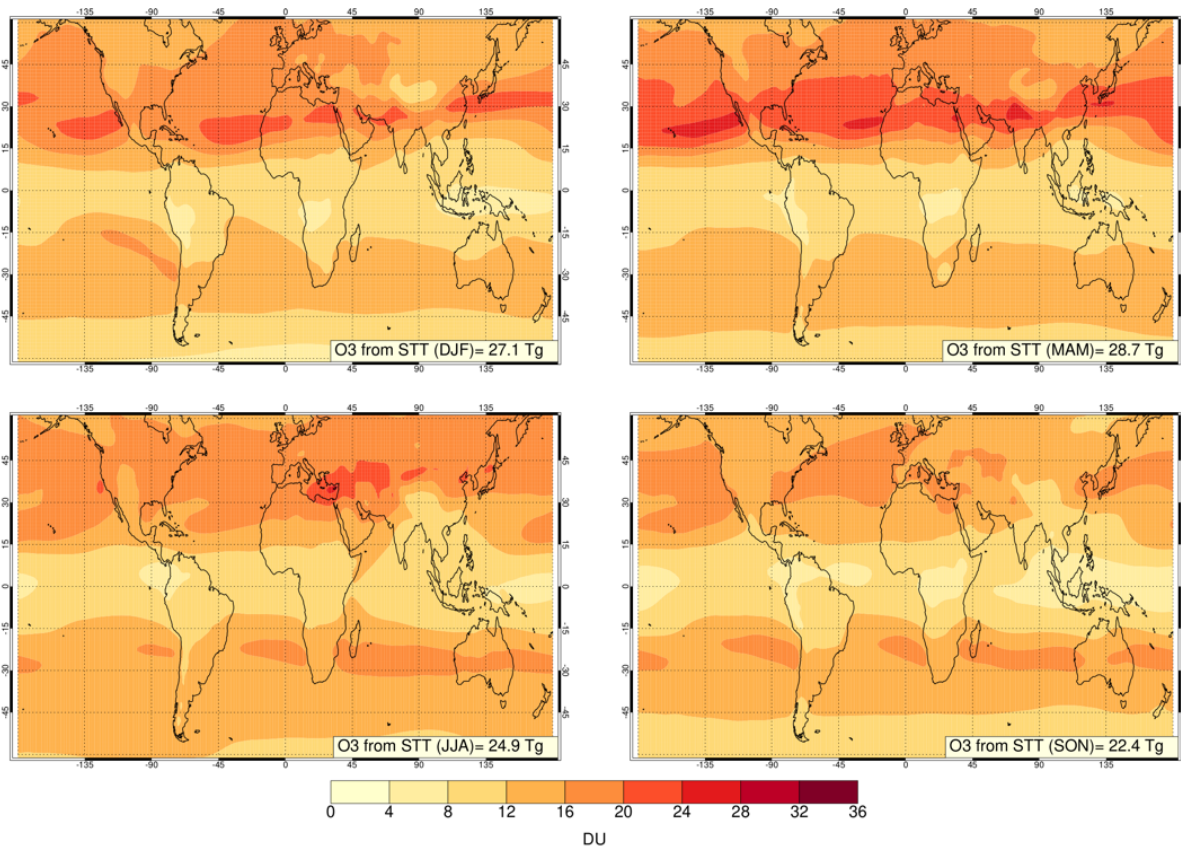
55 Model integrations were performed using a nudged (Telford et al., 2008) configuration of the UKESM1 Earth system model  
56 (Sellar et al., 2019) at Unified Model version 11.5. For nudged model integrations, the horizontal wind fields and potential  
57 temperature are relaxed to either the ERA-Interim (Dee et al., 2011) or ERA-5 (Hersbach et al., 2020) datasets using an e-  
58 folding relaxation timescale of 6 h. Sea-surface temperatures and sea-ice fields were prescribed from the Reynolds dataset  
59 (Reynolds et al., 2002). Atmospheric composition was simulated using the UKCA chemistry module, applying the  
60 stratosphere-troposphere chemical mechanism of Archibald et al. (2020) with the 2-moment prognostic aerosol scheme as  
61 described in Mulcahy et al. (2020). Simulations were performed from 1981 to 2014 using CMIP historical forcings (labelled  
62 as HIST) and continued until 2019 (ERA-Interim) or 2020 (ERA-5) using SSP3-7.0 forcings (labelled as SCEN) as per the  
63 AerChemMIP experiment definition (Collins et al., 2017) (see Table 6) for details.

64  
65 In order to identify the impact of transport on modelled tropospheric ozone in the North Atlantic, the following diagnostic  
66 tracers were also defined:

- 67 • 4 different stratospheric ozone tracers ( $O_3s$ ) were added. These are constrained in the stratosphere and evolve freely  
68 in the troposphere where they follow equivalent loss processes to the prognostic ozone field simulated by the model  
69 . The 4  $O_3s$  tracers are described below:
  - 70 1. Stratospheric concentrations are set to the prognostic ozone field above a model diagnosed tropopause  
71 defined by the 2PV+380K surface.
  - 72 2. Stratospheric concentrations are fixed at 1 ppmv above a model diagnosed tropopause defined by the  
73 2PV+380K surface.
  - 74 3. Stratospheric concentrations are set to the prognostic ozone field above a model diagnosed tropopause  
75 defined by the WMO tropopause definition.
  - 76 4. Stratospheric concentrations are fixed at 1 ppmv above a model diagnosed tropopause defined by the WMO  
77 tropopause definition.

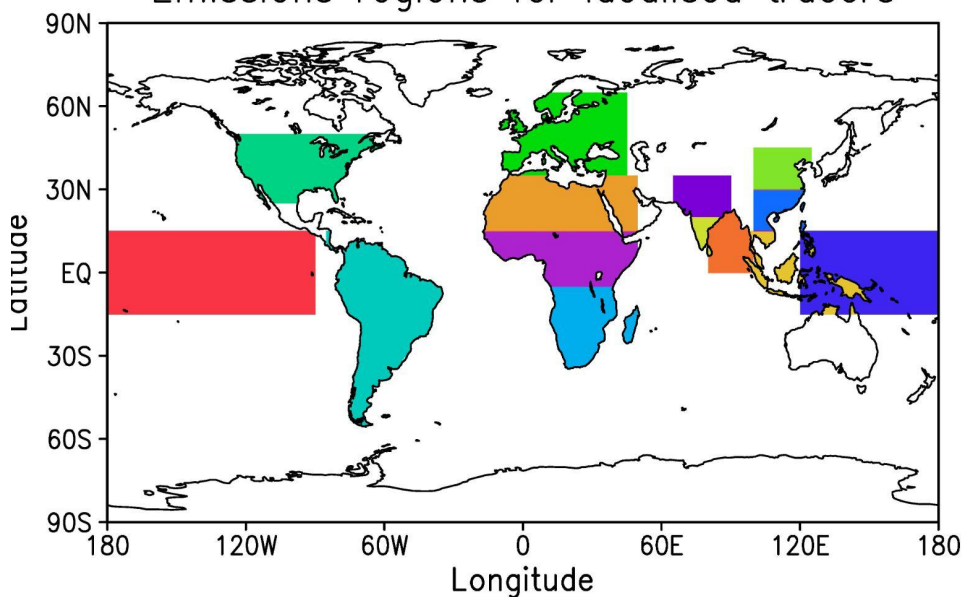
78 Tracer 1 and 3 are similar to the  $O_3s$  tracers used in the CCMI experiments (Abalos et al., 2020) and represent tropospheric  
79 ozone originating from the stratosphere, while tracer 2 and 4 (also referred to as constant  $O_3s$  tracers or  $O_3s-c$ ) give a  
80 complementary measure of downward transport from the stratosphere that is not affected by stratospheric ozone geographical  
81 distribution or trends (Russo et al., 2023). An example of tracer 1 tropospheric column and its seasonal variation is given in  
82 Figure 7a.

- 83 • 30 regionally emitted tracers were included to diagnose long range transport into the North Atlantic region. These  
84 have either a lifetime of 5 or 30 days and emission regions are sketched in Figure 7b.



.85

### Emissions regions for idealised tracers



.86





87 **Figure 7.** a) Integrated tropospheric column for the O<sub>3</sub>s tracer defined using prognostic ozone and the 2PV+380K tropopause,  
88 averaged over 2005-2017 using HIST1 and SCEN1 simulations (see Table 6 for details). b) Emission regions for the 5 day and  
89 30 day regional tracers.

90  
91 The simulations performed are listed in Table 6. The experimental design was focussed around providing simulations and  
92 output that could support observational campaigns and allowed for a detailed analysis of model transport and composition  
93 processes. As well as all the chemical and aerosol fields, fluxes through all chemical reactions and deposition processes were  
94 output as monthly means. Model restart files were also saved to allow for re-running short sections with an increased (and  
95 higher frequency) output request to compare against flight campaigns. Updates to the experiments were made throughout the  
96 project, incorporating bugfixes and model improvements.

97  
98 **Table 6.** Description of the UKESM1 model simulations.

Simulation	Nudging Dataset	Time Period	Notes	Rose suite ID
HIST1	ERA-Interim	1981-2014	Settings as per UKESM1.	u-bv711 (01/1981-11/1991) and u-bw316 (12/1991-12/2014)
HIST2	ERA-5	1982-2014	Includes code-changes described in Ranjithkumar et al. (2021)	u-bw784 (01/1982-12-2014)
HIST3	ERA-5	1982-2014	Includes code-changes described in Ranjithkumar et al. (2021), technical improvements to the top-boundary condition of the tracers, updated photolysis rates, and the improved heterogeneous chemistry of Dennison et al. (2019)	u-bv828 (01/1982-05/2008) and u-bx320 (06/2008-12/2014)
SCEN1	ERA-Interim	2015-2019	Continuation of HIST1	u-by117 (SSP3-7.0)
SCEN2	ERA-5	2015-2020	Continuation of HIST2	u-by803 (SSP3-7.0)
SCEN3	ERA-5	2015-2020	Continuation of HIST3	u-by808 (SSP3-7.0)

99  
00 **2.4.1 Data archive**



.01 892 Tb of UKESM1 model data were generated through the ACSIS project. A huge number of model diagnostics were output,  
.02 including high time frequency fields (hourly) across the North Atlantic basin. These are listed here:  
.03 <https://www.ukca.ac.uk/wiki/index.php/AC SIS/u-bv711/STASH>. Owing to the large nature of the model data set, selected  
.04 core chemical species and tracers are available to download as monthly mean files from the CEDA dataset  
.05 <https://data.ceda.ac.uk/badc/acsis/UKESM1-hindcasts>, Abraham (2024), these include ozone and ozone precursors (O<sub>3</sub>, NO,  
.06 NO<sub>2</sub>, CO and methane) and the idealised tracers used to diagnose transport in the North Atlantic (four stratospheric tracers and  
.07 thirty regionally emitted tracers). This data is available for all the model runs described in Table 6. The data is in Met Office  
.08 PP format, which can be read using open access Python libraries held at <https://ncas-cms.github.io/cf-python>. If desired, users  
.09 may also apply for a Met Office MASS (offline tape archive) account on the UK JASMIN data facility (<https://jasmin.ac.uk>)  
.10 and search the Rose Suite IDs given in Table 6 for access to data from the specific experiments performed.

### .11 **3 Ocean data sets**

.12 The North Atlantic Ocean is a major component of the overall North Atlantic Climate system and one of the key objectives of  
.13 the ACSIS programme was to document the significant changes in ocean circulation and heat content which have taken place  
.14 since the mid 20<sup>th</sup> century, to investigate the physical processes responsible and to identify their external drivers. Another  
.15 objective was to understand how the ocean might change in the next several decades and to evaluate the potential impacts of  
.16 these changes on human society and activities. In order to fulfil these objectives we compiled a substantial number of new data  
.17 products and new model simulations.

.18  
.19 The data products were compiled on the underlying principle of estimating components of the North Atlantic heat budget plus  
.20 the sea surface temperature and sea surface height (dynamic and thermosteric) as these latter two are key to the wider impacts  
.21 of the ocean on the atmosphere and on coastal sea level. Thus we brought together two basin scale observational estimates of  
.22 the horizontal ocean volume and heat transports at 26°N described in previous publications (RAPID -  
.23 <https://rapid.ac.uk/rapidmoc/>, McCarthy et al 2015; Moat et al., 2020) and at ~55°N (OSNAP - <https://www.ukosnap.org/>,  
.24 Lozier et al., 2019), a new high spatial and temporal resolution Atlantic sea surface temperature dataset previously described  
.25 by Williams and Berry (2020) and a new water mass preserving objectively interpolated ocean temperature and salinity dataset  
.26 based on the international Argo float array described in Section 3.1 below (King, 2023). On the modelling side, we undertook  
.27 new cutting edge NEMO forced ocean model simulations with a variety of surface forcing datasets at resolutions of ¼° and  
.28 1/12°, described in Section 3.2.

.29  
.30 Taken together, this new collection of model and observation based data has allowed us make significant advances in our  
.31 understanding of North Atlantic variability including phenomena such as the impact of subpolar heat loss on the Atlantic  
.32 Meridional Overturning Circulation (Megann et al., 2021a), the subpolar fingerprints of changes in the AMOC (Smeed et al.,





.33 2018), , the origin of interannual changes in subpolar SST (Josey and Sinha 2022), the link between subpolar SST and European  
.34 winter weather (Grist et al., 2019) and summer heat waves (Mecking et al., 2019), the relationship between decadal variability  
.35 in surface and subsurface temperature (Moat et al., 2019) and the impact of subpolar freshwater input on the North Atlantic  
.36 atmosphere (Oltmans et al., 2020) to name just a few of the studies enacted under ACSIS.

.37

### .38 **3.1 Ocean temperature and salinity, and upper ocean heat content**

.39 As part of ACSIS the NOC has produced new ocean temperature and salinity datasets based on the Argo float array using  
.40 sophisticated optimal interpolation techniques which preserve ocean water masses. The dataset covers the period 2004-present  
.41 and extends to depths of up to 2000m. Two versions are available with spatial resolutions of 2 degrees and 1 degree  
.42 respectively. During ACSIS the main use of this dataset has been to calculate subtropical and subpolar heat content alongside  
.43 other available estimates in order to understand the interannual to decadal variability of the North Atlantic heat budget.

.44

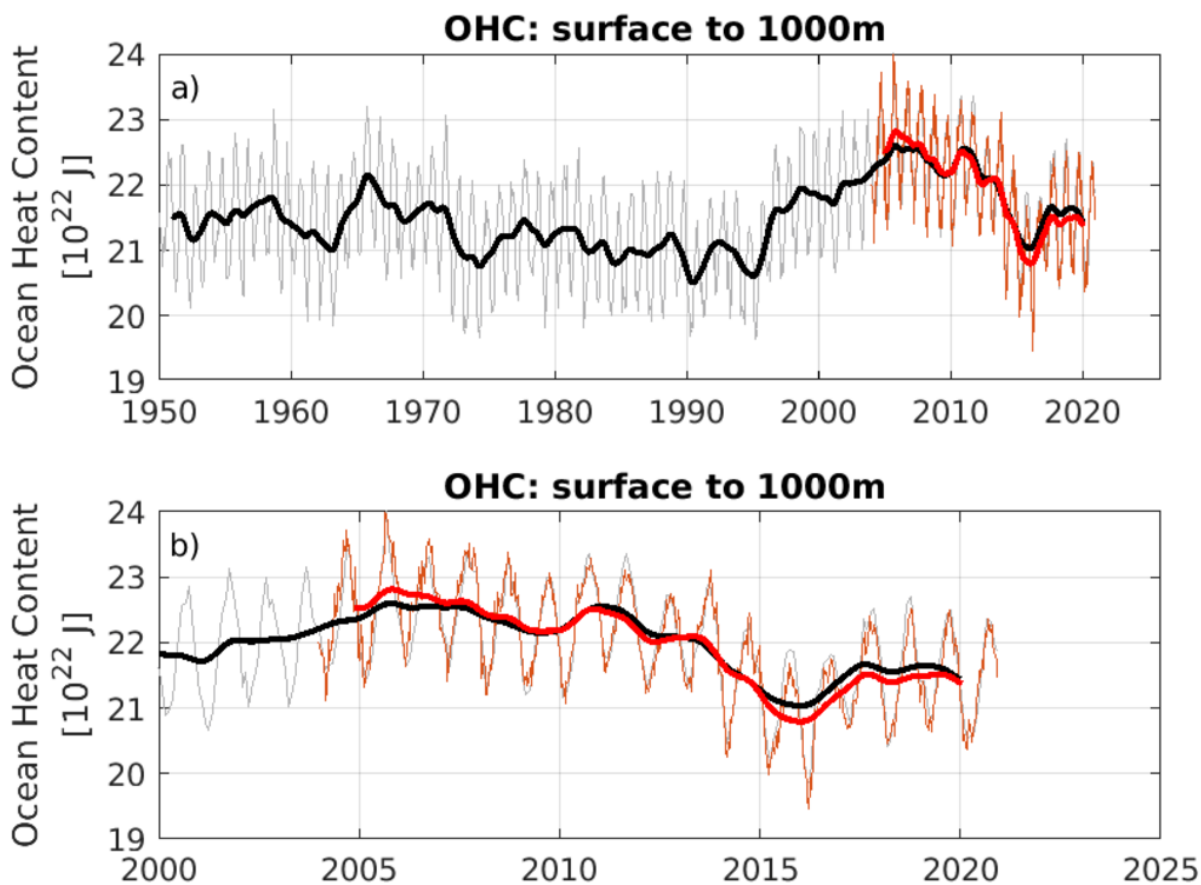
.45 Here we illustrate the subpolar Ocean heat content (SOHC), which is an indicator of long-term changes in the heat supply to  
.46 the North Atlantic region (Figure 8). Changes in SOHC are thought to be important precursors of Atlantic Multidecadal  
.47 Variability (e.g. Sutton et al., 2018), and have been linked to changes in climate extremes, for example the number of Atlantic  
.48 hurricanes (Dunstone et al., 2011). The ACSIS SOHC time series are integrated from the region between 45°N to 67°N, and  
.49 80°W to 0E. The time series are calculated from gridded EN4.2.2 (Good et al., 2013) and Argo objectively mapped 1 x 1  
.50 degree temperature data sets (King, 2023). The SOHC calculated from the new dataset developed during ACSIS is shown in  
.51 red (based only on Argo measurements) while another calculation using the standard Met Office product EN4 (based on Argo,  
.52 hydrographic and remote sensing measurements) is shown in black. The two datasets agree well over the overlapping period  
.53 2004-present and the differences between the decadal filtered lines gives a useful indication of the uncertainty in the heat  
.54 content estimates due to the method of calculation.

.55

#### .56 **3.1.1 Data archive**

.57 Objectively mapped temperature and salinity data and are available for download from BODC as self describing NetCDF  
.58 (<http://doi.org/10.5065/D6H70CW6>) files: <https://doi.org/10.5285/fe8e524d-7f04-41f3-e053-6c86abc04d51> (King et al.,  
.59 2023) as are upper ocean heat content timeseries, also in NetCDF format :<https://doi.org/10/g6wm>, <https://doi.org/10/g8g2>  
.60 (Moat et al. (2021a-b)).

.61



62  
63 **Figure 8.** Subpolar ocean heat content index in units of  $10^{22}$  J using EN4 (black) and ARGO OI (red) a) 1950-2020 and b)  
64 during the Argo period 2004-2020). Thick lines have an annual low pass filter applied.  
65

### 66 3.2 Forced Ocean-ice simulations

#### 67 3.2.1 $\frac{1}{4}^\circ$ ocean models forced with three different surface meteorological datasets.

68 Three integrations of a global ocean and sea ice configuration, consisting of Global Ocean v6 (GO6, Storkey et al, 2018) and  
69 Global Sea Ice v8.1 (GSI8.1, Ridley et al, 2018) were carried out, as a deliverable for Work Package 2.3 of ACSIS, intended  
70 to provide a tool for scientific investigation of the mechanisms of variability of the AMOC and other modes of variability of  
71 the Atlantic Ocean. GO6 is based on NEMO v3.6 (Madec 2016), and GSI8.1 on CICE v5.2.1 (Hunke & Lipscomb, 2010;  
72 Ridley et al., 2018) The GO6 ocean configuration was chosen to be the same as that developed under the JMMP collaborative  
73 programme (<http://www.jwcrp.org.uk/under/jmmp.asp>) as the ocean component of the UK's submissions under CMIP6,  
74 namely GC3.1 (Williams et al., 2017) and UKESM1 (Sellar et al., 2019), and informed choices made in the UK OMIP (Ocean

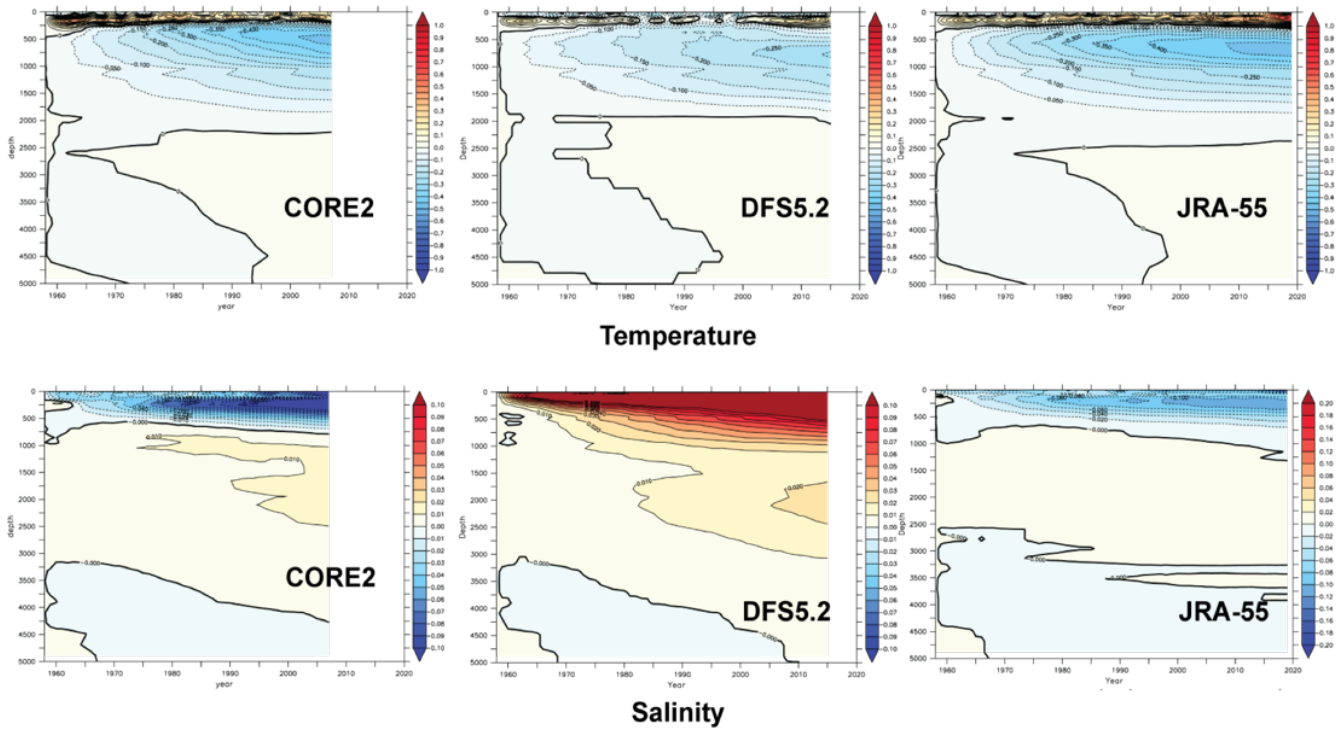


.75 Model Intercomparison Project – Griffies et al., 2016) integrations. Three forcing datasets were used to assess the sensitivity  
.76 of the models to the choice of forcing data. These were the CORE2 (Large and Yeager 2009), DFS5.2 (Brodeau et al 2010)  
.77 and JRA-55 (Tsuji et al., 2018) datasets, each supplying gridded surface met variables (air temperature, humidity, and  
.78 surface winds at subdaily intervals), surface radiative heat fluxes (downwelling shortwave and longwave at daily intervals)  
.79 and freshwater input (snow and precipitation at monthly intervals).

.80 The simulations were run on a global domain on the eORCA025 1/4° grid, with 75 vertical levels. The integrations were run  
.81 from 1958 to 2007 (CORE2); from 1958 to 2015 (DFS5.2) and from 1958 to 2020 (JRA-55), and monthly means are archived.  
.82 Variables archived include full-depth potential temperature and salinity, horizontal and vertical velocity components, surface  
.83 fluxes of heat, freshwater and momentum; mixed-layer depth. Sea ice cover and thickness, but many other state and process  
.84 variables were also archived. Note that sea ice files from the JRA-forced run are only available for years 1990-2001 and 2002-  
.85 2020. These forced ocean-ice simulations use the same configuration as the ocean component of the coupled simulations  
.86 described in section 3.1.

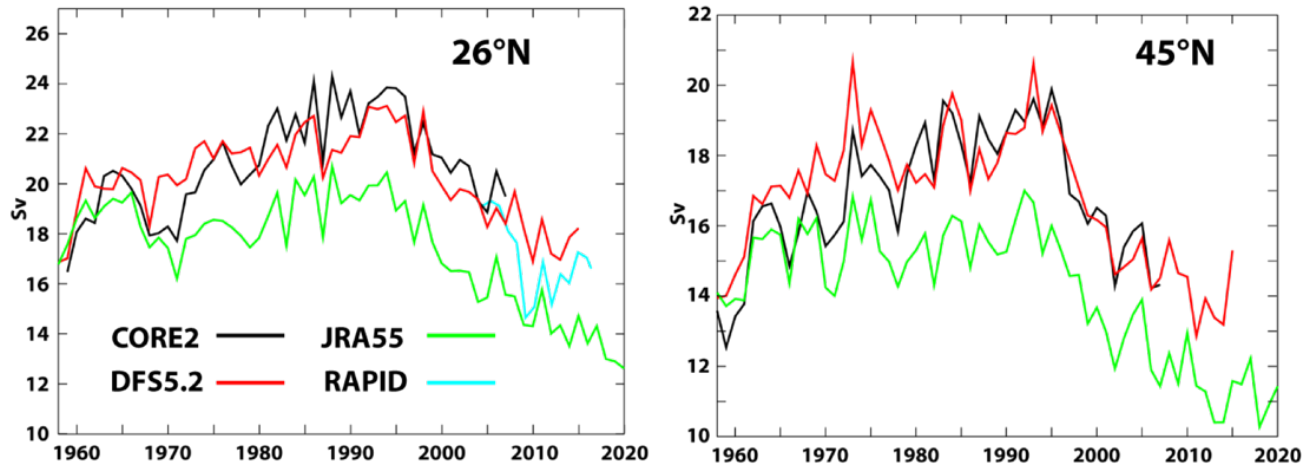
.87  
.88 A comparison of the model drifts in globally averaged temperature and salinity is shown in figure 9. In particular there is a  
.89 large positive drift in upper ocean salinity in the DFS5.2 forced simulation and the relatively large freshening in the CORE2  
.90 simulations. Overall the JRA55 forced simulation shows moderate drift in both variables. Nonetheless simulated interannual  
.91 to multidecadal changes to Atlantic Ocean circulation are similar between the models (Fig 10). More details on the simulations  
.92 and the AMOC in the three simulations are given by Megann et al (2021a). We expect these simulations will be extremely  
.93 useful to investigate the role of surface forcing in generating model biases and in determining the mean ocean circulation and  
.94 its variability.

.95



.96  
 .97  
 .98  
 .99  
 .00  
 .01

**Figure 9.** Annual drifts in global mean temperature (K) (top) and salinity (psu) (bottom) as a function of depth in the ACSIS  $\frac{1}{4}^\circ$  forced ocean model simulations. Left panels are from the CORE2 forced simulation, centre panels are from the DFS5.2 forced simulation and right panels are from the JRA-55 forced simulation.



**AMOC time series in ACSIS GO6 integrations at (left) 26°N and (right) 45°N.**

.02  
 .03



04 **Figure 10.** AMOC timeseries (Sv), 1960-2020 from the ACSIS  $\frac{1}{4}^\circ$  forced ocean model simulations at  $26^\circ\text{N}$  (left) and  $45^\circ\text{N}$   
05 (right). Timeseries from all three integrations are shown on each panel: CORE2 forced simulation (black); DFS5.2 forced  
06 simulation (red) and JRA-55 forced simulation (green). The AMOC derived from observations at  $26^\circ\text{N}$  (the RAPID-MOCHA  
07 array), available from 2004 onwards, are plotted on the left panel (cyan).

08

### 09 **3.2.2 $\frac{1}{4}^\circ$ and $1/12^\circ$ “twin” simulations**

10 Two integrations of the Global Ocean v8p7 (GO8p7) ocean and sea ice configuration simulation were run under the ACSIS  
11 programme. This is based on NEMO v4.0.4 (Madec et al., 2019), including the SI3 sea ice model, and has been developed  
12 under the Joint Marine Modelling Programme (JMMP see <http://www.jwcrp.org.uk/under/jmmp.asp>). The simulations are  
13 identical apart from the ocean horizontal resolution: one on a  $\frac{1}{4}^\circ$  grid, and the other a  $1/12^\circ$  grid. They are forced with the  
14 JRA-55 surface forcing dataset (T sujino et al, 2018) from 1958 to 2021. The integrations are intended to provide a tool for  
15 scientific investigation of the mechanisms of variability of the AMOC and ocean heat content of the Atlantic Ocean at an eddy-  
16 rich resolution. The GO8p7 configuration is close to that expected to be incorporated in the GC5.1 coupled climate model and  
17 the UKESM2 earth system model, both aimed at CMIP7. The configuration was implemented at the two resolutions, with the  
18 parameter and physics setting as close as possible (there are some necessary changes to lateral friction which are required for  
19 numerical stability at higher resolution), to investigate the sensitivity of the circulation, numerical mixing and other metrics to  
20 the resolution.

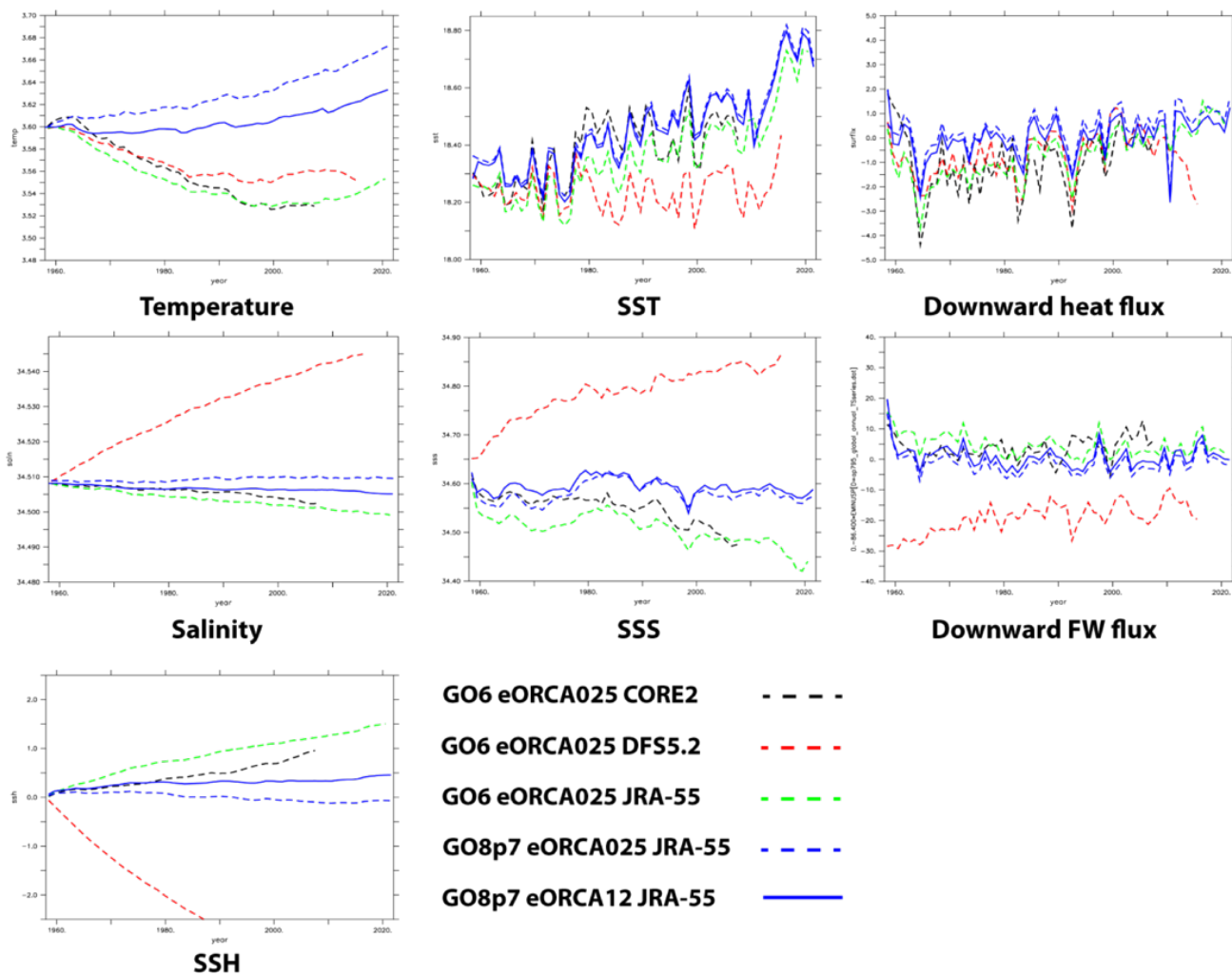
21 As for section 4.4.1 The integrations were carried out on a global domain on eORCA025  $1/4^\circ$  and eORCA12  $1/12^\circ$  grids, with  
22 75 vertical levels. The integrations were run from 1958 to 2020 and monthly and annual means of the 3-D and 2-D model  
23 fields were saved (including full-depth potential temperature and salinity, horizontal and vertical velocity components, surface  
24 fluxes of heat, freshwater and momentum; mixed-layer depth, and sea ice cover and thickness). 5-day means of a selection of  
25 surface fields (including SST, mixed layer depth and sea-surface height) are also archived.

26

27 To illustrate the simulations we show timeseries of some key globally integrated variables from the twin simulations and also,  
28 for context, from the three  $\frac{1}{4}^\circ$  simulations already described in section 4.4.1 (Fig 11). Global mean temperature drifts are of  
29 order 0.05K over the  $\sim 50$  year integrations or  $0.001\text{K yr}^{-1}$ . The  $1/12^\circ$  simulation has a smaller drift than its twin  $\frac{1}{4}$  degree  
30 resolution. The twin simulations show positive temperature drift while the other simulations show a negative drift. We expect  
31 to see an SST warming trend under the influence of anthropogenic warming superimposed on interannual and decadal  
32 variability. All the simulations show strong interannual variability with about the same amplitude and timing, forced by  
33 interannual changes in wind stress and buoyancy forcing, and not influenced by global temperature and salinity drifts. On  
34 decadal and longer timescales the difference between variability, secular trends and model drifts can be blurred. The models  
35 all show a small reduction in global mean SST from initialisation to the late 1970s. The DFS5.2 forced simulation then  
36 continues to reduce its SST until the mid 1980s after which the SST remains more or less stable until about 2010, however all  
37 the other simulations increase their SST at a fairly steady rate throughout the 1980s, 90s and 2000s. from about 2010 onwards



38 all the simulations experience strong surface warming. Globally integrated downward surface heat flux is consistent with the  
39 global mean surface temperature evolution with a negative net surface flux in the early decades for the three simulations with  
40 different surface flux forcing and a positive net flux for the twin simulations. The net heat flux for the twin simulations is  
41 generally positive whereas for the other simulations it only becomes positive around the year 2000 and this is when the global  
42 mean temperature in those simulations starts to rise. The downward heat flux clearly shows the signals of large volcano  
43 eruptions (Agung, 1964, el Chichon 1982 and Pinatubo 1991) as well as the 1997 El Nino event (see Balmaseda et al 2013).  
44 The sharp downward dip in 2009 is interesting and possibly linked to the sudden AMOC reduction at that time, but further  
45 research is required to investigate this. With the exception of the DFS5.2 forced simulations, global mean salinity and global  
46 mean surface salinity show quite small trends consistent with a reasonably balanced surface freshwater flux. The DFS5.2  
47 forced simulation shows strong salinification consistent with a net loss of freshwater through the surface. The twin runs show  
48 best conservation of freshwater. Finally, the net heating/cooling and freshening/salinification of the simulations is reflected in  
49 the global mean sea surface height which is most stable in the twin simulations.



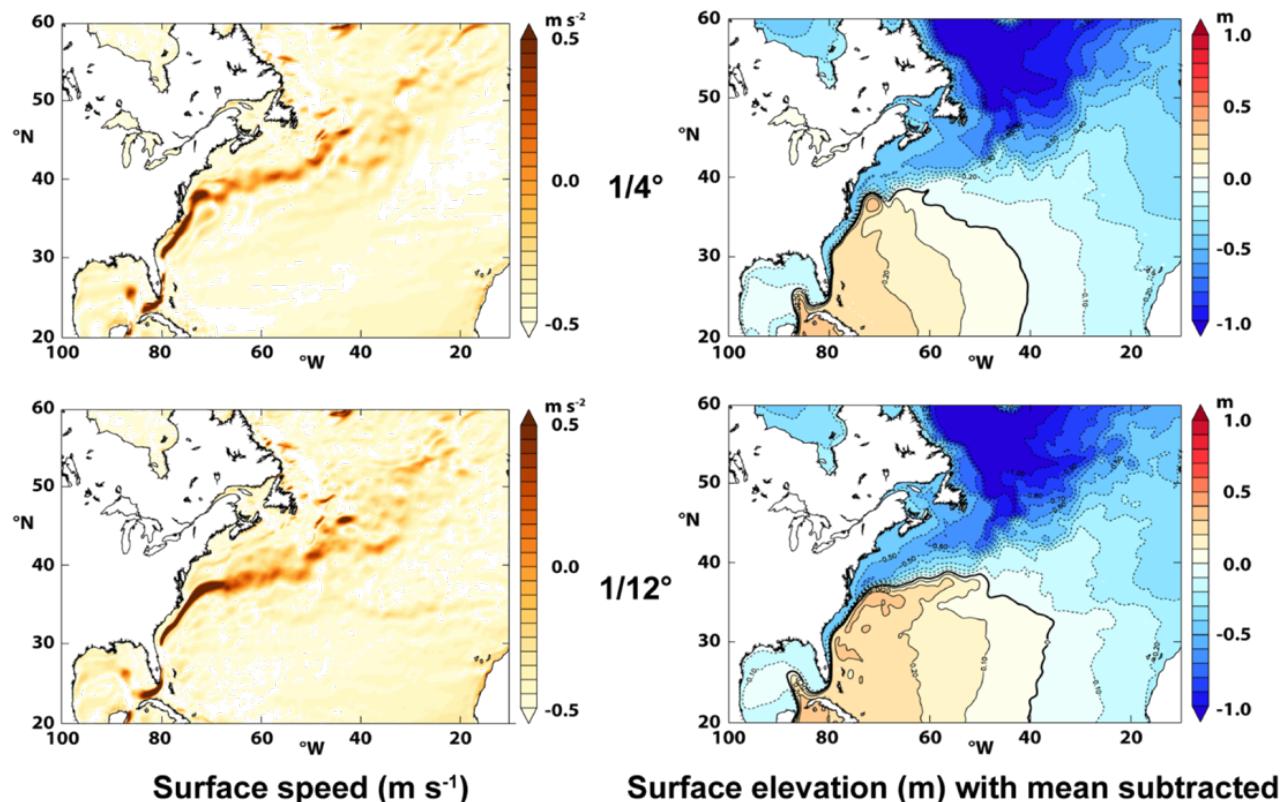
50

51 **Figure 11.** Trends in key variables in the ACSIS  $\frac{1}{4}^\circ$  and  $\frac{1}{2}^\circ$  forced ocean simulations. The variables plotted are global mean  
 52 temperature (top left), global mean sea-surface temperature (top centre), global mean net downward air-sea heat flux (top  
 53 right), global mean salinity (second row left), global mean sea-surface salinity (second row centre), downward freshwater flux  
 54 (second row right) and global mean sea-surface height (bottom left). Dashed lines are from the  $\frac{1}{4}$  degree model (CORE2 forced  
 55 – black, DFS5.2 forced – red, JRA-55 forced,  $\frac{1}{4}^\circ$  twin simulation – blue) whilst the solid blue line is from the  $\frac{1}{12}^\circ$  twin  
 56 simulation. Note that the green and blue lines are both from JRA-55 forced model simulations but with different model code  
 57 versions and configurations (see text).

58

59





**Surface circulation in 2000-2009 of ACSIS GO8p7 runs**

60  
61

62 **Figure 12.** Surface North Atlantic circulation from the ACSIS twin simulations averaged over years 2000-2009. Anomalous  
63 surface current magnitude ( $\text{m s}^{-2}$ ) for the  $1/4^\circ$  simulation (top left) and for the  $1/12^\circ$  simulation (bottom left), Anomalous mean  
64 sea surface height (m) for the  $1/4^\circ$  simulation (top right) and the  $1/12^\circ$  simulation (bottom right).

65

66 A final illustration shows the mean surface circulation in the North Atlantic from the twin simulations (Fig 12). The most  
67 obvious difference in the surface velocity (left hand panels) is that the Gulf Stream separation is more realistic in the  $1/12^\circ$   
68 simulation where the current moves northeastwards off Cape Hatteras ( $\sim 38^\circ\text{N}$ ). This contrasts with the  $1/4^\circ$  simulation where  
69 the current shifts direction anticlockwise to remain quite close to the coast. The kink in the Gulf Stream Extension at the  
70 Northwest corner ( $\sim 50^\circ\text{W}$ ,  $40^\circ\text{N}$ ) is also more realistic in the  $1/12^\circ$  simulation and there is also a discernible signature of the  
71 Azores current (zonal feature around  $34^\circ\text{N}$ ) which is missing in the  $1/4^\circ$  simulation. Similar features can be seen in the mean  
72 sea surface height from the two simulations (right panels). One interesting difference is in the penetration of the Labrador  
73 Current much further south in the  $1/12^\circ$  simulation – where the low sea surface heights characteristic of the subpolar gyre  
74 penetrate south west along the North American shelf/slope region north of the Gulf stream extension (between  $80^\circ\text{W}$  and  $50^\circ\text{W}$   
75 and  $35^\circ\text{N}$  to  $45^\circ\text{N}$ ). Decadal variability in the position of the Gulf Stream has been shown to be linked to salinity anomalies





76 that are advected southwards by the Labrador Current (New et al., 2022) so these differences between the simulations are  
77 likely to impact on their simulation of AMOC variability.

78

### 79 **3.2.3 Data archive**

80

81 Data from all the ocean simulations are archived in NetCDF format, with separate files for variables defined on the T, U, V  
82 and W grids (one for each month of simulation) as is standard for NEMO. Each variable has a long name which gives a detailed  
83 description of the variable (see Madec, 2016, 2019 for an explanation of the data output format). Separate monthly NetCDF  
84 files contain sea ice variables and lagrangian iceberg properties trajectories on the CICE grid. The data are archived at CEDA  
85 (Megann et al., 2021b, c, d):

86

87 CORE2-forced run: <https://dx.doi.org/10.5285/119a5d4795c94d2e94f610647640edc0> (Megann et al., 2021b,

88 DFS5.2-forced run: <https://dx.doi.org/10.5285/a0708d25b4fc44c5ab1b06e12fef2f2e>, (Megann et al., 2021c)

89 JRA55-forced run: <https://dx.doi.org/10.5285/4c545155dfd145a1b02a5d0e577ae37d> (Megann et al., 2021d)

90  $\frac{1}{4}^\circ$  “twin” simulation: <https://dx.doi.org/10.5285/e02c8424657846468c1ff3a5acd0b1ab> (Megann et al., 2022a)

91  $1/12^\circ$  “twin” simulation: <https://dx.doi.org/10.5285/399b0f762a004657a411a9ea7203493a> (Megann et al., 2022b).

## 92 **4 Ice data sets.**

### 93 **4.1 Advanced Sea Ice model simulations**

94 Results from 6 forced ocean-ice simulations and 2 stand-alone ice simulations are included to document the impact of sea ice  
95 physics and atmospheric forcing data on the Arctic sea ice evolution. All of them use the same sea ice model CICE  
96 configuration GSI8.1 (Ridley et al., 2018) and the ocean-ice simulations use the same ocean model NEMO GO6.0 (Storkey et  
97 al., 2018) as the forced ocean ice simulations of section 4.4 and the HadGEM3 climate model of sections 3.1. Three different  
98 atmospheric forcing data set are applied: NCEP Reanalysis-2 (NCEP2) data (Kanamitsu et al., 2002, updated 2020), CORE2  
99 surface data (Large & Yeager, 2009) and the atmospheric forcing data set DFS5.2 (Dussin et al., 2016). Regarding the sea ice  
100 component, we use the default CICE setup as in HadGEM3 (CICE-default) and an advanced setup (CICE-best) in which a  
101 new process is added (snow loss due to drifting snow) and some adjustments have been made to model physics and parameters.  
102 See Schroeder et al. (2019) and Table 7 for details.

103

104 **Table 7.** Overview of model simulations with default and improved sea ice processes.

Simulation	Atmospheric forcing	Ocean model	CICE setup	Time period
------------	---------------------	-------------	------------	-------------



CICE-default	NCEP2	Mixed-layer	CICEv5.1.2 with prognostic melt pond model and EAP rheology	1980-2020
CICE-best	NCEP2	Mixed-layer	As CICE-default, but with several modifications including snow drift scheme, bubbly conductivity scheme, increased sea ice emissivity and reduced melt pond max fraction parameter (see Schroeder et al., 2019)	1980-2020
NEMO-CICE-1deg-default-CORE	CORE II	NEMOv3.6	CICEv5.1.2 with prognostic melt pond model	1960-2009
NEMO-CICE-1deg-best-CORE	CORE II	NEMOv3.6	As CICE-best	1960-2009
NEMO-CICE-1deg-best-DFS	DFS5.2	NEMOv3.6	As CICE-best	1960-2015
NEMO-CICE-1deg-best-NCEP	NCEP2	NEMOv3.6	As CICE-best	2000-2020
NEMO-CICE-1/4deg-default-DFS	DFS5.2	NEMOv3.6	CICEv5.1.2 with prognostic melt pond model	1979-2015
NEMO-CICE-1/4deg-best-DFS	DFS5.2	NEMOv3.6	As CICE-best, but with increased ice and snow conductivity instead of snow drift scheme	1979-2015

i05

i06 The impact of our changes to the sea ice model on the fidelity of the model sea ice simulation is shown in Figure 13. All  
 i07 simulations with the default CICE setup (thin lines) underestimate the mean Arctic sea ice thickness during winter. Figure 13  
 i08 shows that the mean Arctic Cyrosat-2 sea ice thickness is more than 50cm thicker in April than in those simulations. By  
 i09 applying the advanced CICE setup, all simulations (stand-alone, NEMO-CICE 1° and NEMO-CICE 1/4°, thick lines) show  
 i10 realistic mean April sea ice thickness. The advanced setup leads to improvements in simulating summer sea ice extent, too  
 i11 (not shown) and highlights the importance of sea ice physics for accurate model simulations for the Arctic.

i12

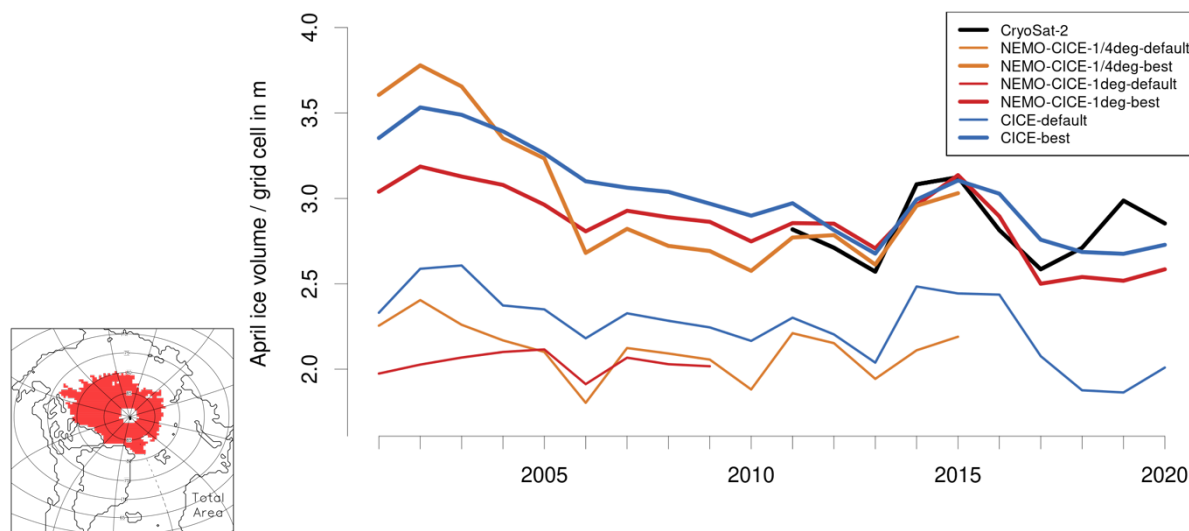
#### i13 **4.1.1 Data archive**

i14

i15 Data from the global ocean simulations with advanced sea ice are archived in NetCDF format as described in section 3.2.3  
 i16 above. Standalone sea ice simulations are similar but output consist of a single NetCDF file containing sea ice variables on the  
 i17 CICE grid for each month of simulation. The data is accessible via CEDA:  
 i18 <http://catalogue.ceda.ac.uk/uuid/770a885a8bc34d51ad71e87ef346d6a8> (see Megann et al., 2021e).



i19



i20

i21 **Figure 13.** Mean April Arctic Sea ice volume over red region for several model simulations in comparison to Cryosat-2  
i22 estimates. The selected region represents the area over which Cryosat-2 data are available for the whole period from 2010 to  
i23 2020 (October to April). Table 7 provides more information about the setup of the model simulations.

i24

## i25 5. Previously published ACSIS datasets

i26

i27 The new datasets described in the previous sections should be viewed in the context of (and potentially used in conjunction  
i28 with) several other datasets generated in whole or in part by the ACSIS programme and already published and described in the  
i29 scientific literature. Here we provide a brief overview of these other datasets and include links to where they can be accessed.

### i30 5.1 Stratospheric Aerosol Surface Area Density from Explosive Volcanic Eruptions

i31 The “MajorVolc” UM-UKCA volcanic aerosol datasets are model simulations of the monthly progression of the volcanic  
i32 aerosol clouds from the 3 largest volcanic eruptions of the 20th century – 1963 Agung, 1982 El Chichon and 1991 Pinatubo.  
i33 The interactive stratospheric aerosol model experiments break new ground, being an advance on the 2D global aerosol model  
i34 simulations that generated the CMIP6 volcanic aerosol dataset (Arfeuille et al., 2013; Luo, 2016), the stratospheric circulation  
i35 and dynamics progressing in 3D, within the high-top N96L85 GA4 UM-UKCA composition-climate model (Walters et al.,  
i36 2014). The simulations apply the v8.2 of the GLOMAP-mode aerosol microphysics module (Mann et al., 2010; Dhomse et al.,  
i37 2014; Mann et al., 2015) including recent adaptations for the stratosphere (Brooke et al., 2017; Dhomse et al., 2020). This  
i38 upgraded capability predicts the volcanic forcings with very high fidelity, each of the steps in the formation, growth and  
i39 sedimentation of the sulphuric acid aerosol particles, the UM-UKCA model also calculating the oxidation rate of the volcanic  
i40 SO<sub>2</sub>, consistently with the depletion and replenishment of oxidants that occurs for the amount of SO<sub>2</sub> emitted.



i41  
i42 Within ACSIS, the volcanic forcings were published as monthly-varying global 2D zonal-mean datasets for 4 key aerosol  
i43 properties (stratospheric AOD, surface area density, particle effective radius, aerosol extinction at 550nm & 1020nm) on an  
i44 open-access data archive (Dhomse, 2020). The variables align directly with Figures in the peer-reviewed journal article  
i45 (Dhomse et al., 2020), and retain the 2 key parent resolutions of the model (1.25° latitude vs 1 km altitude to 40km).

i46  
i47 Following the protocols for the co-ordinated Historical Eruption SO<sub>2</sub> Emission Assessment (HErSEA) experiment within the  
i48 international ISA-MIP activity for interactive stratospheric aerosol models (Timmreck et al., 2018), three different datasets  
i49 were produced for each eruption, at upper-limit, lower-limit and mid-range emission of SO<sub>2</sub> (e.g. 10, 14, 20 Tg of SO<sub>2</sub> for  
i50 Pinatubo). For each SO<sub>2</sub> emission amount, 3 ensemble members were run, each initialised from a timeslice control run whose  
i51 stratosphere was spun-up for the decade's GHG & ODS loadings, re-start points chosen to enact the QBO phase transition for  
i52 that eruption (see Dhomse et al., 2020).

i53  
i54 Monthly mean volcanic forcing data is stored in netCDF format. Files are archived for each variable, all 3 ensemble members  
i55 for each “eruption realisation” (SO<sub>2</sub> emission amount) within 1 file (e.g. “Pin10Tg\_saod\_2Ms\_mon.nc”). The dataset  
i56 identifier is <https://doi.org/10.17632/n3g2htz9hk.1> (Dhomse (2020)).

i57  
i58 Whereas the MajorVolc volcanic aerosol datasets provide globally gridded aerosol properties such as Surface Area Density  
i59 and aerosol extinction, in order to enact volcanic forcing in a climate model requires one to specify the aerosol optical  
i60 properties across the solar and terrestrial spectral ranges: mapping extinction, absorption and asymmetry parameters ( $Q_{ext}$ ,  $Q_{abs}$ ,  
i61  $g$ ) to the wavebands of the radiative transfer module within the climate model. This was done for the Major Volc datasets  
i62 generated as part of ACSIS, described above, and these data are available as described in Feng et al. (2021) and Dhomse et al.  
i63 (2021a, b):

i64  
i65 Pinatubo (<https://doi.org/10.5281/zenodo.4739170> (Feng et al., 2021)); El Chichon (<https://doi.org/10.5281/zenodo.4744633>  
i66 (Dhomse et al., 2021a)); Agung (<https://doi.org/10.5281/zenodo.4744686> (Dhomse et al., 2021b)).

## i67 i68 **5.2 CMIP6 HighResMIP global climate model simulations**

i69 The 6th Coupled Model Intercomparison Project (CMIP6) HighResMIP (<https://www.highresmip.org/>) sub project aimed to  
i70 increase the atmosphere and ocean resolution of global climate models to at least 50 km in the atmosphere and 0.25° in the  
i71 ocean, and to assess the effect of these increases in resolution on process representation and model fidelity (Haarsma et al.  
i72 2016, Roberts et al. 2018). The UK contribution to CMIP6 HighResMIP, based on the HadGEM3 climate model (Hewitt et al  
i73 2011), was delivered as part of the EU Horizon 2020 PRIMAVERA project (<https://www.primavera-h2020.eu/>). Some of the  
i74 HadGEM3 PRIMAVERA simulations were co-funded by ACSIS and are referenced here (Table 8). These consisted of



atmosphere only simulations with horizontal resolutions of N256 (~50km) and N512 (~25km) (Table 8, rows 1-12), and analogous fully coupled simulations with an ocean resolution of 0.25 degrees (Table 8, rows 13-24). The simulations were conducted in pairs consisting of a historical simulation from 1950-2014 and a future simulation from 2015-2050. The terminology is detailed in Haarsma et al. (2016) and Roberts et al. (2019). All these simulations are available on the Earth System Grid Federation (ESGF, <https://esgf.llnl.gov/>). Output is in CF-compliant NetCDF for all simulations. The NEMO ocean component in these simulations is the same configuration as the forced ocean model simulations described in section 3.2.

Two further cutting edge simulations were performed at even higher resolution in both ocean and atmosphere, 1/12°, and 50km (N512) respectively (Table 8, rows 25-26). The first was a control 1950s climate running from 1950-2014 and the second was a future simulation (SSP5-8.5) from 2015-2050. See Roberts et al., (2020) for an assessment of the simulated Atlantic Meridional Overturning Circulation in this and other HigResMIP simulations.

**Table 8.** Summary of HighResMIP global climate model simulations. The first 12 rows refer to SST-forced atmosphere only simulations, the remaining rows refer to coupled ocean-atmosphere simulations.

Model	Experiment	Resolution (Atm./Ocn.)	Period	Ensembl e member	DOI
HadGEM3- GC31-MM	highresSS T-present	N216	1950-2014	r1i1p1fl	<a href="http://doi.org/10.22033/ESGF/C&lt;br/&gt;MIP6.6029">http://doi.org/10.22033/ESGF/C MIP6.6029</a> Roberts (2017a)
HadGEM3- GC31-MM	highresSS T-future	N216	2015-2050	r1i1p1fl	<a href="http://doi.org/10.22033/ESGF/C&lt;br/&gt;MIP6.6013">http://doi.org/10.22033/ESGF/C MIP6.6013</a> Roberts (2019a)
HadGEM3- GC31-MM	highresSS T-present	N216	1950-2014	r1i2p1fl	<a href="http://doi.org/10.22033/ESGF/C&lt;br/&gt;MIP6.6029">http://doi.org/10.22033/ESGF/C MIP6.6029</a> Roberts (2017a)
HadGEM3- GC31-MM	highresSS T-future	N216	2015-2050	r1i2p1fl	<a href="http://doi.org/10.22033/ESGF/C&lt;br/&gt;MIP6.6013">http://doi.org/10.22033/ESGF/C MIP6.6013</a> Roberts (2019a)
HadGEM3- GC31-MM	highresSS T-present	N216	1950-2014	r1i3p1fl	<a href="http://doi.org/10.22033/ESGF/C&lt;br/&gt;MIP6.6029">http://doi.org/10.22033/ESGF/C MIP6.6029</a> Roberts (2017a)
HadGEM3- GC31-MM	highresSS T-future	N216	2015-2050	r1i3p1fl	<a href="http://doi.org/10.22033/ESGF/C&lt;br/&gt;MIP6.6013">http://doi.org/10.22033/ESGF/C MIP6.6013</a> Roberts (2019a)
HadGEM3- GC31-HM	highresSS T-present	N512	1950-2014	r1i1p1fl	<a href="http://doi.org/10.22033/ESGF/C&lt;br/&gt;MIP6.6024">http://doi.org/10.22033/ESGF/C MIP6.6024</a> Roberts (2017b)
HadGEM3- GC31-HM	highresSS T-future	N512	2015-2050	r1i1p1fl	<a href="http://doi.org/10.22033/ESGF/C&lt;br/&gt;MIP6.6008">http://doi.org/10.22033/ESGF/C MIP6.6008</a> Roberts (2019b)



HadGEM3- GC31-HM	highresSS T-present	N512	1950-2014	rli2p1fl	<a href="http://doi.org/10.22033/ESGF/C&lt;br/&gt;MIP6.6024">http://doi.org/10.22033/ESGF/C MIP6.6024</a> Roberts (2017b)
HadGEM3- GC31-HM	highresSS T-future	N512	2015-2050	rli2p1fl	<a href="http://doi.org/10.22033/ESGF/C&lt;br/&gt;MIP6.6008">http://doi.org/10.22033/ESGF/C MIP6.6008</a> Roberts (2019b)
HadGEM3- GC31-HM	highresSS T-present	N512	1950-2014	rli3p1fl	<a href="http://doi.org/10.22033/ESGF/C&lt;br/&gt;MIP6.6024">http://doi.org/10.22033/ESGF/C MIP6.6024</a> Roberts (2017b)
HadGEM3- GC31-HM	highresSS T-future	N512	2015-2050	rli3p1fl	<a href="http://doi.org/10.22033/ESGF/C&lt;br/&gt;MIP6.6008">http://doi.org/10.22033/ESGF/C MIP6.6008</a> Roberts (2019b)
HadGEM3- GC31-HM	hist-1950	N512, 0.25°	1950-2014	rli1p1fl	<a href="http://doi.org/10.22033/ESGF/C&lt;br/&gt;MIP6.6040">http://doi.org/10.22033/ESGF/C MIP6.6040</a> Roberts (2018a)
HadGEM3- GC31-HM	highres- future	N512, 0.25°	2015-2050	rli1p1fl	<a href="http://doi.org/10.22033/ESGF/C&lt;br/&gt;MIP6.5984">http://doi.org/10.22033/ESGF/C MIP6.5984</a> Roberts (2019c)
HadGEM3- GC31-HM	hist-1950	N512, 0.25°	1950-2014	rli2p1fl	<a href="http://doi.org/10.22033/ESGF/C&lt;br/&gt;MIP6.6041">http://doi.org/10.22033/ESGF/C MIP6.6041</a> Schiemann et al. (2019a)
HadGEM3- GC31-HM	highres- future	N512, 0.25°	2015-2050	rli2p1fl	<a href="http://doi.org/10.22033/ESGF/C&lt;br/&gt;MIP6.5985">http://doi.org/10.22033/ESGF/C MIP6.5985</a> Schiemann et al. (2019b)
HadGEM3- GC31-HM	hist-1950	N512, 0.25°	1950-2014	rli3p1fl	<a href="http://doi.org/10.22033/ESGF/C&lt;br/&gt;MIP6.6040">http://doi.org/10.22033/ESGF/C MIP6.6040</a> Roberts et al. (2018a)
HadGEM3- GC31-HM	highres- future	N512, 0.25°	2015-2050	rli3p1fl	<a href="http://doi.org/10.22033/ESGF/C&lt;br/&gt;MIP6.5984">http://doi.org/10.22033/ESGF/C MIP6.5984</a> Roberts et al 2019c
HadGEM3- GC31-HH	hist-1950	N512, 1/12°	1950-2014	rli1p1fl	<a href="https://doi.org/10.22033/ESGF/C&lt;br/&gt;MIP6.5881">https://doi.org/10.22033/ESGF/C MIP6.5881</a> Roberts (2018b)
HadGEM3- GC31-HH	highres- future	N512, 1/12°	2015-2050	rli1p1fl	<a href="https://doi.org/10.22033/ESGF/C&lt;br/&gt;MIP6.1822">https://doi.org/10.22033/ESGF/C MIP6.1822</a> Coward and Roberts (2018)



89

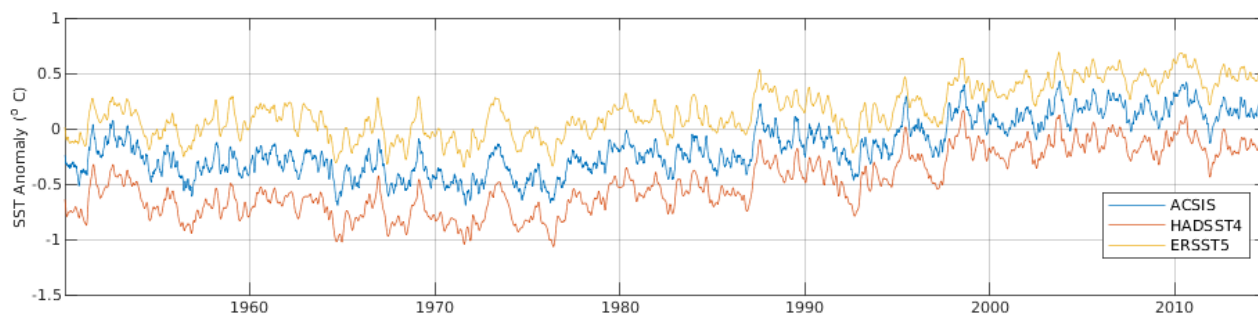
### 90 5.3 Sea surface temperature

91 The ACSIS Atlantic Ocean medium resolution SST dataset is a 5-day field of Sea Surface Temperature (SST) on a  $\frac{1}{2}^\circ$  by  $\frac{1}{2}^\circ$   
92 grid from 1950 to 2014 and covers the Atlantic Ocean (<http://dx.doi.org/10.5285/83b0cd7e7cc6495a90b4cb967ead3577>,  
93 Williams and Berry (2020)).

94 The dataset is based on *in situ* ship and buoy SST observations from the International Comprehensive Ocean-Atmosphere Data  
95 Set (ICOADS) Revision 3. Measurements which fail initial quality control checks were rejected and for each grid box where  
96 there is data a trimmed mean and sample standard deviation was calculated to produce super-observations. These were then  
97 expressed as anomalies from the 1981-2014 Climatology (mean, annual, semi-annual and tri-annual) from the European Space  
98 Agency (ESA) Climate Change Initiative (CCI) SST dataset (version 2.0) derived from satellite observations. The  
99 measurements were then interpolated using Kriging to infill gaps and estimate uncertainties. The spatial covariance used in  
00 the Kriging was derived from the CCI SST analysis residuals (CCI SST analysis minus the CCI SST climatology). After  
01 interpolation, bias corrections derived from the HadSST.4.0.0.0 dataset are applied.

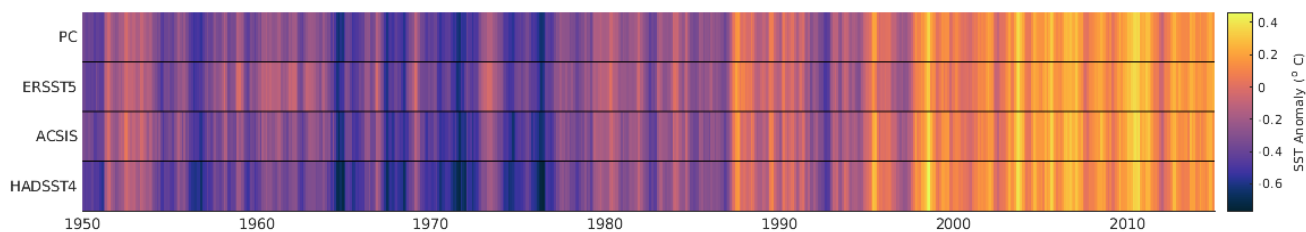
02 The dataset is available as annual CF compliant NetCDF files, with a total of 65 annual files available. Each file contains: the  
03 5 day mean sea surface temperature; the corresponding climatological value, the sea surface temperature anomaly and the  
04 uncertainty in the sea surface temperature.

05 The new dataset has been developed as part of the ACSIS for use in validation and comparison with regional climate models.  
06 Other potential uses include boundary forcing for regional reanalyses, monitoring and assessment of regional climate change  
07 and other studies requiring SST at a resolution higher than typical for *in situ* products (i.e.  $< 1$  month,  $< 1^\circ$ ) and spanning the  
08 satellite and pre-satellite era. In Figure 14a we compare the new SST dataset with two other leading SST datasets over the  
09 whole Atlantic domain and find good agreement of the basin averaged variability and trends. Fig 14b shows the data in a  
10 barcode type plot emphasising Atlantic climate warming. Additionally Figure 14b shows a first principal component time  
11 series from an EOF analysis of the three timeseries.



12



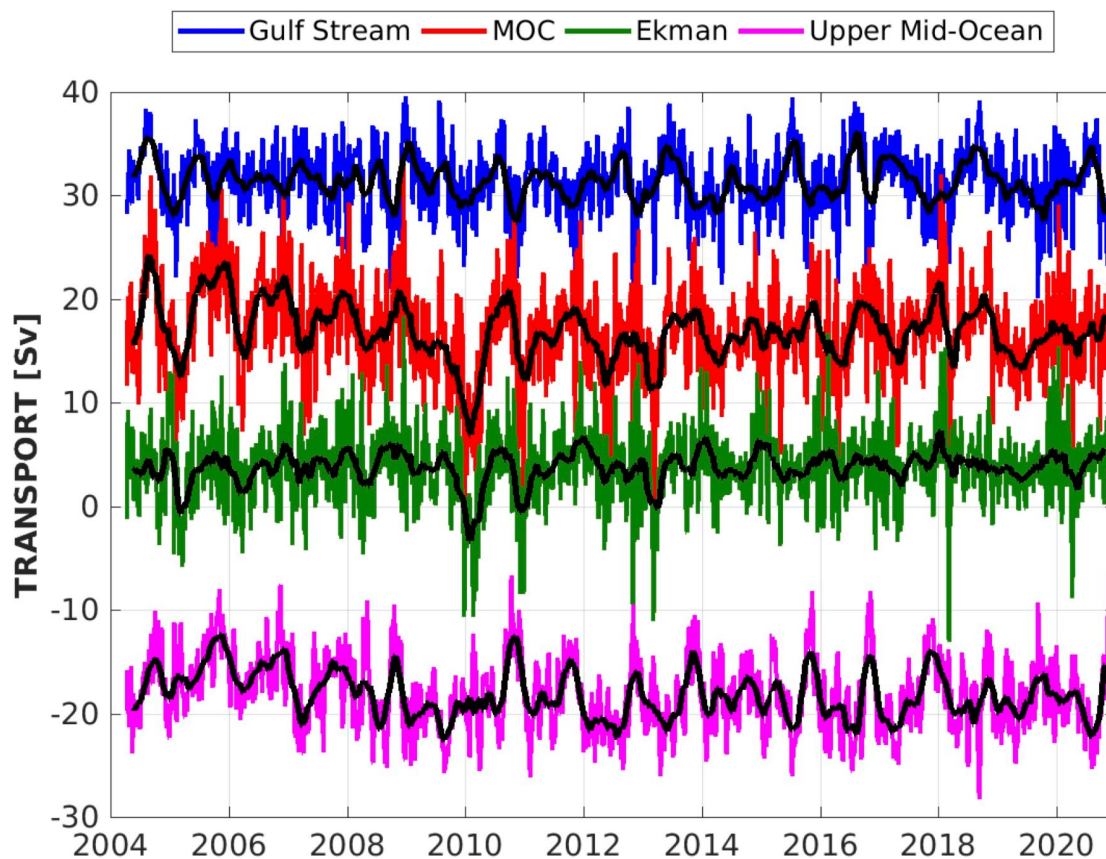


'13  
'14 **Figure 14.** (a) SST anomalies time series averaged over the whole Atlantic (60°S to 68°N and 98°W to 20°E) of the new  
'15 ACSIS dataset (blue) compared two leading global SST datasets, HadSST4 (Kennedy et al., 2019) and ERSST5 (Huang et al.,  
'16 2017). (b) The three datasets as a barcode plot. A timeseries of the principal component of the EOF of the three SST timeseries  
'17 is plotted at the top of the barcode. SST anomalies are relative to a 1981-2014 climatology.

'18

#### '19 5.4 Atlantic Meridional Overturning Circulation (AMOC) observed at 26.5°N

'20



'21





'22  
'23 **Figure 15.** The Atlantic Meridional Overturning Circulation (AMOC) index (red) and its components the Gulf Stream/Florida  
'24 Strait transport (blue), the Ekman transport (green) and the upper mid-ocean transport (magenta) at 26.5°N derived from the  
'25 RAPID array observations. Units are in Sverdrups (Sv) where  $1\text{Sv} = 10^6 \text{ m}^3\text{s}^{-1}$ . Coloured lines are 10-day values while black  
'26 lines have had a three month filter applied. The AMOC index is the maximum of the AMOC streamfunction which is defined  
'27 as the zonal integral of the area weighted velocity, summed downwards with depth from the surface. The depth of the maximum  
'28 is variable but generally lies in the depth range 700-1000m (McCarthy et al., 2015).

'29  
'30 The AMOC is an iconic index of North Atlantic ocean circulation and numerous observational and modelling studies have  
'31 established the importance of its associated northwards heat and salt transport to the mean climate and interannual-decadal  
'32 variability of the subpolar North Atlantic region (Robson et al., 2018, Moat et al., 2019), to regional climate elsewhere on the  
'33 globe (Monerie et al., 2018), and to global climate via its connection to the global thermohaline circulation. Whilst the RAPID  
'34 observations have been supported by separate funding, ACSIS provided essential support for the processing and analysis of  
'35 RAPID observations. ACSIS scientists have analysed many important phenomena uncovered by the RAPID array, including  
'36 the origin, impact and predictability of the extreme AMOC reduction in 2010 (Germe et al., 2022), the transition to a weaker  
'37 AMOC after 2008 (Smeed et al., 2018), possible AMOC recovery from 2009 (Moat et al., 2020), and its subsequent impact  
'38 on ocean conditions in the eastern subpolar gyre (Bryden et al., 2020). Figure 15 shows the entire timeseries from 2004 to the  
'39 present day including the separately measured components due to the near surface Ekman transport (green), the transport  
'40 through the Florida Straits (blue) and the geostrophic transport east of the Bahamas (magenta). The net transport (red) clearly  
'41 shows the reduction in magnitude since 2008 and the major downturn in 2010. Note that at the time of writing the AMOC has  
'42 yet to recover to its pre 2008 value. AMOC time series data can be downloaded directly from the RAPID project website  
'43 (<https://rapid.ac.uk/rapidmoc>, Moat et al., 2022)

'44  
'45 **5.5 Ice observations**

'46 Pan-Arctic sea ice thickness is estimated using satellite data from ESA's CryoSat-2 (CS2) mission. Launched in 2010, CryoSat-  
'47 2's main payload is a Ku-band radar altimeter (SIRAL), which measures the elevation of Earth's surface. Sea ice freeboard  
'48 (the portion of an ice floe above the waterline) is measured by differencing the elevation of the sea ice floe and that of the  
'49 surrounding ocean. Sea ice freeboard is then converted to thickness by assuming that sea ice floats in hydrostatic equilibrium  
'50 in the ocean, and assuming values for snow depth, and snow, ice and ocean density. CryoSat-2's orbit repeats every ~30 days,  
'51 providing Arctic-wide sea ice thickness estimates every month from October-April. The method and dataset are detailed in  
'52 full in Tilling et al., (2018), and monthly sea ice thickness, gridded at 5km, are available from the CPOM data portal  
'53 <http://www.cpom.ucl.ac.uk/csopr/seaice.php>.

'54



'55 For the purposes of the ACSIS project, we binned individual CryoSat-2 sea ice thickness estimates provided by CPOM into  
'56 the five default ice thickness categories of the sea ice model CICE on a rectangular 50 km grid: (1) ice thickness  $h < 0.6$  m, (2)  
'57  $0.6 \text{ m} < h < 1.4$  m, (3)  $1.4 \text{ m} < h < 2.4$  m, (4)  $2.4 \text{ m} < h < 3.6$  m, and (5)  $h > 3.6$  m (Schroeder et al, 2019). The mean area fraction and  
'58 mean thickness are then derived for each thickness category. One of the key motivations of binning the CS2 along-track data  
'59 into sub-grid ice thickness classes is to assess the role of the ice thickness distribution (ITD) in model initialisation and to  
'60 quantify the realism of the CS2 ITD against independent estimates from airborne data. In addition to the bespoke data described  
'61 above, monthly (October-April, 2010-2021) 5km-gridded sea ice thickness estimates are available (in ASCII and NetCDF  
'62 formats) on the CPOM data portal: <http://www.cpom.ucl.ac.uk/csopr/seaice.php>.

'63

## '64 **6 Summary**

'65 We have described the multidisciplinary model and observational datasets that were produced by the UK ACSIS programme  
'66 and how and where the data can be accessed. The scope of ACSIS was very broad, covering atmospheric composition,  
'67 atmospheric circulation, ocean circulation, ice sheets, sea ice, and their interactions, and this breadth is reflected in the rich  
'68 variety of datasets generated. We note that whilst the focus of the ACSIS programme was the North Atlantic, most of the  
'69 model products covered the global domain, and many of the observational products have both global and regional significance.  
'70 Despite its great size and scope, the ACSIS programme had finite resources and so was not able to fully exploit the data it  
'71 generated. The landmark ACSIS papers cited here can be seen as starting points for further research. Therefore we believe  
'72 there is a major opportunity to repurpose our data for new research studies to build on the substantial financial and intellectual  
'73 investment that ACSIS represents and we express the hope that the ACSIS datasets provide a lasting legacy to the international  
'74 environmental science community.

'75

## '76 **Appendix A: Overview of select aircraft composition instruments**

### '77 ***UoM Time of Flight Chemical Ionisation Mass Spectrometer***

'78 The University of Manchester High Resolution-Time of Flight-Chemical Ionisation Mass Spectrometer (ToF-CIMS), been  
'79 described in detail by Matthews et al., (2013) for aircraft deployment. Briefly, iodide ions cluster with sample gases in the ion-  
'80 molecule reaction region (IMR) region creating a stable adduct. The flow is then sampled through a critical orifice into the  
'81 first of the four differentially pumped chambers in the TOF-CIMS, the short segmented quadrupole (SSQ). Quadrupole ion  
'82 guides transmit the ions through these stages. The ions are then subsequently pulsed into the drift region of the ToF-CIMS  
'83 where the arrival time is detected with a pair of microchannel plate detectors with an average mass resolution of 4000 ( $m/\Delta m$ ).  
'84 The inlet design is an atmospheric pressure, rearward facing, short residence time inlet, consisting of 3/8" diameter  
'85 polytetrafluoroethylene (PTFE) tubing with a total length to the instrument of 48 cm. A constant flow of 12 SLM is mass flow  
'86 controlled to the ion-molecule reaction region (IMR) using a rotary vane pump (Picolino VTE-3). 1 SLM is then subsampled  
'87 into the IMR for measurement.

'88



:89 An Iris system as described by Lee et al. (2018) was employed to pressurise and mass flow control the sample flow into the  
:90 instrument, avoiding sensitivity changes that would be associated with variations in pressure inflight that is not controlled  
:91 sufficiently by the constant flow inlet. This works upon the principle of the manipulation of the size of the critical orifice in  
:92 response to changes in the IMR pressure. As with the Lee et al., (2018) design, this works by having a stainless steel plate with  
:93 a critical orifice and a movable PTFE plate on top of this, also with a critical orifice. These orifices either align fully and allow  
:94 maximum flow into the instrument or misalign to reduce flow. This movement is controlled by the 24VDC output of the IMR  
:95 Pirani pressure gauge in relation to the set point and was designed collaboratively with Aerodyne Research Inc. The IMR set  
:96 point was  $72\pm 3$  mbar for the aircraft campaigns which is set through a combination of pumping capacity on the region (Agilent  
:97 IDP3), mass flow controlled reagent ion flow and sample flow. The reagent ion flow is 1 SLM of ultra-high purity (UHP)  
:98 nitrogen mixed with 2 SCCM of a pressurised known concentration gas mix of CH<sub>3</sub>I in nitrogen, passed through the radioactive  
:99 source, <sup>210</sup>Po. The total flow through the IMR is measured (MKS MFM) at the exhaust of the Agilent IDP3 pump so that not  
:00 only is the IMR pressure monitored but also the sample flow. All mass flow controllers and mass flow meters are measured  
:01 and controlled using the standard Aerodyne Inc EyeOn control unit and software.

:02 A pressure controller is also employed on the short segmented quadrupole (SSQ) region to make subtle adjustments in this  
:03 region independently of any small IMR changes that may occur inflight. This works upon the principle controlling an  
:04 electrically actuated solenoid valve in a feedback loop with the SSQ pressure gauge to actively control a leak of air into the  
:05 SSQ pumping line. The SSQ is pumped using an Ebara PDV 250 pump and held at  $1.8\pm 0.01$  mbar.

:06  
:07 Instrument backgrounds are programmatically run for 6 seconds every minute for the entire flight, by overflowing the inlet  
:08 with ultra high purity (UHP) nitrogen at the point of entry into the IMR. Here a 1/16th inch PTFE line enters through the  
:09 movable PTFE top plate, ensuring that the flow exceeds that of the sample flow. Inlet backgrounds are also run multiple times  
:10 during campaigns manually by overflowing as close to the end of the inlet as possible with UHP nitrogen. Data is taken at 4Hz  
:11 during a flight, which is routinely averaged to 1 Hz for analysis. Of the 6 points in each background, the first 2 and last point  
:12 are unused and the mean of the background is calculated using custom python scripting. Backgrounds are humidity corrected  
:13 and using linear interpolation, a time series of the instrument background is determined and then subtracted to give the final  
:14 time series (Matthews, 2023).

### :16 *UoM Aerosol Mass Spectrometer*

:17 The chemical composition of non-refractory submicron aerosols (organic (OA), sulphate, nitrate, ammonium and non-sea-salt  
:18 chloride) can be measured by a compact time-of-flight Aerosol Mass Spectrometer (C-ToF-AMS, Aerodyne Research Inc,  
:19 Billerica, MA, USA) (Drewnick et al., 2005), which provides chemical characterization across a range of ion mass-to-charge  
:20 ( $m/z$ ) ratios from 10 to 500. The detailed operation of the AMS, including calibration and correction factors, during aircraft  
:21 deployment has been described previously (Morgan et al., 2009). In brief, aerosols enter the instrument via an aerodynamic



lens inlet, focusing the incoming particles into a narrow beam. The aerodynamic lens system of the AMS in this study is tailored to sample submicron aerosols. Particles exit the aerodynamic lens into the particle-sizing chamber, which is evacuated to progressively lower pressures as the particle beam passes through and removes the majority of the gaseous material. Non-refractory components of the particles are then flash vaporised on a resistively heated porous tungsten surface. The resultant gaseous molecules are ionised by a 70-eV electron beam released from a tungsten filament. These fragment ions are analysed by a Time-of-Flight mass spectrometer (ToF-MS). The AMS mass spectra were recorded every 8 or 15 s during the ACSIS campaign (AC SIS-1 and 3-6). The AMS data was processed using the standard SQUIRREL (SeQUential Igor data RetRiEval, v.1.65C) ToF-AMS software package. The AMS data was also calibrated using monodisperse ammonium nitrate and ammonium sulfate particles. A time- and composition-dependent collection efficiency (CE) was applied to the data based on the algorithm by Middlebrook et al. (2012).

### ***UoY LIF-SO<sub>2</sub>***

The University of York LIF-SO<sub>2</sub> instrument is a custom-built system for the highly sensitive detection of SO<sub>2</sub> via laser-induced fluorescence, and is based on the system originally demonstrated by Rollins et al. 2016. The basic operating principle is the excitation of SO<sub>2</sub> at 216.9 nm, generated from the fifth harmonic of a custom-built tuneable fibre-amplified semiconductor diode laser system at 1084.5 nm, and the subsequent detection of the resultant fluorescence photons. The laser wavelength is rapidly (~10 Hz) tuned on and off a strong SO<sub>2</sub> transition, with the difference between these signals being directly proportional to the SO<sub>2</sub> concentration within the sample cell. The laser wavelength is tracked using a reference cell containing a known SO<sub>2</sub> concentration.

The ACSIS-7 experiment was part of the first field deployment for the York LIF-SO<sub>2</sub>, and was thus in part a learning experience on the operation of the instrument aboard an aircraft. The sample flow rate was maintained at 2 slpm and the use of a ram inlet allowed both the sample and reference cells to be operated at 400 mbar for the full altitude range of the campaign to maximise instrument sensitivity. Multi-point calibrations were carried out across the expected concentration range approximately every half an hour to ensure the instrument sensitivity was well characterised. To assess the possible quenching effect of excited SO<sub>2</sub> by water vapour, or increased wall losses when sampling humid air, calibrations in both stable ambient air and dry zero air were carried out, for which this effect proved negligible. The uncertainty in the LIF-SO<sub>2</sub> measurements was calculated predominantly from the uncertainty in the instrument sensitivity (typically 6 %). However, due to inconsistencies in the laser power and laser linewidth, the sensitivity was seen to vary during the course of each flight. Therefore, a mean sensitivity has been applied and this variation has been conservatively added to the sensitivity uncertainty on a flight-by-flight basis to give an overall uncertainty of ~ 15 % (using the mean of this variation). The 3  $\sigma$  precision of 225 ppt has also been determined conservatively from stable ambient measurements due to issues with completely overflowing the instrument inlet with zero air in flight.



53 **Code/Data availability**

54 Code availability is not applicable for this article. All data is deposited in reliable data repositories and access is detailed in  
55 Table 1 of this article.

56 **Author contributions**

57 ATA and BS prepared the original draft with input from TJB, LJC, EM, KR, MRR, FAS, KR, LT, LW, HW, MY  
58 BS, EM and MRR edited the original draft, all authors reviewed the manuscript.  
59 SJJ, TJB, EM, CR, FAS, LT, NT, LW, HW acquired data.  
60 ATA, LJC, HC, PE, JL, BS, MY, acquired funding

61 **Competing interests**

62 There are no competing interests.

63 **Acknowledgements**

64 We gratefully acknowledge the financial support provided by the UK Natural Environment Research Council for the extensive  
65 data provided by the ACSIS project. Airborne data were obtained using the BAe-146 Atmospheric Research Aircraft flown by  
66 Airtask Ltd and managed by FAAM Airborne Laboratory, jointly operated by UK Research and Innovation and the University  
67 of Leeds. We would like to give special thanks to the Airtask pilots and engineers and all staff at FAAM Airborne Laboratory  
68 for their hard work in helping plan and execute successful flight campaigns during ACSIS. PE and LT were supported by  
69 NERC awards NE/T008555/1 and NE/S007458/1 for the development and operation of the LIF-SO<sub>2</sub>. MY, TB, and the Penlee  
70 Point Atmospheric Observatory measurements were supported by the NERC projects ACSIS (NE/N018044/1) and MOYA  
71 (NE/N015932/1). TS and the Plymouth sunphotometer measurements were supported by the NERC project ACRUISE  
72 (NE/S005390/1) and by the Western Channel Observatory, which is funded by NERC through its National Capability Long-  
73 term Single Centre Science Programme, Climate Linked Atlantic Sector Science (NE/R015953/1). We further thank Frances  
74 Hopkins, Jani Pewter, Daniel Phillips, and Simone Louw for instrument maintenance at Penlee Point Atmospheric  
75 Observatory. We thank Luis Neves, Instituto Nacional de Meteorologia e Geofísica, São Vicente (INMG), Mindelo, Cabo  
76 Verde and, Shalini Punjabi, WACL, for technical assistance in the CVAO measurements. Model simulations were performed  
77 at NCAS, NOC and CPOM under ACSIS grants NE/N018001/1 and NE/N018044/1.



## 78 References

- 79 Abalos, M., Orbe, C., Kinnison, D. E., Plummer, D., Oman, L. D., Jöckel, P., Morgenstern, O., Garcia, R. R., Zeng, G., Stone,  
80 K. A., and Dameris, M.: Future trends in stratosphere-to-troposphere transport in CCM1 models, *Atmos. Chem. Phys.*, 20,  
81 6883–6901, <https://doi.org/10.5194/acp-20-6883-2020>, 2020.
- 82 Abraham, L.: Data provided by UKESM1 Hindcast simulations for the North Atlantic Climate System Integrated Study  
83 (ACSIS). accessed 31 January 2024, <https://data.ceda.ac.uk/badc/acsis/UKESM1-hindcasts>, 2024.
- 84 Andersen, S. T., Carpenter, L. J., Nelson, B. S., Neves, L., Read, K. A., Reed, C., Ward, M., Rowlinson, M. J., and Lee, J. D.:  
85 Long-term NO<sub>x</sub> measurements in the remote marine tropical troposphere, *Atmos. Meas. Tech.*, 14, 3071–3085,  
86 <https://doi.org/10.5194/amt-14-3071-2021>, 2021.
- 87 Andersen, S. T. and Nelson, B. S. and Read, K. A. and Punjabi, S. and Neves, L. and Rowlinson, M. J. and Hopkins, J. and  
88 Sherwen, T. and Whalley, L. K. and Lee, J. D. and Carpenter, L. J.: Fundamental oxidation processes in the remote marine  
89 atmosphere investigated using the NO-NO<sub>2</sub>-O<sub>3</sub> photostationary state, *Atmospheric Chemistry and Physics*, 22, (24) 15747-  
90 15765, <https://doi.org/10.5194/acp-22-15747-2022>, 2022.
- 91
- 92 Andersen, S. T., Carpenter, L. J., Reed, C., Lee, J. D., Chance, R., Sherwen, T., Vaughan, A. R., Stewart, J., Edwards, P. M.,  
93 Bloss, W. J., Sommariva, R., Crilley, L. R., Nott, G. J., Neves, L., Read, K., Heard, D. E., Seakins, P. W., Whalley, L. K.,  
94 Boustead, G. A., Fleming, L. T., Stone, D. and Fomba, K. W.: Extensive field evidence for the release of HONO from the  
95 photolysis of nitrate aerosols, *Sci. Adv.*, <https://doi.org/10.1126/sciadv.add6266>, 2023
- 96
- 97 Archibald, A.T., Folberth, G., Wade, D.C. and Scott, D.: A world avoided: impacts of changes in anthropogenic emissions on  
98 the burden and effects of air pollutants in Europe and North America, *Faraday Discussions*, 200, pp.475-500, 2017.
- 99 Archibald, A.T, M O'Connor, F., Luke Abraham, N., Archer-Nicholls, S., P Chipperfield, M., Dalvi, M., A Folberth, G.,  
100 Dennison, F., S Dhomse, S., T Griffiths, P., Hardacre, C., J Hewitt, A., S Hill, R., E Johnson, C., Keeble, J., O Köhler, M.,  
101 Morgenstern, O., P Mulcahy, J., Ordóñez, C., J Pope, R., T Rumbold, S., R Russo, M., H Savage, N., Sellar, A., Stringer, M.,  
102 T Turnock, S., Wild, O. and Zeng, G.: Description and evaluation of the UKCA stratosphere-troposphere chemistry scheme  
103 (StratTrop vn 1.0) implemented in UKESM1, *Geosci. Model Dev.*, <https://doi.org/10.5194/gmd-13-1223-2020>, 2020.
- 104 Arfeuille, F. et al.: Volcanic forcing for climate modeling: a new microphysics-based data set covering years 1600–present,  
105 *Climate of the Past*, 10, 359–375, <https://doi.org/10.5194/cp-10-359-2014>, 2014.
- 106 Balmaseda M. A., Trenberth K. E., Källén E.: Distinctive climate signals in reanalysis of global ocean heat content,  
107 *Geophysical Res. Lett.* 40 (9), 1754–1759, <https://doi.org/10.1002/grl.50382>, 2013.
- 108 Behrenfeld, M. J., Moore, R. H., Hostetler, C. A., Graff, J., Gaube, P., Russell, L. M., Chen, G., Doney, S. C., Giovannoni, S.,  
109 Liu, H., Proctor, C., Bolaños, L. M., Baetge, N., Davie-Martin, C., Westberry, T. K., Bates, T. S., Bell, T. G., Bidle, K. D.,  
110 Boss, E. S., Brooks, S. D., Cairns, B., Carlson, C., Halsey, K., Harvey, E. L., Hu, C., Karp-Boss, L., Kleb, M., Menden-Deuer,  
111 S., Morison, F., Quinn, P. K., Scarino, A. J., Anderson, B., Chowdhary, J., Crosbie, E., Ferrare, R., Hair, J. W., Hu, Y., Janz,  
112 S., Redemann, J., Saltzman, E., Shook, M., Siegel, D. A., Wisthaler, A., Martin, M. Y., and Ziemba, L.: The North Atlantic  
113 Aerosol and Marine Ecosystem Study (NAAMES): Science Motive and Mission Overview, *Front. Mar. Sci.*, 6,  
114 122, <https://doi.org/10.3389/fmars.2019.00122>, 2019.
- 115 Boylan, P., Helmig, D., Oltmans, S. and Miller, L.A.: Ozone in the Atlantic Ocean marine boundary layer, *Elementa: Science*  
116 *of the Anthropocene*, 3, 000045, <https://doi.org/10.12952/journal.elementa.000045>, 2015.
- 117 Brodeau, L. Barnier, B., Treguier, A.-M., Penduff, T., Gulev, S.: An ERA40-based atmospheric forcing for global ocean  
118 circulation models. *Ocean Modelling* 31 (2010) 88–104 ISSN 1463-5003, 2010.





- 19 Brooke, J. S. A. et al.: Meteoric smoke deposition in the polar regions: A comparison of measurements with global atmospheric  
20 models, *J. Geophys. Res.*, 122, pp. 11,112–11,130, 2017.
- 21 Bryden, H. L., Johns, W. E., King, B. A., McCarthy, G., McDonagh, E. L., Moat, B. I., Smeed, D. A.: Reduction in ocean  
22 heat transport at 26°N since 2008 cools the eastern subpolar gyre of the North Atlantic Ocean, *Journal of Climate*, 33 (5).  
23 1677–1689. <https://doi.org/10.1175/JCLI-D-19-0323.1>, 2020.
- 24 Carpenter, L. J., Fleming, Z. L., Read, K. A., Lee, J. D., Moller, S. J., Hopkins, J. R., Purvis, R. M., Lewis, A. C., Müller, K.,  
25 Heinold, B., Herrmann, H., et al.: Seasonal characteristics of tropical marine boundary layer air measured at the Cape Verde  
26 Atmospheric Observatory, *Journal of Atmospheric Chemistry*, 67(2), pp.87–140. 2010.
- 27 Collins, W. J., Lamarque, J.-F., Schulz, M., Boucher, O., Eyring, V., Hegglin, M. I., Maycock, A., Myhre, G., Prather, M.,  
28 Shindell, D., and Smith, S. J.: AerChemMIP: quantifying the effects of chemistry and aerosols in CMIP6, *Geosci. Model Dev.*,  
29 10, 585–607, <https://doi.org/10.5194/gmd-10-585-2017>, 2017.
- 30 Coward, Andrew; Roberts, Malcolm (2018). *NERC HadGEM3-GC31-HH model output prepared for CMIP6 HighResMIP*.  
31 Version 20240131. Earth System Grid Federation. <https://doi.org/10.22033/ESGF/CMIP6.1822>  
32
- 33 Daskalakis, N., Tsigaridis, K., Myriokefalitakis, S., Fanourgakis, G. S. and Kanakidou, M.: Large gain in air quality compared  
34 to an alternative anthropogenic emissions scenario. *Atmospheric Chemistry and Physics*, 16(15), pp.9771–9784, 2016.
- 35 Dee, D. P., Uppala, S. M., Simmons, A. J., Berrisford, P., Poli, P., Kobayashi, S., Andrae, U., Balmaseda, M. A., Balsamo, G.,  
36 Bauer, P., Bechtold, P., Beljaars, A. C. M., van de Berg, L., Bidlot, J., Bormann, N., Delsol, C., Dragani, R., Fuentes, M.,  
37 Geer, A. J., Haimberger, L., Healy, S. B., Hersbach, H., Hólm, E. V., Isaksen, I., Kållberg, P., Köhler, M., Matricardi, M.,  
38 McNally, A. P., Monge-Sanz, B. M., Morcrette, J.-J., Park, B.-K., Peubey, C., de Rosnay, P., Tavolato, C., Thépaut, J.-N., and  
39 Vitart, F.: The ERA-Interim reanalysis: configuration and performance of the data assimilation system, *Q. J. Roy. Meteor.*  
40 *Soc.*, 137, 553–597, <https://doi.org/10.1002/qj.828>, 2011 (data available at: [https://www.ecmwf.int/en/forecasts/datasets/  
41 reanalysis-datasets/era-interim](https://www.ecmwf.int/en/forecasts/datasets/reanalysis-datasets/era-interim), last access: 12 January 2023).
- 42 Dennison, F., Keeble, J., Morgenstern, O., Zeng, G., Abraham, N. L. and Yang, X.: Improvements to stratospheric chemistry  
43 scheme in the um-ukca (v10. 7) model: Solar cycle and heterogeneous reactions, *Geoscientific Model Development*, 12(3),  
44 pp.1227–1239. 2019.
- 45 Dhomse, S.: *UMUKCA\_Volcanic\_Forcing\_Data\_Dhomse2020*, Mendeley Data, V1, <https://doi.org/10.17632/n3g2htz9hk.1>,  
46 2020.
- 47 Dhomse, S. S. et al.: Aerosol microphysics simulations of Pinatubo eruption with UKCA composition-climate model, *Atmos.*  
48 *Chem. Phys.*, 14, pp. 11221–11246, 2014. <https://doi.org/10.5194/acp-14-11221-2014>, 2014.
- 49 Dhomse, S. S. et al.: Evaluating the simulated radiative forcings, aerosol properties, and stratospheric warmings from the 1963  
50 Mt Agung, 1982 El Chichón, and 1991 Mt Pinatubo volcanic aerosol clouds, *Atmos. Chem. Phys.*, 20, 13627–13654, 2020,  
51 <https://doi.org/10.5194/acp-20-13627-2020>, 2020.
- 52 Dhomse, S., Feng, W., Rap, A., Carslaw, K., Bellouin, N., and Mann, G.: SMURPHS/ACSIS El Chichon volcanic forcing  
53 dataset (mapped to UM wavebands) -- from HERSEA ensemble of interactive strat-aerosol GA4 UM-UKCA runs (Dhomse et  
54 al., 2020, ACP) (Version v1) [Data set], Zenodo, <https://doi.org/10.5281/zenodo.4744634>, 2021a.
- 55 Dhomse, S., Feng, W., Rap, A., Carslaw, K., Bellouin, N., and Mann, G.: SMURPHS/ACSIS Agung volcanic forcing dataset  
56 (mapped to UM wavebands) -- from HERSEA ensemble of interactive strat-aerosol GA4 UM-UKCA runs (Dhomse et al.,  
57 2020, ACP) (Version v1) [Data set], Zenodo, <https://doi.org/10.5281/zenodo.4744687>, 2021b.
- 58 Drewnick, F., Hings, S. S., DeCarlo, P., Jayne, J. T., Gonin, M., Fuhrer, K., Weimer, S., Jimenez, J. L., Demerjian, K. L.,  
59 Borrmann, S., and Worsnop, D. R.: A new time-of-flight aerosol mass spectrometer (TOF-AMS) – Instrument description and  
60 first field deployment, *Aerosol Sci. Tech.*, 39, 637–658, <https://doi.org/10.1080/02786820500182040>, 2005.





- '61 Dunstone, N. J., Smith, D. M., and Eade, R.: Multi-year predictability of the tropical Atlantic atmosphere driven by the high-  
'62 latitude North Atlantic Ocean. *Geophys. Res. Lett.*, **38**, L14701, <https://doi.org/10.1029/2011GL047949>, 2011.
- '63 Dussin, R., Barnier, B., Brodeau, L., and Molines, J. M.: The making of the DRAKKAR forcing set DFS5. DRAKKAR  
'64 (MyOcean report 01-04-16), LGGE, Grenoble, France, 2016.
- '65 Facility for Airborne Atmospheric Measurements; Natural Environment Research Council; Met Office; Archibald, A.;  
'66 Matthews, E.; Squires, F.; Wu, H.; Temple, L.: ACSIS: Merged airborne chemistry data from instruments on board the FAAM  
'67 aircraft. NERC EDS Centre for Environmental Data Analysis, <https://doi:10.5285/6285564c34a246fc9ba5ce053d85e5e7>,  
'68 2024
- '69
- '70 Feng, W., Dhomse, S., Rap, A., Carslaw, K., Bellouin, N., and Mann, G.: SMURPHS/ACIS Pinatubo volcanic forcing dataset  
'71 (mapped to UM wavebands) -- from HERSEA ensemble of interactive strat-aerosol GA4 UM-UKCA runs (Dhomse et al.,  
'72 2020, ACP) (v1), <https://doi.org/10.5281/zenodo.4739171>, 2021.
- '73 Germe, A.; Hirschi, J. J.-M., Blaker, A. T., Sinha, B.: Chaotic variability of the Atlantic meridional overturning circulation at  
'74 subannual time scales, *Journal of Physical Oceanography*, *52* (5). 929-949. <https://doi.org/10.1175/JPO-D-21-0100.1,2022>.
- '75 Good, S. A., Martin, M. J. and Rayner, N. A.: 2013. EN4: quality controlled ocean temperature and salinity profiles and  
'76 monthly objective analyses with uncertainty estimates, *Journal of Geophysical Research: Oceans*,  
'77 <https://doi.org/10.1002/2013JC009067>, 2013.
- '78 Griffies, S. M., Danabasoglu, G., Durack, P. J., Adcroft, A. J., Balaji, V., Böning, C. W., Chassignet, E. P., Curchitser, E.,  
'79 Deshayes, J., Drange, H., Fox-Kemper, B., Gleckler, P. J., Gregory, J. M., Haak, H., Hallberg, R. W., Heimbach, P., Hewitt,  
'80 H. T., Holland, D. M., Ilyina, T., Jungclaus, J. H., Komuro, Y., Krasting, J. P., Large, W. G., Marsland, S. J., Masina, S.,  
'81 McDougall, T. J., Nurser, A. J. G., Orr, J. C., Pirani, A., Qiao, F., Stouffer, R. J., Taylor, K. E., Treguier, A. M., Tsujino, H.,  
'82 Uotila, P., Valdivieso, M., Wang, Q., Winton, M., and Yeager, S. G.: OMIP contribution to CMIP6: experimental and  
'83 diagnostic protocol for the physical component of the Ocean Model Intercomparison Project, *Geosci. Model Dev.*, *9*, 3231-  
'84 3296, <https://doi.org/10.5194/gmd-9-3231-2016>, 2016.
- '85 Griffiths, P. T., Murray, L. T., Zeng, G., Shin, Y. M., Abraham, N. L., Archibald, A. T., Deushi, M., Emmons, L. K., Galbally,  
'86 I. E., Hassler, B., Horowitz, L. W., Keeble, J., Liu, J., Moeini, O., Naik, V., O'Connor, F. M., Oshima, N., Tarasick, D., Tilmes,  
'87 S., Turnock, S. T., Wild, O., Young, P. J., and Zanis, P.: Tropospheric ozone in CMIP6 simulations, *Atmos. Chem. Phys.*, *21*,  
'88 4187–4218, <https://doi.org/10.5194/acp-21-4187-2021>, 2021.
- '89 Grist, J. P., Sinha, B., Hewitt, H. T., Duchez, A., MacLachlan, C., Hyder, P., Josey, S. A., Hirschi, J. J.-M., Blaker, A. T.,  
'90 New, A. L., Scaife, A. A., Roberts, C. D.: Re-emergence of North Atlantic subsurface ocean temperature anomalies in a  
'91 seasonal forecast system. *Climate Dynamics*, *22*, pp. <https://doi.org/10.1007/s00382-019-04826-w>, 2019.
- '92 Haarsma, R. J., Roberts, M. J., Vidale, P. L., Senior, C. A., Bellucci, A., Bao, Q., et al.: High Resolution Model Intercomparison  
'93 Project (HighResMIP v1.0) for CMIP6, *Geoscientific Model Development*, *9*(11), 4185–4208. <https://doi.org/10.5194/gmd-9-4185-2016>, 2016.
- '94
- '95 Helmig, D., Muñoz, M., Hueber, J., Mazzoleni, C., Mazzoleni, L., Owen, R.C., Val-Martin, M., Fialho, P., Plass-Duelmer, C.,  
'96 Palmer, P.I. and Lewis, A.C.: Climatology and atmospheric chemistry of the non-methane hydrocarbons ethane and propane  
'97 over the North AtlanticNMHC at Pico Mountain, *Elementa: Science of the Anthropocene*, *3*, 54, ISSN 2325-1026, 2015.
- '98 Helmig, D., Rossabi, S., Hueber, J. et al.: Reversal of global atmospheric ethane and propane trends largely due to US oil and  
'99 natural gas production, *Nature Geosci* *9*, 490–495, <https://doi.org/10.1038/ngeo2721>, 2016.
- '00 Hersbach, H., Bell, B., Berrisford, S., Hirahara, A., Horányi, J., Muñoz-Sabater, et al.: The ERA5 global reanalysis, *Q. J. R.*  
'01 *Meteorol. Soc.*, *146*, 1999-2049, 2020.
- '02



- 003 Hewitt, H. T. Hill, R. S. R. Copsey, D. Culverwell, I. D. Harris, C. M. Keen, A. B. McLaren, A. J. et al.: Design and  
004 implementation of the infrastructure of HadGEM3: the next generation Met Office climate modelling system. *Geoscientific*  
005 *Model Development*. 4(2), 2011.
- 006 Hirschi, J. J.-M., Barnier, B., Böning, C., Biastoch, A., Blaker, A. T., Coward, A., Danilov, S., Drijfhout, S., Getzlaff, K.,  
007 Griffies, S. M., Hasumi, H., Hewitt, H., Iovino, D., Kawasaki, T., Kiss, A. E., Koldunov, N., Marzocchi, A., Mecking, J. V.,  
008 Moat, B., Molines, J.-M., Myers, P. G., Penduff, T., Roberts, M., Treguier, A.-M., Sein, D. V., Sidorenko, D., Small, J., Spence,  
009 P., Thompson, L., Weijer, W., Xu, X.: The Atlantic meridional overturning circulation in high resolution models, *Journal of*  
010 *Geophysical Research: Oceans*, 125 (4), e2019JC015522. <https://doi.org/10.1029/2019JC015522>, 2020.
- 011 Huang, B., Thorne, P. W., et. al.: Extended Reconstructed Sea Surface Temperature version 5 (ERSSTv5), Upgrades,  
012 validations, and intercomparisons, *J. Climate*, <https://doi.org/10.1175/JCLI-D-16-0836>, 2017.
- 013 Hunke, E. C., and Lipscomb, W. H.: Cice: The Los Alamos Sea ice model, documentation and software user's manual, version  
014 4.1 (Tech. Rep.). Los Alamos National Laboratory, 2010.
- 015 Jackson, R. B. et al.: Increasing anthropogenic methane emissions arise equally from agricultural and fossil fuel sources,  
016 *Environ. Res. Lett.* 15, 071002, 2020.
- 017 Josey, S. A. ; Sinha, B.: Subpolar Atlantic Ocean mixed layer heat content variability is increasingly driven by an active ocean,  
018 *Communications Earth & Environment*, 3 (1). <https://doi.org/10.1038/s43247-022-00433-6>, 2022.
- 019 Kanamitsu, M., et al.: NCEP–DOE AMIP-II reanalysis (R-2), *Bull. Amer. Meteor. Soc.*, **83**, 1631–1644,  
020 <https://doi.org/10.1175/BAMS-83-11-1631>, 2002.
- 021 Keeble, J., Hassler, B., Banerjee, A., Checa-Garcia, R., Chiodo, G., Davis, S., Eyring, V., Griffiths, P. T., Morgenstern, O.,  
022 Nowack, P., Zeng, G., Zhang, J., Bodeker, G., Burrows, S., Cameron-Smith, P., Cugnet, D., Danek, C., Deushi, M., Horowitz,  
023 L. W., Kubin, A., Li, L., Lohmann, G., Michou, M., Mills, M. J., Nabat, P., Olivie, D., Park, S., Seland, Ø., Stoll, J., Wieners,  
024 K.-H., and Wu, T.: Evaluating stratospheric ozone and water vapour changes in CMIP6 models from 1850 to 2100, *Atmos.*  
025 *Chem. Phys.*, 21, 5015–5061, <https://doi.org/10.5194/acp-21-5015-2021>, 2021.
- 026 Kennedy, J. J., Rayner, N. A., Atkinson, C. P., and Killick, R. E.: An ensemble data set of sea-surface temperature change  
027 from 1850: the Met Office Hadley Centre HadSST.4.0.0.0 data set, *Journal of Geophysical Research: Atmospheres*, 124.  
028 <https://doi.org/10.1029/2018JD029867>, 2019.
- 029 King B. A.: Objectively mapped Argo profiling float data and RAPID moored microcat data from the North Atlantic Ocean,  
030 2004-2022. NERC EDS British Oceanographic Data Centre NOC. [https://doi.org/10.5285/fe8e524d-7f04-41f3-e053-](https://doi.org/10.5285/fe8e524d-7f04-41f3-e053-6c86abc04d51)  
031 [6c86abc04d51](https://doi.org/10.5285/fe8e524d-7f04-41f3-e053-6c86abc04d51), 2023.
- 032
- 033 Kumar, A., Wu, S., Weise, M. F., Honrath, R., Owen, R. C., Helmig, D., Kramer, L., Val Martin, M. and Li, Q.: Free-  
034 troposphere ozone and carbon monoxide over the North Atlantic for 2001–2011: *Atmospheric Chemistry and Physics*, 13(24),  
035 12537-12547, 2013.
- 036 Large, W. G., and Yeager, S. G.: The global climatology of an interannually varying air–sea flux data set, *Climate Dynamics*,  
037 33(2), 341– 364. <https://doi.org/10.1007/s00382-008-0441-3>, 2009.
- 038 Lawler, M. J. et al.: HOCl and Cl<sub>2</sub> observations in marine air, *Atmos. Chem. Phys.*, 11, 7617-7628. 2011.
- 039 Lee, B. H., Lopez-Hilfiker, F. D., Mohr, C., Kurtén, T., Worsnop, D. R., and Thornton, J. A.: An iodide-adduct high-resolution  
040 time-of-flight chemical-ionization mass spectrometer: Application to atmospheric inorganic and organic compounds,  
041 *Environmental science & technology*, 48(11), 6309-6317, 2018.
- 042



- 143 Loades, D. C., Yang, M., Bell, T. G., Vaughan, A. R., Pound, R. J., Metzger, S., Lee, J. D., and Carpenter, L. J.: Ozone  
144 deposition to a coastal sea: comparison of eddy covariance observations with reactive air-sea exchange models, *Atmos. Meas.*  
145 *Tech.*, 13, 6915-6931, 10.5194/amt-13-6915-2020, 2020.
- 146 Lozier, M.S., Li, F., Bacon, S., Bahr, F., Bower, A., Cunningham, S., de Jong, F., de Steur, L., de Young, B., Fischer, J., Gary,  
147 S., Greenan, B., Holliday, N. P., Houk, A., Houpert, L., Inall, M., Johns, B., Johnson, H., Johnson, C., Karstensen, J., Koman,  
148 G., LeBras, I., Lin, X., Mackay, N., Marshall, D., Mercier, H., Oltmanns, M., Pickart, R., Ramsay, A., Rayner, D., Straneo, F.,  
149 Thierry, V., Torres, D., Williams, R., Wilson, C., Yang, J., Yashayaev, I., Zhao, J.: A sea change in our view of overturning  
150 in the Subpolar North Atlantic Program, *Science* 01 Feb 2019:Vol. 363, Issue 6426, pp. 516-521  
151 <https://doi.org/10.1126/science.aau6592>, 2019.
- 152 Luo, B.: Stratospheric aerosol data for use in CMIP6 models, available at:  
153 [ftp://iacftp.ethz.ch/pub\\_read/luo/CMIP6/Readme\\_Data\\_Description.pdf](ftp://iacftp.ethz.ch/pub_read/luo/CMIP6/Readme_Data_Description.pdf), 2016 .
- 154 Madec et al.: NEMO ocean engine, Note du Po<sup>le</sup> de mode<sup>l</sup>isation de l'Institut Pierre-Simon Laplace No 27 ISSN No 1288-  
155 1619, 2016.
- 156 Madec, G., and the NEMO System Team: NEMO ocean engine, *Scientific Notes of Climate Modelling Center (27) – ISSN*  
157 *1288-1619*, <https://doi.org/10.5281/zenodo.1464816>, 2019.
- 158 Mann, G. W. et al.: “Description and evaluation of GLOMAP-mode: a modal global aerosol microphysics model for the UKCA  
159 composition-climate model”, *Geosci. Mod. Dev.*, 3, 519–551, 2010, <https://doi.org/10.5194/gmd-3-519-2010>, 2010.
- 160 Mann, G. W. et al.: Evolving particle size is the key to improved volcanic forcings, *Past Global Change*, vol. 23, no. 2, 52-53,  
161 <https://doi.org/10.22498/pages.23.2.52>, 2015.
- 162 Matthews, E., Bannan, T. J., Khan, M. A. H., Shallcross, D. E., Stark, H., Browne, E. C., Archibald, A. T., Mehra, A.,  
163 Bauguitte, S. J. B., Reed, C., Thamban, N. M., Wu, H., Barker, P., Lee, J., Carpenter, L. J., Yang, M., Bell, T. G., Allen, G.,  
164 Jayne, J. T., Percival, C. J., McFiggans, G., Gallagher, M., Coe, H: Airborne observations over the North Atlantic Ocean reveal  
165 the importance of gas-phase urea in the atmosphere. *National Academy of Sciences. Proceedings*, 120(25), Article  
166 e2218127120. <https://doi.org/10.1073/pnas.2218127120>, 2023
- 167 Matthews E, Examining novel atmospheric chemistry in the marine environment with an iodide chemical ionisation mass  
168 spectrometer. Ph. D. Thesis. The University of Manchester, 2023.
- 169 McCarthy, G. D., Smeed, D. A., Johns, W. E., Frajka-Williams, E., Moat, B. I. Rayner, D., Baringer, M.O., Meinen, C.S.,  
170 Collins, J., Bryden, H.L.: Measuring the Atlantic Meridional Overturning Circulation at 26°N, *Progress in Oceanography*, 130:  
171 91-111. <https://doi.org/10.1016/j.pocean.2014.10.006>, 2015.
- 172 McFiggans, G. B., et al.: Novel findings in the Reactive Halogens in the Marine Boundary Layer (RHAMBLe) project,  
173 *Geochimica Et Cosmochimica Acta*, 73, A857-A857, 2009.
- 174 Mecking, J. V., Drijfhout, S. S., Hirschi, J. J.-M., Blaker, A. T.: Ocean and atmosphere influence on the 2015 European  
175 heatwave, *Environmental Research Letters*, 14(11) 114035, <https://doi.org/10.1088/1748-9326/ab4d33>, 2019.
- 176 Megann, A., Blaker, A., Josey, S., New, A., and Sinha, B.: Mechanisms for late 20th and early 21st Century decadal AMOC  
177 variability, *JGR: Oceans*, 126, e2021JC017865. <https://doi.org/10.1029/2021JC017865>, 2021a.
- 178 Megann, A., Sinha, B., and Blaker, A.: Monthly ocean and sea-ice output from 1/4° NEMO GO6 integration forced by CORE2  
179 data, <https://doi.org/10/gm8vf7>, 2021b .
- 180 Megann, A., Sinha, B. and Blaker, A.: Monthly ocean and sea-ice output from 1/4° NEMO (GO6 integration forced by DFS5.2  
181 data. NERC EDS British Oceanographic Data Centre. <https://doi.org/10/gm8vf5>, 2021c.
- 182 Megann, A., Sinha, B. and Blaker, A.: Monthly ocean and sea-ice output from 1/4° NEMO GO6 integration forced by JRA55  
183 data. NERC EDS British Oceanographic Data Centre. <https://doi.org/10/gm8vf8>, 2021d.



- 184 Megann, A., Sinha, B., Blaker, A., Schroeder, D., Feltham, D.: The North Atlantic Climate System Integrated Study: model  
185 run output. NERC EDS British Oceanographic Data Centre NOC, accessed 27 March 2023,  
186 <http://catalogue.ceda.ac.uk/uuid/770a885a8bc34d51ad71e87ef346d6a8>, 2021e.
- 187 Megann, A., Blaker, A., Coward, A., Guiavarc'h, C., Storkey, D.: Model output from 1/4° global JRA55-forced integration of  
188 GO8p7 global ocean-sea ice model from 1958 to 2021. NERC British Oceanographic Data Centre, 20 October 2022.  
189 doi:10.5285/e02c8424657846468c1ff3a5acd0b1ab, 2022a.
- 190 Megann, A., Blaker, A., Coward, A., Guiavarc'h, C., Storkey, D.: Model output from 1/12° global JRA55-forced integration  
191 of GO8p7 global ocean-sea ice model from 1958 to 2021, NERC British Oceanographic Data Centre, 20 October 2022.  
192 doi:10.5285/399b0f762a004657a411a9ea7203493a, 2022b.
- 193 Middlebrook, A. M., Bahreini, R., Jimenez, J. L., and Canagaratna, M. R.: Evaluation of composition-dependent collection  
194 efficiencies for the aerodyne aerosol mass spectrometer using field data, *Aerosol Sci. Tech.*, 46, 258–271,  
195 <https://doi.org/10.1080/02786826.2011.620041>, 2012.
- 196 Moat, B. I., Sinha, B., Josey, S. A., Robson, J., Ortega, P., Sévellec, F., Holliday, N. P., McCarthy, G. D., New, A. L., Hirschi,  
197 J. J.-M.: Insights into decadal North Atlantic sea surface temperature and ocean heat content variability from an eddy-  
198 permitting coupled climate model, *Journal of Climate*, 32(18). 6137-6161. <https://doi.org/10.1175/JCLI-D-18-0709.1>, 2019.
- 199 Moat, B. I.; Smeed, D. A.; Frajka-Williams, E.; Desbroyères, D. G.; Beaulieu, C.; Johns, W. E.; Rayner, D.; Sanchez-Franks,  
200 A.; Baringer, M. O.; Volkov, D.; Jackson, L. C.; Bryden, H. L.: Pending recovery in the strength of the meridional overturning  
201 circulation at 26° N, *Ocean Science*, 16 (4). 863-874. <https://doi.org/10.5194/os-16-863-2020>, 2020.
- 202 Moat, B.I.; King, B.A.; Macintosh, C.R. (2021a): Subpolar North Atlantic ocean heat content (surface to 1000m) using the  
203 EN4.2.2 temperature data set. NERC EDS British Oceanographic Data Centre NOC, <https://doi.org/10/g6wm>, 2021a
- 204 Moat, B. I., King, B. A., Macintosh, C. R.: Subpolar North Atlantic ocean heat content (surface to 1000m) using objectively  
205 mapped Argo profiling float data, NERC EDS British Oceanographic Data Centre NOC. <https://doi.org/10/g8g2>, 2021b.
- 206 Moat, B. I., Frajka-Williams, E., Smeed, D. A., Rayner, D., Johns, W. E., Baringer, M. O., Volkov, D., and Collins, J.: Atlantic  
207 meridional overturning circulation observed by the RAPID-MOCHA-WBTS (RAPID-Meridional Overturning Circulation and  
208 Heatflux Array-Western Boundary Time Series) array at 26N from 2004 to 2020 (v2020.2), British Oceanographic Data Centre  
209 - Natural Environment Research Council, UK. <https://doi.org/10.5285/e91b10af-6f0a-7fa7-e053-6c86abc05a09>, 2022.
- 210 Monerie, P.-A., Robson, J., Dong, B. and Dunstone, N.: A role of the Atlantic Ocean in predicting summer surface air  
211 temperature over North East Asia? *Climate Dynamics*, 51 (1-2). pp. 473-491. ISSN 0930-7575,  
212 <https://doi.org/10.1007/s00382-017-3935-z>, 2018.
- 213 Monks, P. S., Archibald, A. T., Colette, A., Cooper, O., Coyle, M., Derwent, R., Fowler, D., Granier, C., Law, K. S., Mills, G.  
214 E., Stevenson, D. S., Tarasova, O., Thouret, V., von Schneidemesser, E., Sommariva, R., Wild, O., and Williams, M. L.:  
215 Tropospheric ozone and its precursors from the urban to the global scale from air quality to short-lived climate forcer, *Atmos.*  
216 *Chem. Phys.*, 15, 8889–8973, <https://doi.org/10.5194/acp-15-8889-2015>, 2015.
- 217 Morgan, W. T., Allan, J. D., Bower, K. N., Capes, G., Crosier, J., Williams, P. I., and Coe, H.: Vertical distribution of sub-  
218 micron aerosol chemical composition from North-Western Europe and the North-East Atlantic, *Atmos. Chem. Phys.*, 9, 5389–  
219 5401, <https://doi.org/10.5194/acp-9-5389-2009>, 2009.
- 220 Mulcahy, J. P., Johnson, C., Jones, C. G., Povey, A. C., Scott, C. E., Sellar, A., Turnock, S. T., Woodhouse, M. T., Abraham,  
221 N. L., Andrews, M. B., Bellouin, N., Browse, J., Carslaw, K. S., Dalvi, M., Folberth, G. A., Glover, M., Grosvenor, D. P.,  
222 Hardacre, C., Hill, R., Johnson, B., Jones, A., Kipling, Z., Mann, G., Mollard, J., O'Connor, F. M., Palmieri, J., Reddington,  
223 C., Rumbold, S. T., Richardson, M., Schutgens, N. A. J., Stier, P., Stringer, M., Tang, Y., Walton, J., Woodward, S., and Yool,  
224 A.: Description and evaluation of aerosol in UKESM1 and HadGEM3-GC3.1 CMIP6 historical simulations, *Geosci. Model*  
225 *Dev.*, 13, 6383–6423, <https://doi.org/10.5194/gmd-13-6383-2020>, 2020.



- 26 National Centre for Atmospheric Science; Carpenter, L.J.; Hopkins, J.R.; Lewis, A.C.; Neves, L.M.; Moller, S.; Pilling, M.J.;  
27 Read, K.A.; Young, T.D.; Lee, J.D. (2010): Continuous Cape Verde Atmospheric Observatory Observations. NCAS British  
28 Atmospheric Data Centre, accessed 31 January, 2024.  
29 <http://catalogue.ceda.ac.uk/uuid/81693aad69409100b1b9a247b9ae75d5>.
- 30 Nisbet, E. G., Manning, M. R., Dlugokencky, E. J., Fisher, R. E., Lowry, D., Michel, S. E., Myhre, C. L., Platt, S. M., Allen,  
31 G., Bousquet, P. and Brownlow, R.: Very strong atmospheric methane growth in the 4 years 2014–2017: Implications for the  
32 Paris Agreement, *Global Biogeochemical Cycles*, 33(3), pp.318–342. 2019.
- 33 Oltmanns, M., Karstensen, J., Moore, G. W. K., and Josey, S. A.: Rapid cooling and increased storminess triggered by  
34 freshwater in the North Atlantic, *Geophysical Research Letters*, 47, e2020GL087207, <https://doi.org/10.1029/2020GL087207>,  
35 2020.
- 36 Parrington, M., Palmer, P. I., Henze, D. K., Tarasick, D. W., Hyer, E. J., Owen, R. C., Helmig, D., Clerbaux, C., Bowman, K.  
37 W., Deeter, M. N., Barratt, E. M., Coheur, P.-F., Hurtmans, D., Jiang, Z., George, M., and Worden, J. R.: The influence of  
38 boreal biomass burning emissions on the distribution of tropospheric ozone over North America and the North Atlantic during  
39 2010, *Atmos. Chem. Phys.*, 12, 2077–2098, <https://doi.org/10.5194/acp-12-2077-2012>, 2012.
- 40 Phillips, D. P., Hopkins, F. E., Bell, T. G., Liss, P. S., Nightingale, P. D., Reeves, C. E., Wohl, C., and Yang, M.: Air–sea  
41 exchange of acetone, acetaldehyde, DMS and isoprene at a UK coastal site. *Atmos. Chem. Phys.*, 21, 10111–10132,  
42 <http://doi.org/10.5194/acp-21-10111-2021>, 2021.
- 43 Plymouth Marine Laboratory; Yang, M. (2017): Penlee Point Atmospheric Observatory: Meteorological and chemical  
44 observations 2014– present. Centre for Environmental Data Analysis, accessed 31 January, 2024.  
45 <https://catalogue.ceda.ac.uk/uuid/8f1ff8ea77534e08b03983685990a9b0>.
- 46 Prather, M. J., Zhu, X., Flynn, C. M., Strode, S. A., Rodriguez, J. M., Steenrod, S. D., Liu, J., Lamarque, J.-F., Fiore, A. M.,  
47 Horowitz, L. W., Mao, J., Murray, L. T., Shindell, D. T., and Wofsy, S. C.: Global atmospheric chemistry – which air matters,  
48 *Atmos. Chem. Phys.*, 17, 9081–9102, <https://doi.org/10.5194/acp-17-9081-2017>, 2017.
- 49 Priestley, M., Le Breton, M., Bannan, T. J., Leather, K. E., Bacak, A., Reyes-Villegas, E., ... and Percival, C. J.: Observations  
50 of Isocyanate, Amide, Nitrate, and Nitro Compounds From an Anthropogenic Biomass Burning Event Using a ToF-CIMS,  
51 *Journal of Geophysical Research: Atmospheres*, 123(14), 7687–7704, 2018.
- 52 Ranjithkumar, A., Gordon, H., Williamson, C., Rollins, A., Pringle, K., Kupc, A., Abraham, N. L., Brock, C. and Carslaw, K.:  
53 Constraints on global aerosol number concentration, SO<sub>2</sub> and condensation sink in UKESM1 using ATom measurements,  
54 *Atmospheric Chemistry and Physics*, 21(6), pp.4979–5014. 2021.
- 55 Read K. A. et al.: Extensive halogen-mediated ozone destruction over the tropical Atlantic Ocean, *Nature*, 453, 1232–1235.  
56 2008.
- 57 Reed, C., Evans, M. J., Crilley, L. R., Bloss, W. J., Sherwen, T., Read, K. A., Lee, J. D., and Carpenter, L. J.: Evidence for  
58 renoxification in the tropical marine boundary layer, *Atmos. Chem. Phys.*, 17, 4081–4092, <https://doi.org/10.5194/acp-17-4081-2017>, 2017.  
59  
60
- 61 Reeves, C. E., Penkett, S. A., Bauguitte, S., Law, K. S., Evans, M. J., Bandy, B. J., Monks, P. S., Edwards, G. D., Phillips, G.,  
62 Barjat, H. and Kent, J.: Potential for photochemical ozone formation in the troposphere over the North Atlantic as derived  
63 from aircraft observations during ACSOE, *Journal of Geophysical Research: Atmospheres*, 107(D23), pp.ACH-14. 2002.
- 64 Reynolds, R. W., Rayner, N. A., Smith, T. M., Stokes, D. C. and Wang, W.: An improved in situ and satellite SST analysis  
65 for climate, *Journal of climate*, 15(13), pp.1609–1625. 2002.
- 66 Ridley, J. K., Blockley, E. W., Keen, A. B., Rae, J. G. L., West, A. E., and Schroeder, D., 2018: The sea ice model component  
67 of HadGEM3-GC3.1, *Geosci. Model Dev.*, 11, 713–723, <https://doi.org/10.5194/gmd-11-713-2018>. Roberts, Malcolm





- 68 **(2017a)**. *MOHC HadGEM3-GC31-MM model output prepared for CMIP6 HighResMIP highresSST-present*. Version  
69 20240131. Earth System Grid Federation. <https://doi.org/10.22033/ESGF/CMIP6.6029>.
- 70 Roberts, Malcolm **(2017b)**. *MOHC HadGEM3-GC31-HM model output prepared for CMIP6 HighResMIP highresSST-*  
71 *present*. Version 20240131. Earth System Grid Federation. <https://doi.org/10.22033/ESGF/CMIP6.6024>
- 72 Roberts, Malcolm **(2018a)**. *MOHC HadGEM3-GC31-HM model output prepared for CMIP6 HighResMIP hist-1950*. Version  
73 20240131. Earth System Grid Federation. <https://doi.org/10.22033/ESGF/CMIP6.6040>.
- 74 Roberts, Malcolm **(2018b)**. *MOHC HadGEM3-GC31-HH model output prepared for CMIP6 HighResMIP control-1950*.  
75 Version 20240131. Earth System Grid Federation. <https://doi.org/10.22033/ESGF/CMIP6.5881>.
- 76 Roberts, Malcolm **(2019a)**. *MOHC HadGEM3-GC31-MM model output prepared for CMIP6 HighResMIP highresSST-future*.  
77 Version 20240131. Earth System Grid Federation. <https://doi.org/10.22033/ESGF/CMIP6.6013>.
- 78 Roberts, Malcolm **(2019b)**. *MOHC HadGEM3-GC31-HM model output prepared for CMIP6 HighResMIP highresSST-future*.  
79 Version 20240131. Earth System Grid Federation. <https://doi.org/10.22033/ESGF/CMIP6.6008>.
- 80
- 81 Roberts, Malcolm **(2019c)**. *MOHC HadGEM3-GC31-HM model output prepared for CMIP6 HighResMIP highres-future*.  
82 Version 20240131. Earth System Grid Federation. <https://doi.org/10.22033/ESGF/CMIP6.5984>.
- 83 Roberts, M. J., Vidale, P. L., Senior, C., Hewitt, H. T., Bates, C., Berthou, S., et al.: The Benefits of Global High Resolution  
84 for Climate Simulation: Process Understanding and the Enabling of Stakeholder Decisions at the Regional Scale, *Bulletin of*  
85 *the American Meteorological Society*, 99(11), 2341–2359. <https://doi.org/10.1175/BAMS-D-15-00320.1>, 2018.
- 86 Roberts, M. J., Baker, A., Blockley, E. W., Calvert, D., Coward, A., Hewitt, H. T., et al.: Description of the resolution hierarchy  
87 of the global coupled HadGEM3-GC3.1 model as used in CMIP6 HighResMIP experiments, *Geoscientific Model*  
88 *Development*, 12(12), 4999–5028. <https://doi.org/10.5194/gmd-12-4999-2019>, 2019.
- 89 Roberts, M. J., Jackson, L. C., Roberts, C. D., Meccia, V., Docquier, D., Koenigk, T., Ortega, P., Moreno-Chamarro, E.,  
90 Bellucci, A., Coward, A., Drijfhout, S., Exarchou, E., Gutjahr, O., Hewitt, H., Iovino, D., Lohmann, K., Putrasahan, D.,  
91 Schiemann, R., Seddon, J., Terray, L., Xu, X., Zhang, Q., Chang, P., Yeager, S. G., Castruccio, F. S., Zhang, S., Wu, L.:  
92 Sensitivity of the Atlantic meridional overturning circulation to model resolution in CMIP6 HighResMIP simulations and  
93 implications for future changes. *Journal of Advances in Modeling Earth Systems*, 12 (8), e2019MS002014,  
94 <https://doi.org/10.1029/2019MS002014>, 2020.
- 95 Robson, J., Sutton, R. T., Archibald, A., Cooper, F., Christensen, M., Gray, L. J., Holliday, N. P., Macintosh, C., McMillan,  
96 M., Moat, B., Russo, M., Tilling, R., Carslaw, K., Desbruyères, D., Embury, O., Feltham, D. L., Grosvenor, Daniel P., Josey,  
97 S., King, B., Lewis, A., McCarthy, G. D., Merchant, C., New, A. L., O'Reilly, C. H., Osprey, S. M., Read, K., Scaife, A.,  
98 Shepherd, A., Sinha, B., Smeed, D., Smith, D., Ridout, A., Woollings, T., Yang, M.: Recent multivariate changes in the North  
99 Atlantic climate system, with a focus on 2005–2016, *International Journal of Climatology*, 38 (14), 5050–5076,  
100 <https://doi.org/10.1002/joc.5815>, 2018.
- 101 Robson, J., Aksenov, Y., Bracegirdle, T. J., Dimdore-Miles, O., Griffiths, P. T., Grosvenor, D. P., Hodson, D. L. R., Keeble,  
102 J., Megann, A., Osprey, S., Povey, A. C., Schröder, D., Yang, M., Archibald, A. T., Carslaw, K. S., Gray, L., Jones, C.,  
103 Kerridge, B., Knappett, D., Kuhlbrodt, T., Russo, M., Sellar, A., Siddans, R., Sinha, B., Sutton, R., Walton, J., Wilcox, L. J.:  
104 The evaluation of the North Atlantic climate system in UKESM1 historical simulations for CMIP6, *Journal of Advances in*  
105 *Modeling Earth Systems*, 12 (9), e2020MS002126. <https://doi.org/10.1029/2020MS002126>, 2020.
- 106 Rollins, A. W., Thornberry, T. D., Ciciora, S. J., McLaughlin, R. J., Watts, L. A., Hanisco, T. F., Baumann, E., Giorgetta, F.  
107 R., Bui, T. V., Fahey, D. W., and Gao, R.-S.: A laser-induced fluorescence instrument for aircraft measurements of sulfur  
108 dioxide in the upper troposphere and lower stratosphere, *Atmos. Meas. Tech.*, 9, 4601–4613, [https://doi.org/10.5194/amt-9-](https://doi.org/10.5194/amt-9-4601-2016)  
109 4601-2016, 2016



- 10 Russo, M. R., Kerridge, B. J., Abraham, N. L., Keeble, J., Latter, B. G., Siddans, R., Weber, J., Griffiths, P. T., Pyle, J. A., and  
11 Archibald, A. T.: Seasonal, interannual and decadal variability of tropospheric ozone in the North Atlantic: comparison of  
12 UM-UKCA and remote sensing observations for 2005–2018, *Atmos. Chem. Phys.*, 23, 6169–6196,  
13 <https://doi.org/10.5194/acp-23-6169-2023>, 2023.
- 14 Schiemann, R.; Vidale, P.; Hatcher, R.; Roberts, M. (2019a). *NERC HadGEM3-GC31-HM model output prepared for CMIP6*  
15 *HighResMIP hist-1950*. Version 20240131. Earth System Grid Federation. <https://doi.org/10.22033/ESGF/CMIP6.6041>.  
16
- 17 Schiemann, R.; Vidale, P. L.; Hatcher, R.; Roberts, M. (2019b). *NERC HadGEM3-GC31-HM model output prepared for*  
18 *CMIP6 HighResMIP highres-future*. Version 20240131. Earth System Grid Federation.  
19 <https://doi.org/10.22033/ESGF/CMIP6.5985>.  
20
- 21 Schroeder, D., Feltham, D. L., Tsamados, M., Ridout, A. and Tilling, R.: New insight from CryoSat-2 sea ice thickness for sea  
22 ice modelling, *The Cryosphere* 13(1), 125-139. ISSN 1994-0424. <https://doi.org/10.5194/tc-13-125-2019>, 2019.
- 23 Schultz, M. G., Schröder, S., Lyapina, O., Cooper, O. R., Galbally, I., Petropavlovskikh, I., Von Schneidemesser, E., Tanimoto,  
24 H., Elshorbany, Y., Naja, M. and Seguel, R. J. et al.: Tropospheric Ozone Assessment Report: Database and metrics data of  
25 global surface ozone observations, *Elementa: Science of the Anthropocene*, 5, 58, <https://doi.org/10.1525/elementa.244>, 2017.
- 26 Sellar, A. A., Jones, C. G., Mulcahy, J. P., Tang, Y., Yool, A., Wiltshire, A., O'Connor, F. M., Stringer, M., Hill, R., Palmieri,  
27 J., Woodward, S., de Mora, L., Kuhlbrodt, T., Rumbold, S. T., Kelley, D. I., Ellis, R.; Johnson, C. E., Walton, J., Abraham, N.  
28 L., Andrews, M. B., Andrews, T., Archibald, A. T., Berthou, S., Burke, E., Blockley, E., Carslaw, K., Dalvi, M., Edwards, J.,  
29 Folberth, G. A., Gedney, N., Griffiths, P. T., Harper, A. B., Hendry, M. A., Hewitt, A. J., Johnson, B., Jones, A., Jones, C. D.,  
30 Keeble, J., Liddicoat, S., Mordenstern, O., Parker, R. J., Predoi, V., Robertson, E., Siahann, A., Smith, R. S., Swaminathan,  
31 R., Woodhouse, M. T., Zeng, G., Zerroukat, M.: UKESM1: description and evaluation of the U.K. Earth System Model,  
32 *Journal of Advances in Modeling Earth Systems*, 11 (12). 4513-4558. <https://doi.org/10.1029/2019MS001739>, 2019.
- 33 Sinclair, K., van Dienenhoven, B., Cairns, B., Alexandrov, M., Moore, R., Ziemba, L. D. and Crosbie, E.: Observations of  
34 aerosol-cloud interactions during the North Atlantic aerosol and marine ecosystem study, *Geophysical Research Letters*, 47(3),  
35 p.e2019GL085851. 2020.
- 36 Smeed, D. A., Josey, S. A., Beaulieu, C., Johns, W. E., Moat, B. I., Frajka-Williams, E, Rayner, D., Meinen, C. S., Baringer,  
37 M. O., Bryden, H. L, and McCarthy, G. D.: The North Atlantic Ocean is in a state of reduced overturning, *Geophysical*  
38 *Research Letters*, 45 (3), 1527-1533, <https://doi.org/10.1002/2017GL076350>, 2018.
- 39 Smyth, T. (2024): ACSIS: Sunphotometer aerosol measurements at Plymouth Marine Laboratory - Version 1. 2001-2023.  
40 NERC EDS Centre for Environmental Data Analysis, *accessed 31 January, 2024*,  
41 <https://catalogue.ceda.ac.uk/uuid/e74491c96ef24df29a9342a3d57b5939>
- 42 Sommariva, R., Hollis, L. D. J., Sherwen, T., et al.: Seasonal and geographical variability of nitryl chloride and its precursors  
43 in Northern Europe, *Atmos Sci Lett.*, 19 (8), <https://doi.org/10.1002/asl.844>, 2018.
- 44 Storkey, D., Blaker, A. T., Mathiot, P., Megann, A., Aksenov, Y., Blockley, E. W., Calvert, D., Graham, T., Hewitt, H. T.,  
45 Hyder, P., Kuhlbrodt, T., Rae, J. G. L., and Sinha, B.: UK Global Ocean GO6 and GO7: a traceable hierarchy of model  
46 resolutions, *Geosci. Model Dev.*, 11, 3187–3213, <https://doi.org/10.5194/gmd-11-3187-2018>, 2018.
- 47 Sutton, R. T., McCarthy, G. D., Robson, J., Sinha, B., Archibald, A. T. and Gray, L. J.: Atlantic multidecadal variability and  
48 the UK ACSIS program, *Bulletin of the American Meteorological Society*, 99(2), 415-425, 2018.
- 49 Telford, P. J., Braesicke, P., Morgenstern, O. and Pyle, J. A.: Description and assessment of a nudged version of the new  
50 dynamics Unified Model, *Atmospheric Chemistry and Physics*, 8(6), 1701-1712, 2008.
- 51 Thompson, R. L. et al.: Variability in atmospheric methane from fossil fuel and microbial sources over the last three decades,  
52 *Geophys. Res. Lett.*, 45, 11499–11508, 2018.





- 53 Tilling, R. L., Ridout, A. and Shepherd, A.: Estimating Arctic sea ice thickness and volume using CryoSat-2 radar altimeter  
54 data. *Advances in Space Research*, 62(6), pp.1203-1225, 2018.
- 55 Timmreck, C. et al.: The Interactive Stratospheric Aerosol Model Intercomparison Project (ISA-MIP): motivation &  
56 experiment design, *Geosci. Mod. Dev.*, 11, 2581-2608, <https://doi.org/10.5194/gmd-11-2581-2018>, 2018.
- 57 Tsujino, H., et al.: JRA-55 based surface dataset for driving ocean-sea ice models (JRA55-do) *Ocean Modelling*, 130, 79-139,  
58 <https://doi.org/10.1016/j.ocemod.2018.07.002>, 2018.
- 59 Turnock, S. T., Butt, E. W., Richardson, T. B., Mann, G. W., Reddington, C. L., Forster, P. M., Haywood, J., Crippa, M.,  
60 Janssens-Maenhout, G., Johnson, C. E. and Bellouin, N.: The impact of European legislative and technology measures to  
61 reduce air pollutants on air quality, human health and climate, *Environmental Research Letters*, 11(2), p.024010, 2016.
- 62 Turnock, S. T., Allen, R. J., Andrews, M., Bauer, S. E., Deushi, M., Emmons, L., Good, P., Horowitz, L., John, J. G., Michou,  
63 M., Nabat, P., Naik, V., Neubauer, D., O'Connor, F. M., Olivić, D., Oshima, N., Schulz, M., Sellar, A., Shim, S., Takemura,  
64 T., Tilmes, S., Tsigaridis, K., Wu, T., and Zhang, J.: Historical and future changes in air pollutants from CMIP6 models,  
65 *Atmos. Chem. Phys.*, 20, 14547–14579, <https://doi.org/10.5194/acp-20-14547-2020>, 2020.
- 66 Van Pinxteren et al.: Marine organic matter in the remote environment of the Cape Verde islands – an introduction and  
67 overview to the MarParCloud campaign, *ACP*, acp-2019-997, 2020.
- 68 Walters, D. et al.: The Met Office Unified Model Global Atmosphere 4.0 and JULES Global Land 4.0 configurations, *Geosci.*  
69 *Model Dev.*, 7, 361–386, <https://doi.org/10.5194/gmd-7-361-2014>, 2014.
- 70 White, C., Ussher, S. J., Fitzsimons, M. F., Atkinson, S., Woodward, E. M. S., Yang, M., Bell, T. G.: Inorganic nitrogen and  
71 phosphorus in Western European aerosol and the significance of dry deposition flux into stratified shelf waters, *Atmospheric*  
72 *Environment*, 261, 118391, <https://doi.org/10.1016/j.atmosenv.2021.118391>, 2021.
- 73 Williams, K. D., Copsey, D., Blockley, E. W., Bodas-Salcedo, A., Comer, C. R., Davis, P., et al.: The Met Office Global  
74 Coupled Model 3.0 and 3.1 (GC3.0 and GC3.1) Configurations, *Journal of Advances in Modeling Earth Systems*, 10, 357–  
75 380, <https://doi.org/10.1002/2017MS001115>, 2017.
- 76 Williams, S. D. P., and Berry, D. I.: ACSIS Atlantic Ocean medium resolution SST dataset: Reconstructed 5-day, ½-degree,  
77 Atlantic Ocean SST (1950-2014). *Geoscience Data Journal*, 7 (2), 135-148, <https://doi.org/10.1002/gdj3.94>, 2020.
- 78 Wilkinson, M. D., Dumontier, M., Aalbersberg, I. J., Appleton, G., Axton, M., Baak, A., Blomberg, N., Boiten, J. W., da Silva  
79 Santos, L. B., Bourne, P. E. and Bouwman, J.: The FAIR Guiding Principles for scientific data management and  
80 stewardship. *Scientific data*, 3(1), 1-9, 2016.
- 81 Wofsy, S. C., Afshar, S., Allen, H. M., Apel, E., Asher, E. C., Barletta, B., Bent, J., Bian, H., Biggs, B. C., Blake, D. R., Blake,  
82 N., Bourgeois, I., Brock, C. A., Brune, W. H., Budney, J. W., Bui, T. P., Butler, A., Campuzano-Jost, P., Chang, C. S., Chin,  
83 M., Commane, R., Correa, G., Crouse, J. D., Cullis, P. D., Daube, B. C., Day, D. A., Dean-Day, J. M., Dibb, J. E., DiGangi,  
84 J. P., Diskin, G. S., Dollner, M., Elkins, J. W., Erdesz, F., Fiore, A. M., Flynn, C. M., Froyd, K., Gesler, D. W., Hall, S. R.,  
85 Hanisco, T. F., Hannun, R. A., Hills, A. J., Hints, E. J., Hoffman, A., Hornbrook, R. S., Huey, L. G., Hughes, S., Jimenez, J.  
86 L., Johnson, B. J., Katich, J. M., Keeling, R. F., Kim, M. J., Kupc, A., Lait, L. R., Lamarque, J.-F., Liu, J., McKain, K.,  
87 McLaughlin, R. J., Meinardi, S., Miller, D. O., Montzka, S. A., Moore, F. L., Morgan, E. J., Murphy, D. M., Murray, L. T.,  
88 Nault, B. A., Neuman, J. A., Newman, P. A., Nicely, J. M., Pan, X., Paplawsky, W., Peischl, J., Prather, M. J., Price, D. J.,  
89 Ray, E., Reeves, J. M., Richardson, M., Rollins, A. W., Rosenlof, K. H., Ryerson, T. B., Scheuer, E., Schill, G. P., Schroder,  
90 J. C., Schwarz, J. P., St. Clair, J. M., Steenrod, S. D., Stephens, B. B., Strode, S. A., Sweeney, C., Tanner, D., Teng, A. P.,  
91 Thames, A. B., Thompson, C. R., Ullmann, K., Veres, P. R., Vieznor, N., Wagner, N. L., Watt, A., Weber, R., Weinzierl, B.,  
92 Wennberg, P., Williamson, C. J., Wilson, J. C., Wolfe, G. M., Woods, C. T., and Zeng, L. H.: *ATom: Merged Atmospheric*  
93 *Chemistry, Trace Gases, and Aerosols*, ORNL DAAC, Oak Ridge, Tennessee, USA, 10.3334/ORNLDAAC/1581, 2018.
- 94 Yang, M. and Fleming, Z. L.: Estimation of atmospheric total organic carbon (TOC)–paving the path towards carbon budget  
95 closure, *Atmospheric Chemistry and Physics*, 19(1), 459-471. 2019.



- .96 Yang, M., Bell, T. G., Hopkins, F. E., and Smyth, T. J.: Attribution of atmospheric sulfur dioxide over the English Channel to  
.97 dimethyl sulfide and changing ship emissions, *Atmos. Chem. Phys.*, 16, 4771–4783, [https://doi.org/10.5194/acp-16-4771-](https://doi.org/10.5194/acp-16-4771-2016)  
.98 2016, 2016a.
- .99 Yang, M., Bell, T. G., Hopkins, F. E., Kitidis, V., Cazenave, P. W., Nightingale, P. D., Yelland, M. J., Pascal, R. W., Prytherch,  
.00 J., Brooks, I. M., and Smyth, T. J.: Air-sea fluxes of CO<sub>2</sub> and CH<sub>4</sub> from the Penlee Point Atmospheric Observatory on the  
.01 south-west coast of the UK, *Atmospheric Chemistry and Physics*, 16, 5745–5761, <https://doi.org/10.5194/acp-16-5745-2016>,  
.02 2016b.
- .03 Yang, M., Prytherch, J., Kozlova, E., Yelland, M. J., Parenkat Mony, D., and Bell, T. G.: Comparison of two closed-path  
.04 cavity-based spectrometers for measuring air–water CO<sub>2</sub> and CH<sub>4</sub> fluxes by eddy covariance, *Atmos. Meas. Tech.*, 9, 5509–  
.05 5522, <https://doi.org/10.5194/amt-9-5509-2016>, 2016c.
- .06 Yang, M., Bell, T. G., Hopkins, F. E., and Smyth, T. J.: Attribution of atmospheric sulfur dioxide over the English Channel to  
.07 dimethyl sulfide and changing ship emissions, *Atmospheric Chemistry and Physics*, 16, 4771–4783,  
.08 <https://doi.org/10.5194/acp-16-4771-2016>, 2016d.
- .09 Yang, M., Bell, T. G., Brown I. J., Fishwick J. R., Kitidis, V., Nightingale, P. D., Rees, A. P., and Smyth T. J.: Insights from  
.10 year-long measurements of air-water CH<sub>4</sub> and CO<sub>2</sub> exchange in a coastal environment, *Biogeosciences*, 16, 961–978,  
.11 <https://doi.org/10.5194/bg-16-961-2019a>, 2019a.
- .12 Yang, M., Norris, S. J., Bell, T. G., and Brooks, I. M.: Sea spray fluxes from the southwest coast of the United Kingdom  
.13 dependence on wind speed and wave height. *Atmos. Chem. Phys.*, 19, 15271–15284, [https://doi.org/10.5194/acp-19-15271-](https://doi.org/10.5194/acp-19-15271-2019)  
.14 2019, 2019b.
- .15 Zawadowicz, M. A., Suski, K., Liu, J., Pekour, M., Fast, J., Mei, F., Sedlacek, A. J., Springston, S., Wang, Y., Zaveri, R. A.,  
.16 Wood, R., Wang, J., and Shilling, J. E.: Aircraft measurements of aerosol and trace gas chemistry in the eastern North Atlantic,  
.17 *Atmos. Chem. Phys.*, 21, 7983–8002, <https://doi.org/10.5194/acp-21-7983-2021>, 2021.